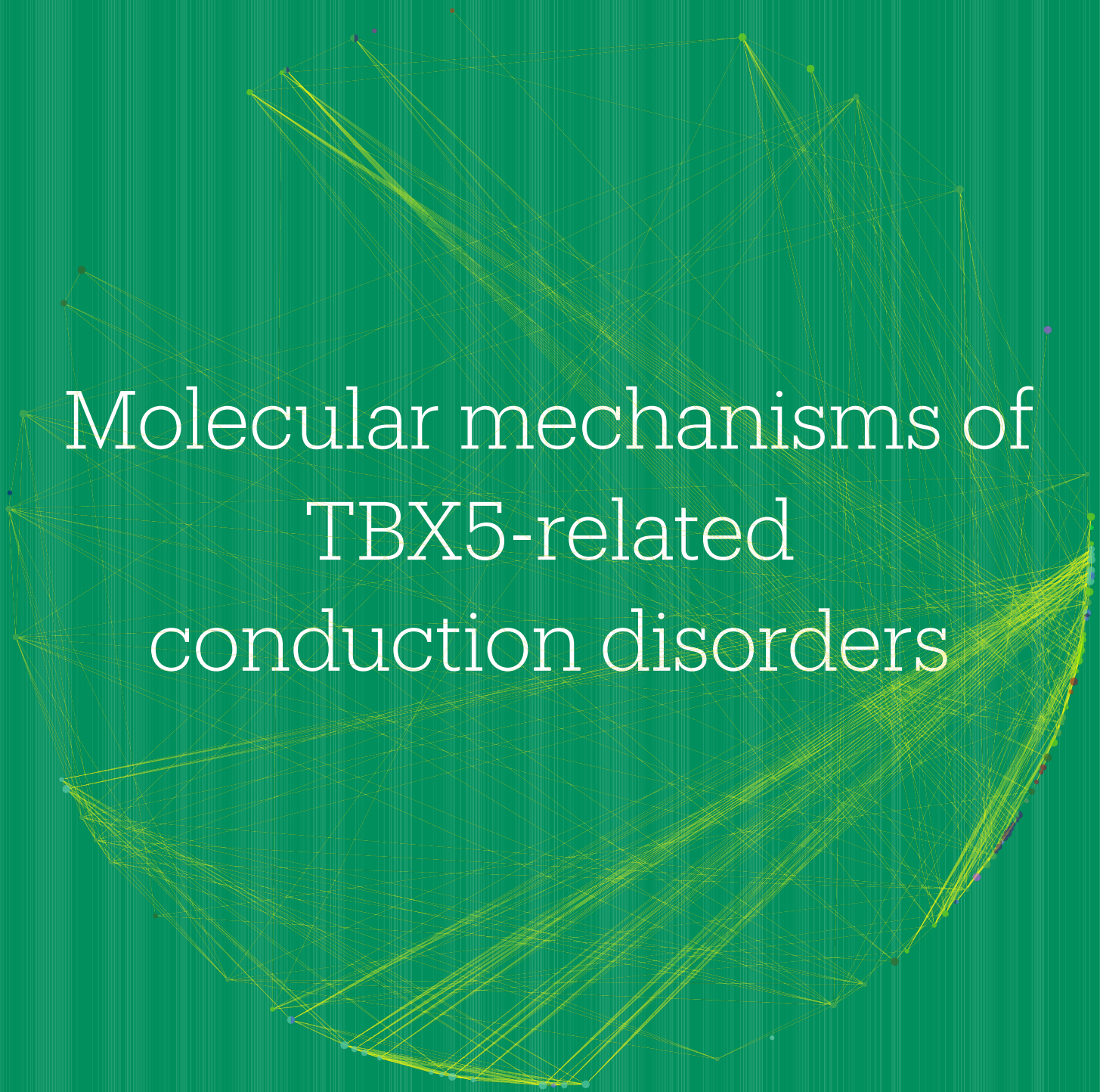

Molecular mechanisms of TBX5-related conduction disorders

Dissertation

Franziska Sophie Rathjens

Georg-August-Universität Göttingen | 05/2020

Molecular Mechanisms of TBX5-related conduction disorders

Dissertation

for the award of the degree

‚Doctor rerum naturalium'

at the Georg-August-Universität Göttingen

within the doctoral programme Molecular Medicine

of the Georg-August University School of Science (GAUSS)

submitted by

Franziska Sophie Rathjens

from Buxtehude

Kassel, 11th of May 2020

Examination Board

Members of the Thesis Advisory Committee:	
Referee: PD Dr. Laura Cecilia Zelarayán	Institute of Pharmacology and Toxicology University Medical Centre Göttingen Robert-Koch-Straße 40 37075 Göttingen laura.zelarayan@med.uni-goettingen.de
Co-referee: Prof. Dr. Elisabeth Zeisberg	Clinic for Cardiology and Pneumology University Medical Centre Göttingen Robert-Koch-Straße 40 37075 Göttingen elisabeth.zeisberg@med.uni-goettingen.de
Prof. Dr. Steven Johnsen	Clinic for General, Visceral and Pediatric Surgery University Medical Centre Göttingen Robert-Koch-Straße 40 37075 Göttingen steven.johnson@med.uni-goettingen.de

Additional members of the Examination Board	
Prof. Dr. Argyris Papantonis	Institute of Pathology University Medical Centre Göttingen Robert-Koch-Straße 40 37075 Göttingen argyris.papantonis@med.uni-goettingen.de
apl. Prof. Dr. Rüdiger Behr	German Primate Center Degenerative Diseases Kellnerweg 4 37077 Göttingen RBehr@dpz.eu
Prof. Dr. Hubertus Jarry	Animal Welfare Officer University Medical Centre Göttingen Robert-Koch-Straße 40 37075 Göttingen hubjarry@med.uni-goettingen.de

List of Figures

List of Tables

1. Acknowledgements

This project has been financially supported by a DZHK Shared Expertise and a Start-Up Grant of the University Medical centre of Göttingen. I was personally supported by a Promotionsstipendium of the Studienstiftung des deutschen Volkes.

I wish to express my deepest gratitude to Dr. Maria Patapia Zafeiriou, who gave me the opportunity to conduct this project in the first place. She took me in in my first practical in my master studies, when I had no idea about research in the university and about standards of scientific writing. I learned a lot of that from scratch under her supervision. She gave me freedom to bring in my own ideas and to attend conferences and workshops which helped me to personally and scientifically develop.

A special thank you goes to PD Dr. Laura Zelarayán for giving feedback and being available for questions. I thank my thesis advisory committee, Prof. Dr. Elisabeth Zeisberg and Prof. Dr. Steven Johnson who were encouraging and gave helpful scientific advice. Also I want to acknowledge Prof. Dr. Argyris Papantonis, Prof. Dr. Rüdiger Behr and Prof. Dr. Hubertus Jarry for volunteering to take part in my examination.

We collaborated with Partners from Göttingen – NGS Integrative Genomics Core Unit conducted RNA- and ChIP-Sequencing and analysed the RNA-Seq. Prof. Dr. Steven Johnson and his group helped us to establish ChIP-Seq. Namely, Dr. Sankari Nagarajan gave input for the sonication part of ChIP and Feda Hamdan shared some insights on ChIP-analysis with me. Dr. Rainer Bohrer from the GWDG very kindly introduced me to the High-Performance Computing Cluster, that finally allowed us to conduct the HOMER motif analysis.

External collaboration partners also helped this project. Prof. Dr. Larissa Fabritz and her team Fahima Syeda and Nashita Kabir conducted the ex-vivo pacing experiments and gave fruitful input in scientific discussions. Prof. Dr. Oliver Müller and his team supported us with the plasmids for cloning the AAV-vectors and produced and provided the final viral particles.

Also, I thank Paul Charlton, who gave me a hard time during our short encounter for presentation trainings – but that did help, and it has brought me forward a lot.

The Institute of Pharmacology and Toxicology was a nice multicultural environment to work in. Several colleagues participated directly in this project: The SFB 1002 Service Project S01 conducted operations and echocardiographic investigations and assisted in general with mouse work. Lavanya was very important for everything concerning ChIP and a cheerful person besides. She conducted some experiments and analyses listed in this thesis as well.

Several research assistants and students worked in this project: Alica, Cord, Denise, Vanessa as well as Alfia, Amara, Yelena and Yi-Ching. Simran provided us with NRCMs.

I learned a lot from Claudia, who gave a lot of helpful advice and taught me how to handle mice. Ines also took a share in that. Krasimira showed me how to work with human stem cells and how to differentiate them to cardiomyocytes.

I appreciated working together with team members Eric, Moni, Cheila of AG Zelarayán. I enjoyed the time with several different office colleagues during the time, Elena, Elif, Eriona, Farah, Funsho, Mina, PL, Satish, Shumon, Tobi. Thank you, Irina and Susanne, for lunch and tea sessions improving the morale.

I thank my mother for always believing in me, letting me make my own decisions and support me when needed.

Life has changed, since Ilverin has entered the world. He made everything more colourful, more intense and he made time fly. Therefore, I would like to thank Pascal for clearing time slots for me to write this Thesis, for all his moral support and for taking care of the visuals during the journey and of this final ‘book’. You two make everything better.

2. Abstract

Background

Cardiovascular disease is a common cause of death. About 60 % of cardiovascular mortality is attributable to sudden cardiac death, mostly caused by arrhythmia. The origin of arrhythmia can be an underlying chronic cardiac disease, but genetic factors are involved as well, especially in younger patients. A genetic factor associated with arrhythmia is the transcription factor T-box 5 (TBX5). Most studies investigated TBX5 in the context of developmental processes or with respect to conduction properties of the heart. Interestingly, TBX5 expression is dysregulated not only due to genetic factors: Ventricular samples from patients or animal models with cardiomyopathy show lower TBX5 expression than controls. Because of this aberrant expression pattern in the working myocardium, we hypothesized, that TBX5 plays an important role for tissue homoeostasis of the ventricular working myocardium.

Methods & Results

To investigate the consequences of TBX5 loss in the working myocardium, we generated an inducible primarily ventricular TBX5 KO model (*vTbx5*KO). This led to reduced heart growth and diastolic dysfunction in the *vTbx5*KO. Moreover, the mice presented with impeded conduction marked by PR- and QRS-prolongation and arrhythmias characterized by atrioventricular block and ventricular tachycardia. The survival of the *vTbx5*KO mice was reduced to 40%, probably attributable to sudden cardiac death.

For the determination of the underlying molecular mechanism, we performed integrative chromatin occupancy and transcriptome analysis. This analysis revealed 47 targets of TBX5 in the adult ventricle. More profound analysis on a subset of genes identified three clusters of novel targets implicated in cardiac electrophysiology (*Gja1, Kcnj5, Kcng2, Cacna1g, Chrm2*), cardioprotection (*Fhl2, Gpr22, Fgf16*) and contraction (*Fstl4, Cmya5, Emilin2, Pdlim4*).

Furthermore, we aimed to evaluate the therapeutic potential of restoration of TBX5 expression to revert arrhythmia and prevent sudden cardiac death. For this purpose, adeno-associated virus (AAV) encoding TBX5 were injected in *vTbx5*KO mice, that already suffered from arrhythmia. Indeed, the AAV led to a restoration of TBX5 and its target genes and more importantly to a normalisation of conduction and reduced arrhythmic propensity.

Conclusions

This study showed that beyond its role in the developing and adult conduction system, TBX5 is required for tissue homoeostasis and electrical signal propagation of the working myocardium. Its restoration after TBX5 loss can normalise target gene expression and cardiac electrophysiology.

3. Zusammenfassung

Hintergrund

Herz-Kreislauferkrankungen zählen zu den häufigsten Todesursachen. Mehr als 60% dieser Todesfälle sind auf den durch Arrhythmien ausgelösten plötzlichen Herztod zurückzuführen. Arrhythmien können sowohl durch chronische Herzerkrankungen als auch durch genetische Faktoren - besonders bei jüngeren Patienten - hervorgerufen werden. Einer dieser Faktoren ist der Transkriptionsfaktor T-box 5 (TBX5), der mit Arrhythmien assoziiert ist. Bisher hat sich die Forschung hauptsächlich auf die Rolle von TBX5 in der Entwicklungsbiologie und Erregungsleitung im Herzen konzentriert. Jedoch ist die Expression von TBX5 nicht nur im Kontext von genetischen Veränderungen, sondern auch in den kardialen Ventrikeln von Patienten oder Tiermodellen mit Herzinsuffizienz reduziert. Wegen dieser verminderten Expression im Arbeitsmyokard, stellten wir die Hypothese auf, dass TBX5 ebenfalls eine wichtige Rolle für die Homöostase des ventrikulären Arbeitsmyokards spielt.

Methoden & Ergebnisse

Um die Folgen des TBX5-Verlusts im Arbeitsmyokard zu untersuchen, generierten wir ein induzierbares TBX5-KO-Modell mit prädominanter ventrikulärer Spezifität (vTbx5KO). Dies hatte ein reduziertes Herzwachstum und eine diastolische Dysfunktion für die vTbx5KO zur Folge. Zudem zeigten die Mäuse eine verlangsamte Erregungsleistung, Arrhythmien wie atrioventrikulären Block und Kammertachykardien, die die Überlebenswahrscheinlichkeit der Mäuse auf 40% reduzierten, vermutlich durch das erhöhte Risiko eines plötzlichen Herztodes.

Um den zugrundeliegenden molekularen Mechanismus zu untersuchen, führten wir eine integrierte Analyse der Chromatinbindung von TBX5 zusammen mit einer Transkriptomanalyse der fehlregulierten Transkripte durch. Diese Analyse zeigte 47 neue Zielgene von TBX5 in den adulten Ventrikeln. Die validierten Zielgene lassen sich drei Gruppen zuordnen: Gene, mit einer Funktion in der kardialen Elektrophysiologie (*Gja1, Kcnj5, Kcng2, Cacna1g, Chrm2*), Kardioprotektion (*Fhl2, Gpr22, Fgf16*) und Kontraktion (*Fstl4, Cmya5, Emilin2, Pdlim4*).

Zur Evaluierung des therapeutischen Potentials einer Wiederherstellung der TBX5 Expression im Hinblick auf Arrhythmiereduzierung und Herztodprävention injizierten wir arrhythmische *vTbx5*KO-Mäuse mit TBX5-codierenden adeno-assoziierten Viren. Tatsächlich konnte diese Transduktion die Expression von TBX5 und seiner Zielgene wiederherstellen und - noch wichtiger - die Erregungsweiterleitung normalisieren und das Arrhythmierisiko reduzieren.

Schlussfolgerungen

Diese Studie zeigt, dass TBX5 nicht nur in der Entwicklung und der Erregungsleitung eine essentielle Rolle spielt, sondern auch für die Homöostase des Arbeitsmyokards essentiell ist. Die Wiederherstellung der TBX5 Expression kann die Zielgenexpression und kardiale Elektrophysiologie normalisieren.

Table of Contents

4. Abbreviations

Table 1. Abbreviations

Abbreviation	Explanation
AAV	adeno-associated virus
AME	Analysis of Motif Enrichment
ANF/ANP	Atrial natriuretic factor/peptide
AngII	Angiotensin II
AP	Alkaline Phosphatase
APD	action potential duration
Armh4	armadillo-like helical domain containing 4
bp	base pairs
BrdU	5-bromo-2'-deoxyuridine
BSA	bovine serum albumine
Cacna1g	calcium channel, voltage-dependent, T-type, alpha 1G subunit
CASQ2	calsequestrin 2
CBFHH	Calcium and bicarbonate free Hanks with HEPES
cDNA	copy DNA
CEAS	cis-regulatory element annotation system
ChIP	chromatin immunoprecipitation
Chrm2	cholinergic receptor, muscarinic 2, cardiac
CM	cardiomyocytes
CMV	cytomegalovirus
Cmya5	Cardiomyopathy associated 5
CP	cardiac progenitor cells
CVD	cardiovascular disease
CX43	Connexin 43 /Gja1
Da	Dalton
DCM	Dilated cardiomyopathy
DMEM	Dulbecco's modified Eagle's medium
DMSO	dimethyl sulfoxide
DNA	deoxyribonucleic acid
dNTP	deoxynucleoside triphosphate
E. coli	Escherichia coli
ECG	electrocardiogram
EHM	engineered human myocardium
Emilin2	Elastin microfibril interface located protein 2
FBS	fetal bovine serum
Fbxo25	F-box protein 25
FD	Fast Digestion
Fgf10	fibroblast growth factor 10
Fgf16	fibroblast growth factor 16
Fgf8	fibroblast growth factor 8
Fhl2	Four-and-a-half LIM domains 2
Fstl4	follistatin-like 4
GAPDH	glyceraldehyde 3-phosphate dehydrogenase
GATA4	GATA binding protein 4
GIRK4	G-protein coupled inward rectifier potassium channel
Gja1	gap junction a1 /Cx43
Gja5	gap junction protein alpha 5
GO	Gene Ontology
Gpr22	G-Protein coupled receptor 22
GREAT	Genomic Regions Enrichment of Annotations Tool
H3K27ac	Histone 3, acetylated at the 27th lysine residue
HDAC	histone deacetylase
HEK	human embryonic kidney
HOMER	Hypergeometric Optimization of Motif EnRichment
HRP	horseradish peroxidase
i.p.	intraperitoneal
ICM	ischemic cardiomyopathy
IgG	Immunoglobulin G
IP	immunoprecipitation
IRX3	Iroquois homeobox 3
kb	kilo basepairs
Kcng2	potassium voltage-gated channel, subfamiliy G, member 2
Kcnj5	potassium inwardly-rectifying channel, subfamily J, member 5 (encodes GIRK4)
kDa	kilodalton
KO	Knock-out
KO-CT	vTbx5KO mice transduced with AAV9-LUC
KO-RE	vTbx5KO mice transduced with AAV9-TBX5
LA	left atrium
LB	Lysogeny Broth
LMP4	LIM mineralization protein 4 (PDZ and LIM domain protein 7 - Pdlim7)
LQT	long QT syndrome
LV	left ventricle
MACS	Model-based Analysis of ChIP-Seq

MCS	multiple cloning site
MEF 2	myocyte enhancer factor 2
MEIS 1/2/3	Meis homeobox 1/2/3
miR	microRNA
mRNA	messenger RNA
Myh6	myosin, heavy polypeptide 6, cardiac muscle, alpha
NF	non-failing hearts
NKX2.5	NKX2 homeobox 5
Nppa/b	natriuretic peptide type A / B
NRCM	neonatal rat cardiomyocyte
NuRD	Nucleosome Remodeling and Deacetylase
NYHA	New York Heart Association
PAGE	Polyacrylamide gel electrophoresis
PBS	phosphate buffered saline
PCR	polymerase chain reaction
Pdlim4	PDZ and LIM domain 4
PFA	paraformaldehyde
POL2	RNA Polymerase II
PVDF	polyvinylidene difluoride
qPCR	quantitative polymerase chain reaction
RA	retinoic acid
rAAV	recombinant adeno-associated virus
RNA	ribonucleic acid
RT	reverse transcription
RV	right ventricle
Sall4	spalt like transcription factor 4
SCD	sudden cardiac death
SCF	Skp, Cullin, F-box containing complex
Scn5a/Nav1.5	sodium channel, voltage-gated, type V, alpha
SDS	sodium dodecyl sulfate
SEM	standard error of the mean
SERM	selective estrogen receptor modulator
Shh	sonic hedgehog
SNP	single nucleotide polymorphism
TAC	transverse aortic constriction
TBE	T-box binding element
TBX5	T-box 5
TGF-β	transforming growth factor, beta 1
TnnT	Troponin T
TPX	poly(4-methyl-1-pentene)
TSS	transcription start site
UPS	ubiquitin-proteasome system
UTR	untranslated region
UV	ultra violet
WB	Western Blot
Wnt	Wingless/Integrated
WT	wild type

5. Introduction

5.1. Cardiovascular disease and sudden cardiac death

Cardiovascular diseases (CVD) accounted for 31% of deaths worldwide with 17 million people dying from CVD in 2008 [Mendis et al., 2011]. About 60 % of cardiovascular deaths can be attributed to out-of-hospital sudden cardiac death (SCD), defined as unexpected death and mostly caused by arrhythmia [Adabag et al., 2010]. SCD can be explained by underlying cardiac disease seen in autopsy in 79.3% of cases, but cannot be explained in 1 out of 5 cases by visible abnormalities. Genetic variants can lead to fatal arrhythmias causing SCD, especially in the young [Eckart et al., 2011]. Genes associated with SCD are mostly ion channel encoding genes. A defect in an ion channel is termed channelopathy and can lead to electrical disturbances, like Brugada syndrom or prolonged or shortened QT-syndroms [Cerrone et al., 2011] [Schwartz et al., 2018]. But not only these channelopathies, also mutations and variants of transcription factors regulating the expression of proteins involved in electrical signal propagation are directly associated with SCD, such as NKX2 homeobox 5 (NKX2-5) [Ellesøe et al., 2016] [Perera et al., 2014], Meis homeobox 1 (MEIS1) [Bouilloux et al., 2016] [Pfeufer et al., 2010] [Smith et al., 2011], iroquois homeobox 3 (IRX3) [Koizumi et al., 2016], myocyte enhancer factor 2 (MEF2) [Naya et al., 2002] and T-box 5 (TBX5).

5.2. T-box 5

T-box 5 (TBX5) is a transcription factor with an essential role in heart development [Horb et al., 1999] and cardiac conduction [Moskowitz et al., 2004]. It regulates the expression of proteins implicated in electrical signal propagation of the heart, such as the sodium channel protein *Scn5a* (sodium voltage-gated channel alpha subunit 5) and the gap junction protein *Gja5* (gap junction protein alpha 5) [Arnolds et al., 2012]. Disturbances of TBX5 expression or activity can lead to congenital heart disease and arrhythmia [Bruneau et al., 2001] [Arnolds et al., 2012] [Nadadur et al., 2016].

5.2.1. Holt-Oram Syndrome

A haploinsufficiency of TBX5 results in a syndrome called Holt-Oram or heart-hand syndrome, which was first described by [Holt et al., 1960]. It occurs mainly via *de novo* mutations, in about 1 of 100,000 newborns [Elek et al., 1991]. Patients show upper-limb malformations, congenital heart defects (mostly atrial or ventricular septal defects) and/or cardiac conduction disorders [Vanlerberghe et al., 2019].

5.2.2. Genome-wide association studies

In humans, a genome wide association study revealed a strong correlation between the single nucleotide polymorphism (SNP) rs3825214 in an intron of TBX5 and atrial fibrillation as well as atrioventricular block. Additionally this SNP was associated with prolongation in QRS-, PR- and QT-interval [Holm et al., 2010].

Two other studies have also found TBX5 to be associated with abnormal PR-intervals in populations of European and African American origin [Pfeufer et al., 2010], [Smith et al., 2011].

5.2.3. Mouse models

Previous studies have studied the role of TBX5 during development and found it to be essential for heart development. Mice with a homozygous Knock-Out (KO) of TBX5 die during embryonic development due to cardiac defects [Bruneau et al., 2001]. A heterozygous global KO of TBX5 in mice leads to increased perinatal death, caused by intrauterine heart failure. These mice show structural (cardiomegaly, atrial septal defects, dilated atria) and functional cardiac abnormalites along with bone defects [Bruneau et al., 2001]. The functional cardiac abnormalities include arrhythmias like atrioventricular block [Bruneau et al., 2001] but also an impairment of diastolic function [Zhou et al., 2005]. This has been recapitulated in a constitutive cardiac specific TBX5 heterozygous KO mouse model (using *Nkx2.5*-Cre mice), in which the mice show diastolic heart failure in the absence of structural defects [Zhu et al., 2008].

Mice with a tissue-specific KO of TBX5 in the adult conduction system show an arrhythmic phenotype including slower AV and ventricular conduction, AV-block and sudden cardiac death [Arnolds et al., 2012]. Inducible global KO of TBX5 leads to atrial fibrillation, that can be attributed to prolonged APD90, early and delayed afterdepolarization and altered Ca^{2+} handling in atrial myocytes [Nadadur et al., 2016].

Outside of heart TBX5 plays a role for the induction of lung morphogenesis by interacting with the Wnt and Shh pathways [Steimle et al., 2018]. In this context, it interacts with different targets compared to the cardiovascular system.

5.2.4. Binding to DNA and interactions with other transcription factors

TBX5 has been shown to synergistically activate the *Nppa* promoter by directly interacting with NKX2.5 and GATA4 (Figure 1A) [Pradhan et al., 2016],[Hiroi et al., 2001],[Garg et al., 2003]. In addition, it interacts with MEF2C and myocardin to activate *Myh6* transcription [Ghosh et al., 2009], [Wang et al., 2011]. TBX5 also physically interacts with Sall4. This interaction either enhances activation by TBX5 - e.g. on *Fgf10* and *Gja5* - or counteracts it - e.g. on the *Nppa* promoter [Koshiba-Takeuchi et al., 2006].

In contrast to its well established function as a transcriptional activator, it has recently been shown, that TBX5 can also repress gene expression by interaction with the Nucleosome Remodeling and Deacetylase (NuRD) complex (Figure 1B) [Waldron et al., 2016]. This complex is involved in chromatin remodelling and represses target gene transcription of e.g. *Mef2b*. The interaction of TBX5 with the NuRD complex is necessary for correct cardiac septation [Boogerd et al., 2016][Waldron et al., 2016].

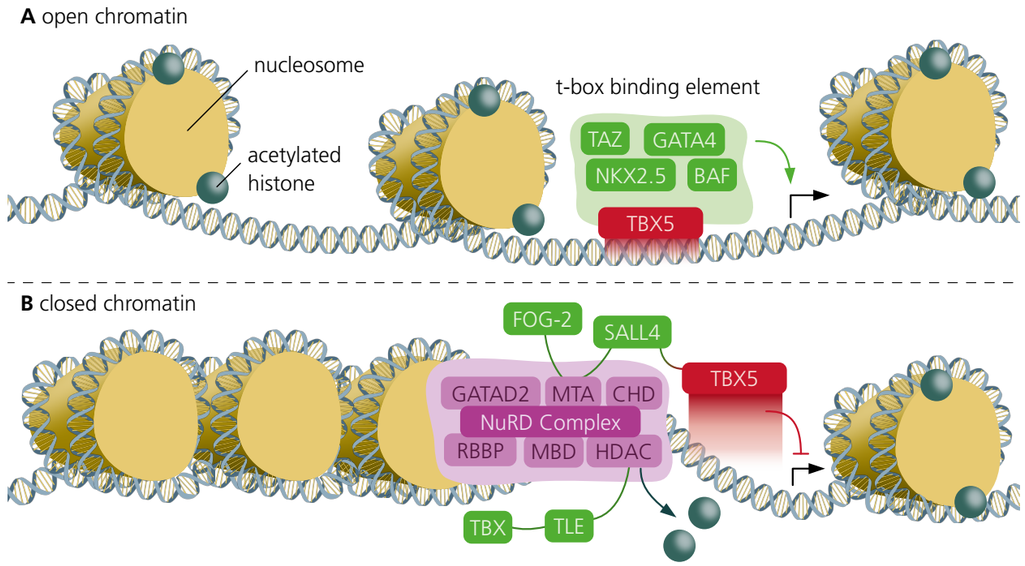

Figure 1. TBX5 acts as a transcriptional activator or repressor depending on interacting factors A. TBX5 interacts with NKX2.5 and GATA4 to activate transcription by binding to enhancers and promoters on open chromatin. **B.** TBX5 interacts with the NuRD-complex to repress transcription by deacetylation of histones thereby remodeling chromatin to an inactive state. Figure adapted from [Boogerd et al., 2016].

5.3. Target genes of TBX5

TBX5 regulates a broad variety of genes, depending on the tissue context and developmental stage. Research studies have focused on embryonic development, especially in the heart, and on cardiac function with regards to electrophysiology in the adult heart. In these contexts several target genes have been identified (Table 2 lists a number of published TBX5 targets).

Known target genes activated by TBX5 include the peptide hormone atrial natriuretic peptide a (*Nppa*) [Bruneau et al., 2001][Koshiba-Takeuchi et al., 2006] secreted by cardiac atria. Others include genes implicated in electrical signalling in the heart like sodium voltage-gated channel alpha subunit 5 (*Scn5a*) [Arnolds et al., 2012][van den Boogaard et al., 2012] or gap junction protein alpha 5 (*Gja5*) [Bruneau et al., 2001][Koshiba-Takeuchi et al., 2006]. A third group of genes are involved in development and cell growth, e.g. *Wnt2/2b* [Steimle et al., 2018] and *Fgf10* [Koshiba-Takeuchi et al., 2006],[Camarata et al., 2006].

In the atria, TBX5 regulates the expression of the transcription factor PITX2 and both regulate *Gja1*, *Scn5a*, *Dsp*, *Atp2a2* and *Ryr2*. TBX5 activates expression and PITX2 represses their activation [Nadadur et al., 2016].

Table 2. Target genes

Gene	Long name	Interacting with	TBX5 action	References
Nppa	atrial natriuretic peptide type A	Myocardin, NKX2.5, SALL4	activation	[Bruneau et al., 2001], [Hiroi et al., 2001], [Koshiba-Takeuchi et al., 2006], [Wang et al., 2011], [Pradhan et al., 2016]
Gja1	gap junction protein, alpha 1	PITX2	activation	[Nadadur et al., 2016]
Gja5	gap junction protein, alpha 5	SALL4	activation	[Bruneau et al., 2001], [Arnolds et al., 2012], [Koshiba-Takeuchi et al., 2006]
Scn5a	sodium channel, voltage-gated, type V, alpha	PITX2	activation	[Arnolds et al., 2012], [van den Boogaard et al., 2012], [Nadadur et al., 2016]
Kcnj5	potassium inwardly rectifying channel subfamily J member 5		activation	[Nadadur et al., 2016]
Fhl2	Four and a half LIM domains 2		activation	[Mori et al., 2006]
Myh6	myosin, heavy polypeptide 6, cardiac muscle, alpha	MEF2C, Myocardin	activation	[Ghosh et al., 2009], [Wang et al., 2011]
Atp2a2	ATPase, Ca++ transporting, cardiac muscle, slow twitch 2	PITX2	activation	[Zhu et al., 2008], [Nadadur et al., 2016]
Ryr2	ryanodine receptor 2, cardiac	PITX2	activation	[Nadadur et al., 2016]
Dsp	desmoplakin	PITX2	activation	[Nadadur et al., 2016]
Pitx2	paired-like homeodomain transcription factor 2		activation	[Nadadur et al., 2016]
Fgf10	fibroblast growth factor 10	SALL4	activation	[Koshiba-Takeuchi et al., 2006],[Camarata et al., 2006]

Wnt2/2b	wingless-type MMTV integration site family, member 2/2B	Shh pathway	activation	[Steimle et al., 2018]
Gad1	glutamate decarboxylase 1		repression	[Waldron et al., 2016]
Kcne3	potassium voltage-gated channel Isk-related subfamily, gene 3		repression	[Waldron et al., 2016]
Kctd16	potassium channel tetramerisation domain containing 16	NuRD-complex	repression	[Waldron et al., 2016]
Nxph4	neurexophilin 4		repression	[Waldron et al., 2016]
Sncb	synuclein, beta		repression	[Waldron et al., 2016]
Col20a1	collagen, type XX, alpha 1		repression	[Waldron et al., 2016]
Mef2b	myocyte enhancer factor 2B	NuRD-complex	repression	[Waldron et al., 2016]
Klf4	krueppel-like factor 4 (gut)		repression	[Waldron et al., 2016]
Casz1	castor zinc finger 1		repression	[Waldron et al., 2016]
Fgf11	fibroblast growth factor 11		repression	[Waldron et al., 2016]
Plekha2	pleckstin homology domain containing A2		repression	[Waldron et al., 2016]

5.3.1. Functional implications of TBX5 target genes

5.3.1.1. *Scn5a*

Scn5a has been identified as a TBX5 target gene. An enhancer shortly downstream of the gene body is responsible for TBX5 induced regulation [Arnolds et al., 2012][van den Boogaard et al., 2012]. *Scn5a* (sodium channel, voltage-gated, type V, alpha) encodes for a subunit of the sodium-selective voltage-dependent channel Nav1.5 and is essential for cardiac contraction [Papadatos et al., 2002]. A complete KO of *Scn5a* is embryonically lethal and a haploinsufficiency leads to a 50% reduction in sodium conductance with the consequence of disturbed conduction in atria and ventricles and re-entrant tachycardia [Papadatos et al., 2002].

5.3.1.2. *Gja1*

Recently *Gja1* has been found to be regulated by TBX5 [Nadadur et al., 2016]. *Gja1* encodes for Connexin 43 (CX43), the major gap junction protein in the working myocardium [Severs et al., 2004]. It is expressed in the atria and ventricles (Figure 2, left and middle panel) and localized at the cell-cell-junctions (Figure 2, right panel) (own unpublished data). Heart-specific KO of CX43 leads to ventricular tachycardia and sudden cardiac death [Gutstein et al., 2001].

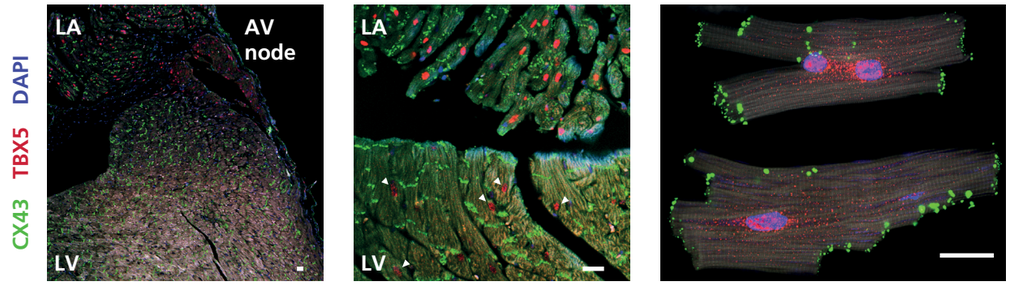

Figure 2. CX43 and TBX5 expression in the myocardium and isolated cardiomyocytes Besides prominent expression in the left atrium (LA) and atrioventricular (AV) node (left panel), TBX5 (red) is expressed to a lower extent in the working myocardium of the left ventricle (LV) (middle panel, arrowheads). In isolated ventricular myocytes, the expression of CX43 (green) and TBX5 in the same cell is obvious (right panel). DAPI (blue) was used to stain nuclei. Scale bars: 20 µm (own unpublished data).

5.3.1.3. *Kcnj5*

Kcnj5 (potassium inwardly-rectifying channel, subfamily J, member 5) encodes for G-protein coupled inward rectifier potassium channel 4 (GIRK4). It forms a heteromer with GIRK1 in the heart [Krapivinsky et al., 1995]. GIRK4 is expressed the intercalated disks of rodent atria and ventricles and its expression could be detected in human ventricles [Liang et al., 2014]. It contributes to ventricular repolarization [Liang et al., 2014]. Therefore, mutations in the *KCNJ5*-gene in humans lead to Long QT syndrome type 13 (LQT13). Long-QT syndromes can be a cause for arrhythmia and sudden cardiac death [Wang et al., 2013].

5.4. Regulation of TBX5

Protein expression and activity can be regulated on several levels, from transcription through translation, post-translational modifications, intracellular localisation to degradation.

5.4.1. Transcriptional regulation

The transcription of the TBX5 gene is activated by retinoic acid (RA) signaling in chicken and mice [Liberatore et al., 2000],[De Bono et al., 2018]. While it has been suggested that this activation is indirectly mediated by *Fgf8* [Zhao et al., 2009], [Cunningham et al., 2013], others found a RA-response element in an intron of TBX5 [Nishimoto et al., 2015]. However, those studies were carried out on the role of TBX5 in limb development and the regulation in the heart might be different. In vitro promoter activation assays showed, that *Tbx5* can be activated by RA, FHL2 and TBX5 itself [Renger, 2012] (Figure 3A).

5.4.2. Translational regulation & Posttranslational modifications

The translation of TBX5 mRNA into protein was suggested to be regulated by miR-10a and miR-10b (Figure 3B), which target the 3'-UTR of TBX5, thereby downregulating TBX5 protein levels [Wang F et al., 2014]. When TBX5 protein is acetylated (e.g. by Histone acetyltransferase p300), its activity increases, whereas deacetylation by histone deacetylase 3 (HDAC3) leads to repression of TBX5 activity [Lewandowski et al., 2014] (Figure 3C).

5.4.3. Intracellular localization & Degradation

TBX5 shuttles between the nucleus and the cytoplasm, where it is bound by LMP4 on actin filaments (Figure 3D). Thereby, the overexpression of LMP4 can inhibit the activity of TBX5 [Camarata et al., 2006]. Lastly the degradation of TBX5 by the ubiquitin-proteasome system (UPS) seems to be regulated by the F-box protein 25 (Fbxo25) (Figure 3E), which facilitates TBX5 and NKX2.5 protein degradation via SCF-mediated ubiquitination [Jeong et al., 2015].

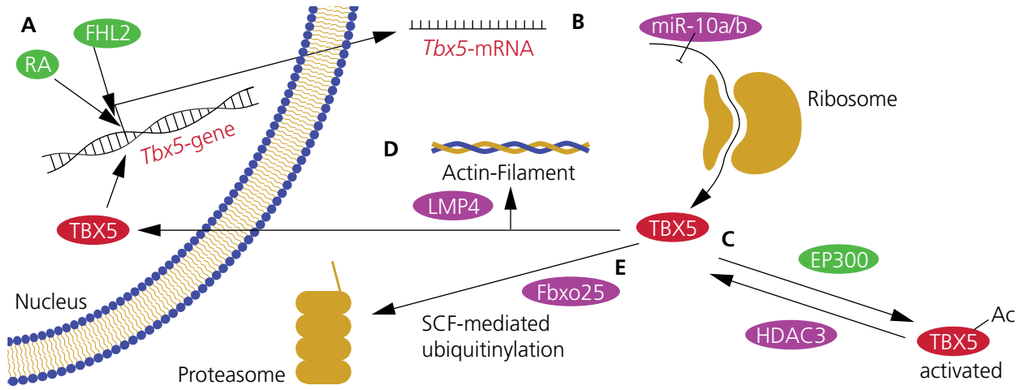

Figure 3. Regulation of TBX5-expression and activity. A. *Tbx5*-transcription can be activated by retinoic acid (RA), FHL2 and TBX5 itself. **B.** *Tbx5*-mRNA can be bound and inhibited by miR-10a and b. **C.** When TBX5 is acetylated (e.g. by EP300) its activity increases, deacetylation (by e.g. HDAC3) renders TBX5 to a more inactive state. **D.** LMP4 induced binding of TBX5 to actin-filaments, prohibits TBX5 from entry into the nucleus and thereby hinders its action. **E.** Degradation of TBX5 in the proteasome is initiated by FBXO25, which induces SCF-mediated ubiquitination. See the text (5.4) for references. Factors coloured in green are enhancing and factors in purple are inhibiting TBX5 expression/activity. Blue and yellow are structural elements.

5.5. TBX5 in the diseased heart

So far, most studies have focused on the role of TBX5 in the context of its developmental function or with respect to genetic alterations of TBX5. But there are a some indications, that TBX5 might have a relevance outside of this context.

5.5.1. Rodent models

In a rodent model of cardiac hypertrophy - induced by the chronic infusion of Angiotensin II, a peptide hormone inducing blood pressure increase and hypertrophy - TBX5 has been found to be downregulated [Baurand Anthony et al., 2007].

Similarly, in a rat heart-on-a-chip model, chronic AngII stimulation resulted in lower TBX5 levels and its target *Scn5a* [Horton et al., 2016].

5.5.2. Dysregulated Expression of TBX5 in human cardiomyopathies

Because TBX5 was dysregulated in a murine model of cardiac hypertrophy, the expression of TBX5 in human cardiac disease was quantified. Indeed, TBX5 expression was reduced in samples from patients receiving a heart transplantation because of dilated (DCM) or ischemic (ICM) cardiomyopathies (Figure 4) (own unpublished data). Interestingly, the medical history of all affected patients included arrhythmic events (Table 3).

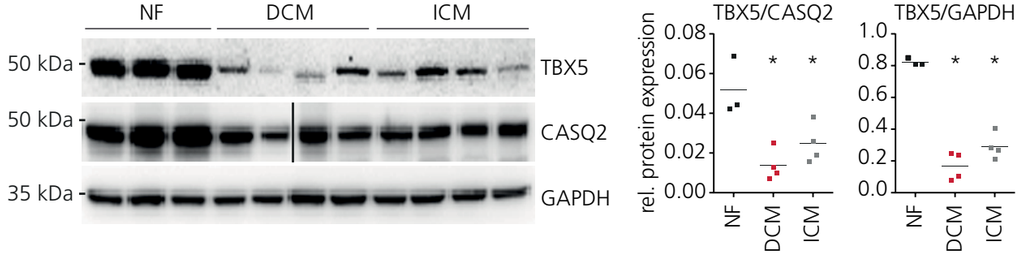

Figure 4. Reduced expression of TBX5 in human cardiomyopathy samples TBX5 protein is expressed at lower levels in left ventricular samples from patients with dilated (DCM) and ischemic (ICM) cardiomyopathy compared to non-faliling (NF) hearts. Analysis was done by immunoblot and quantified by densitometry. Calsequestrin 2 (CASQ2) and Glyceraldehyde 3-phosphate dehydrogenase (GAPDH) were used to normalize protein expression. **Statistics:** One-Way ANOVA, * $p<0.05$

Table 3. DCM and ICM Patient characteristics

	DCM	ICM	NF
n	4	4	3
Age, mean (SD)	54 (10)	52.5 (4)	data not available
Age, range	40-65	47-57	
EF, mean (SD)	22.3 % (10)	26.25 % (8)	
EF, range	15-40 %	20-40 %	
Male, percentage (n)	75% (3)	100% (4)	
Female, percentage (n)	25% (1)		
History of arrhythmia	100% (4)	100% (4)	

5.6. Adeno-associated virus as a re-expression strategy

Since TBX5 is expressed at a reduced level in the diseased heart, it might be a strategy in the treatment of heart failure to restore its expression. Therefore, introducing external DNA into organisms is of great interest, as a research tool as well as for clinical use. An important tool to deliver DNA to mammals in vivo is the use of adeno-associated virus (AAV). To reduce the risk of integration into the genome, wild-type AAVs have been modified by removing the *rep* gene and are termed recombinant AAV (rAAV) [Wang et al., 2019].

Tissue specificity of the AAV-transduction is greatly influenced by the serotype used for virus production. For cardiac gene transfer, the most widely used serotypes are AAV6 and AAV9 [Bass-Stringer et al., 2018]. The choice of the promoter driving the expression of the transgene affects the specificity, but also the expression levels, e.g. the CMV promoter can strongly drive expression, but cardiac specific promoters like Troponin T can lead to better specificity for the heart [Schwab et al., 2018][Mearini et al., 2014].

Already, two recombinant AAVs (rAAVs) have been approved in the European Union and the US for gene therapy in humans [Wang et al., 2019]. More than 160 trials using rAAVs are registered [clinicaltrials.gov].

5.7. Hypotheses and Aims

Based on the expression of TBX5 in the left ventricle (Figure 2) and its dysregulated expression in the diseased myocardium (5.5), we formed the following hypotheses:

- TBX5 is important for homoeostasis of the working myocardium.
- Reduction of TBX5 levels in the ventricles leads to a dysregulation of the transcriptional program and a deterioration of cardiac function and rhythmicity.
- Normalization of TBX5 in a loss-of-function model can rescue the transcriptional and phenotypical consequences.

To test these hypotheses we aimed to:

- Determine the phenotypical consequences of TBX5 loss in the adult heart using echo- and electrocardiographic measurements.
- Uncover the transcriptional consequences of TBX5 loss in the adult heart by integrative RNA- and ChIP-Seq analysis
- Evaluate if TBX5 re-expression in vivo can rescue the phenotype and restore TBX5 driven gene transcription

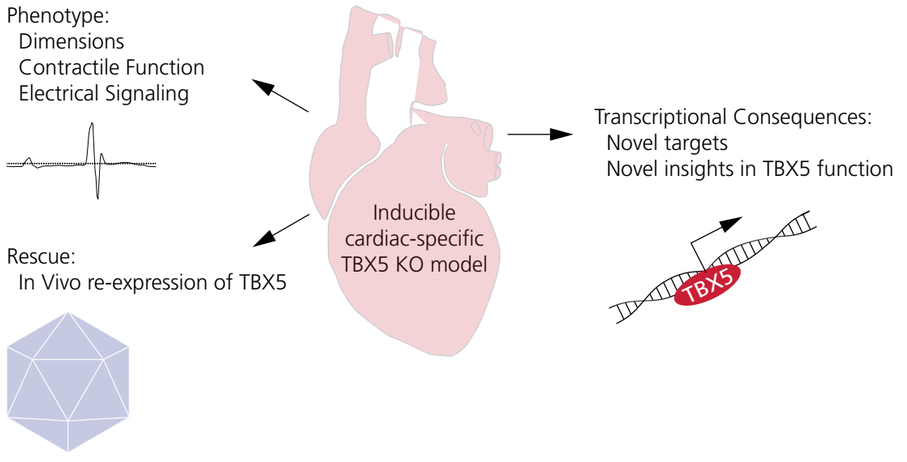

Figure 5. Scheme summarising the project Aims An inducible cardiac-specific TBX5 KO mouse model will be used to determine the phenotypical and molecular consequences of TBX5 loss in the adult working myocardium. A rescue experiment will be performed to reveal if TBX5 re-expression in vivo can reverse the molecular and functional consequences of TBX5 loss.

6. Materials

6.1. Devices

Table 4. Devices used

Device	Type	Manufacturer
Chemiluminescent Imager	ChemiDoc XRS	BioRad
CASY cell counter	Model TT	Roche Innovatis AG
Centrifuges	Biofuge Pico	Heraeus
	3K30	Sigma Laborzentrifugen
	5417R	Eppendorf
Laminar air flow bench	HERAGUARD	Thermoscientific
Incubator	Certomat HK	B. Braun Biotech
	Sanyo	Sanyo
Gel Imager	Gel Doc XR Imaging System	Biorad
SDS-PAGE Equipment	MiniProtean	Biorad
Microscopes	Axiovert 200	Carl Zeiss
	Leica M80	Leica
	LSM 710	Carl Zeiss
Multiplate Reader	FlexStation 3	Molecular Devices
PCR cycler	T Gradient	Biometra
	Veriti® 96-well Thermal Cycler	Applied Biosystems
qRT-PCR device	7900 HT Fast Real-Time PCR system	Applied Biosystems
Spectrophotometer	NanoDrop 1000	Peqlab
Sonicator	Bioruptor Plus	Diagenode
Thermomixer	Thermomixer Compact	Eppendorf
Tissue Lyser	Tissue Lyser II	Qiagen
UV Transilluminators	TI1	Biometra

6.2. Software

Table 5. Software used

Name	Manufacturer
Adobe Illustrator CS6	Adobe
Adobe InDesign CS6	Adobe
Adobe Photoshop CS6	Adobe
AxioVision	Carl Zeiss
Cytoscape	Cytoscape Consortium
Excel	Microsoft
Glowmax 1.9.2	Promega
GraphPad Prism 8	GraphPad Software
Image Lab	Biorad
ND-1000 V3.8.1	Nanodrop Technologies
Ponemah 6.33	DSI
Quantity One 4.6.7	Biorad
SDS 2.4	Applied Biosystems
Serial Cloner 2.6.1	Serial Basics
Soft Max Pro 5.4	Molecular Devices
ZEN 2011	Carl Zeiss
Zotero	Open Source

6.3. Consumables

Table 6. Consumables

Material	Type	Manufacturer
384-well plates (for qPCR)	MicroAmp Optical Reaction	Applied Biosystems
384-well adhesive film	MicroAmp Optical Adhesive Film	Applied Biosystems
96-well (for Bradford)	96-well flat bottom	Sarstedt
Cannula / Syringes		B.Braun
Cell culture plates	6-well, 12-well	Sarstedt
Cell scraper		Sarstedt
Chromatography Paper	3 mm	Whatman
Glass Cover slips	12 mm	Thermo Scientific
PVDF membrane	Roti-PVDF®, 0,45 µm	Roth
Object slides		Thermo Scientific
Osmotic minipumps	1002	Alzet
PVDF membrane	Roti-PVDF®, 0,45 µm	Roth
Telemetric ECG transmitters	ETA-F10	Data Science International
Tissue culture flask	75 cm²	Sarstedt
TPX tubes	1.5 ml Bioruptor® Plus TPX	diagenode

6.4. Chemicals

Table 7. Chemicals	
Acetic acid 100%	Merck
Acrylamid 30%	AppliChem
Agarose Ultra Pure™	AppliChem
Ammonium chloride	Carl Roth
Ammonium persulfate (APS)	Life Technologies
Ampicillin	AppliChem
5-bromo-2'-deoxyuridine (BrdU)	Sigma
Bromophenol blue	AppliChem
Bovine Serum Albumine (BSA)	Sigma
Chemoluminescence reagent (FemtoLucent)	G Biosciences
Chemoluminescence reagent (LumiGlo)	Cell Signaling
Collagen	internal production
β-Mercaptoethanol	AppliChem
Bradford-Reagent (Roti-Quant)	Carl Roth
dNTP PCR Nucleotide Mix (10 mmol/l)	Promega
EDTA	AppliChem
EGTA	AppliChem
embedding solution (Mowiol)	Sigma
Ethanol (99,5%)	Carl Roth
Ethidium bromide	Sigma
Formaldehyde (for ChIP) - 16%, Methanol-free	Polysciences
Paraformaldehyde (Roti-Histofix, for stainings)	Carl Roth
Glycerol	Gerbu
Glycine	AppliChem
Hoechst	Life Technologies
LB Agar	AppliChem
LB Medium	AppliChem
Methanol	Carl Roth
Miglyol (medium-chain triglycerides)	Caelo
Milk, non-fatty dried	Carl Roth
NP-40	Sigma
Phosphatase Inhibitor (PhosSTOP)	Roche
Ponceau S	AppliChem
Potassium bicarbonate	Carl Roth
Potassium chloride	Carl Roth
2-Propanol	AppliChem
Protease Inhibitor Cocktail (cOmplete Mini, EDTA-free)	Roche
Sodiumdodecylsulfate (SDS)	AppliChem
Sodium citrate	Sigma
Sodium chloride	Carl Roth
Tamoxifen	Sigma Aldrich
N,N,N',N'-Tetramethylethylendiamin (TEMED)	AppliChem
Turbofect Transfection Reagent	ThermoScientific
Tris Base, ultrapure	Carl Roth
Tris-hydrochlorid	Carl Roth
Triton X-100	AppliChem
Tween-20	Sigma
SOC-Medium	NEB

6.5. Enzymatic reactions

Table 8. Enzymatic reactions		
Method	**Reagents/Enzymes**	**Manufacturer**
Dephosphorylation	Fast AP Thermosensitive Alkaline Phosphatase 1 U/µl	Thermoscientific
	10x reaction buffer for AP	Thermoscientific
Ligation	T4 DNA Ligase 5 U/µl	Thermoscientific
	10 x T4 Ligase buffer	Thermoscientific
	T4 DNA Ligase 5 U/µl	NEB
	2x Rapid Ligation buffer	NEB
PCR	Phusion DNA Polymerase 2 U/µl	Thermoscientific
	5x Phusion HF Buffer	Thermoscientific
	Dream Taq	Thermoscientific
	10x Dream Taq buffer with MgCl2	Thermoscientific
qPCR	GoTaq® qPCR MasterMix 2x	Promega
	CXR Reference dye	Promega
Restriction	Fast Digest Enzymes	Thermoscientific
	10x Fast Digest Green buffer	Thermoscientific
Reverse Transcription	M-MLV Reverse Transcriptase 200 U/µl	Promega
	M-MLV RT 5x buffer	Promega
ChIP	Proteinase K (20mg/ml)	Pierce

6.6. Antibodies

Table 9. Antibodies used

	Antigen	Species	Manufacturer	Catalog-No.	Dilution WB	Dilution IF
primary	anti-TBX5	rabbit	Sigma	HPA008786	1:1000	
	anti-flag, monoclonal	rabbit	Sigma	F7425		1:100
	anti-flag M2, monoclonal	mouse	Sigma	F1804	1:1000	
	anti-GAPDH	mouse	Millipore	MAB374	1:50000	
	anti-Cx43	rabbit	Millipore	3512	1:1000	1:100
	anti-FHL2	rabbit	abcam	ab 12327	1:1000	
	anti-KCNJ5	rabbit	Sigma	HPA017353	1:250	1:50
	anti-α-actinin (sarcomeric)	mouse	Sigma	A7811		1:200
	normal rabbit IgG	rabbit	SantaCruz	sc-2027		1:100
	IgG (ChIP grade)	rabbit	Millipore	12-370		
secondary	anti-rabbit Alexa Fluor 594	goat	Invitrogen	A11012		1:200
	anti-mouse Alexa Fluor 594	goat	Invitrogen	A11005		1:200
	anti-rabbit Alexa Fluor 488	goat	Invitrogen	A11008		1:200
	anti-mouse Alexa Fluor 488	goat	Invitrogen	A11001		1:200
	HRP-conjugated anti-mouse	rabbit	Dako	P0260	1:10000	
	HRP-conjugated anti-rabbit	goat	Dako	P0448	1:5000	

6.7. Commercial plasmids

Table 10. Commercial plasmids

Name	Manufacturer
pGL4.25	Promega
pGEM-T Easy	Promega
pCMV2C-flag	Sigma

6.8. Primer

Table 11. Primers used for qRT-PCR, annealing temperature 60°C for all listed primer pairs

Primer name	Primer sequence
Tbx5 rec fwd	AGGCAGGGAGGAGAATGTTT
Tbx5 rec rev	GGCTCTGCTTTGCCAGTTAC
Gapdh fwd	ATGTTCCAGTATGACTCCACTCACG
Gapdh rev	GAAGACACCAGTAGACTCCACGACA
Kcnj5 fwd	AGAAGTTAGCCCCAAGGGTTC
Kcnj5 rev	ATGCTCCCAAGTACACCCTG
Gja1 fwd	CACCACTTTGGCGTGCCGGCTT
Gja1 rev	TCAACCGCTGTCCCCAGGAGCC
Kcng2 fwd	AATTCAGGAAAGTGAAAAGTCTTGG
Kcng2 rev	TTGGTCCTCCGTTGAGCTTG
Cacna1g fwd	AGGAGAAGCAGATGGCCGA
Cacna1g rev	GTACACAGGTGGTGGACGAG
Chrm2 fwd	CAGACTCCACCAGATCGCAG
Chrm2 rev	GGATCCAGCCACAAGGACAA
Fhl2 fwd	AAGGAGGAGAACCCACACTG
Fhl2 rev	GTGCCGATCCTTGTAGGACA
Gpr22 fwd	GTGAGCCCAAAGGCCCATAA
Gpr22 rev	CGCACCGTGACGTTTGATTC
Fgf16 fwd	TGATCAGCATCAGGGGAGTG
Fgf16 rev	CAAGGTGGAGGCATAGGTGT
Fstl4 fwd	CCACGTCCTGCAGGTGAAT
Fstl4 rev	GCCAAGAGGGAGAGCTGTTT
Cmya5 fwd	CTGCCGCGTTCTCACTTTTC
Cmya5 rev	TGGGGTTCTAGTCTGGGAGG
Emilin2 fwd	GCAGCTTGTGGAACTGCATC
Emilin2 rev	TCGGTTGCTTCTGAGGGTTC
Pdlim4 fwd	CGGGATCGTGGGAACCATTG
Pdlim4 rev	CCACATCATATCCCTCCGGC

Table 12. Primers used for cloning	
Primer name	**Primer sequence**
Gja1-enh	TATCTCGAGGTTGTAACATCAACTTTATAATGAAATATC
	TATAAGCTTACCACTTGTGCCTGCTG
Kcnj5-enh	CTCGAGGAGGCAGGGCTAGAGAAGA
	GAAGCTTGGTGGGTGAGTTTTGAGCAG
Tbx5-CDS	GCTATAGAATTCTGGCCGATACAGATGAGGG
	TATAGTCGACGCTATTCTCACTCCACTCTG

Table 13. Primers used for ChIP-qPCRs		
Primer	**peak location (mm9)**	**sequences**
Scn5a fwd	chr9: 119,378,722 - 119,379,682	GGTGTGAATGAGGGAGGCAG
Scn5a rev		GGGTGTCTGGGACAGGAGAT
Gja1 fwd	chr10: 56,700,503 - 56,701,066	GGTCACATGGTTGCTCGGTA
Gja1 rev		CAGCTCGCCTAGTCCACTTC
Fhl2 fwd	chr1: 43,304,427 - 43,304,911	CAGTAGCTGTCTGCTGGGAG
Fhl2 rev		CATGTGCACACCTCCCTCTT
Fgf16 fwd	chrX: 102,968,546 - 102,969,107	GCCAGCTTGAAGTAGCCAGA
Fgf16 rev		CTCTCCTAATGAGCGGCCTG
Kcnj5 fwd	chr9: 32,121,467 - 32,122,084	TCCTGGCTCCAAAGGATTCAC
Kcnj5 rev		ATGGAGAAGAGCCCCTGTCT
Cacna1g fwd	chr11: 94,312,360 - 94,313,144	TCCTTGTTCAGACGGTCAGC
Cacna1g rev		GCAAGCATGCCTCCCAGATA
Chrm2 fwd	chr6: 36,457,945 - 36,458,346	GTGTCAGTTAATTGCAGCGG
Chrm2 rev		TATATTTGAGAAGGAAGGCAGTTTG
Gpr22 fwd	chr12: 32,388,826 - 32,389,259	TGGGGTGAGGAAACGACCTT
Gpr22 rev		CACTATCAAGCCCTGGAGCAT

6.9. Western Blot

Table 14. Buffers for SDS-PAGE and Western Blotting		
Bäuerle Buffer	HEPES	4.77 g/l
	NaCl	20.45 g/l
	Glycerol	200 g/l
	$MgCl_2$	0.20 g/l
	EDTA	0.186 g/l
	EGTA	0.038 g/l
	NP-40	10 g/l
	pH adjusted to 7.9; before use Phosphatase and Proteinase Inhibitors were added according to manufacturers instructions	
Lämmli Buffer 4x	Tris-HCl 0,5 mol/l, pH 6,8	2.4 ml
	0,5% Bromphenolblau (in Tris-HCl)	0.5 ml
	SDS	0.8 g
	100% Glycerin	3.0 ml
	water	ad 9ml
	Mercaptoethanol (added to aliquots before use)	1ml
Running buffer (10x)	Tris Base	30.3 g/l
	Glycin	144 g/l
	SDS	10 g/l
	dilute to 1x before use	
Stacking gel (6 %)	Aqua bidest.	
	Acrylamide 30%	
	Tris/HCl 0.5 mol/l, pH 6.8	
	SDS 10%	
	APS 10%	
	TEMED	
Seperating gel (10%)	Aqua bidest.	
	Acrylamide 30%	
	Tris/HCl 1.5 mol/l, pH 8.8	
	SDS 10%	
	APS 10%	
	TEMED	

Transfer buffer (10x)	Tris Base	75.6 g/l
	Glycine	74.4 g/l
	SDS	15 g/l
Transfer buffer (1x)	Transfer buffer (10x)	10 ml
	Methanol	20 ml
	Aqua bidest.	70 ml
TBST	Tris/HCl 1 mol/l, pH 7.6	20 ml
	NaCl 5 mol/l	33 ml
	Tween 20	1 ml
	Aqua bidest.	ad 1 l
Blocking solution (milk)	Non-fat dried milk	50 g/l
	TBST	ad 1 l
Blocking solution (BSA)	BSA	50 g/l
	TBST	ad 1 l

6.10. Immunostainings

Table 15. Buffers for Immunostaining

Permeabilisation buffer	Triton-X-100	3 g/l
	BSA	2 g/l
	dilute in PBS	
Blocking buffer	Triton-X-100	1 g/l
	BSA	50 g/l
	dilute in PBS	
Blocking buffer	Triton-X-100	1 g/l
	BSA	1 g/l
	dilute in PBS	
Nuclear staining buffer	Hoechst	1 µg/ml
	dilute in PBS	

6.11. Agarose Gelelectrophoresis

Table 16. Buffer for Agarose Gelelectrophoresis

TAE buffer (50x)	Tris Base	242.2 g/l
	EDTA	18.6 g/l
	Glacial Acetic Acid	57.1 ml/l
	dilute to 1x before use	

6.12. Kits

Table 17. Kits

Method	Kit	Manufacturer
Plasmid isolation (Mini)	NucleoSpin® Plasmid	Macherey Nagel
Plasmid isolation (Maxi)	NucleoBond® Xtra Midi	Macherey Nagel
RNA isolation	NucleoSpin® RNA	Macherey Nagel
Gel Extraction and PCR Clean up	NucleoSpin® Gel and PCR Clean-Up	Macherey Nagel
DNA Clean up after ChIP	Buffer NTB for NucleoSpin® Gel and PCR Clean-Up	Macherey Nagel
Luciferase assays	Dual-Luciferase Reporter Assay	Promega
NRCM isolation	Neonatal Heart Dissociation Kit	Miltenyi Biotec

6.13. Bacterial Cultivation

Table 18. Bacteria

Species	Type	Manufacturer
E. coli	NEB 10-β competent *E. coli*	NEB
E. coli	*dam*$^-$/*dcm*$^-$ competent *E. coli*	NEB

6.14. Cell culture

Table 19. Cell lines

Cell line	Source
HEK293A	ATCC, CRL-1573

Table 20. Cell culture reagents

Medium	Specification	Manufacturer
DMEM	+ Glucose, - Pyruvate	Gibco
MEM	2.2 g/l $NaHCO_3$, - Glutamine	Gibco
FBS		Gibco
Penicillin/Streptomycin	100x	Gibco
Transfection reagent	Turbofect	Thermoscientific
HEK Medium	10% FBS, 1% Penicillin/Streptomycin in DMEM	
NRCM medium	10% FBS, 1% L-Glutamine, 1% Penicillin/ Streptomycin, 0.1 mmol/l BrdU in MEM	

6.15. Cell isolation

Table 21. Buffers for neonatal rat cardiomyocyte isolation

Calcium- and bicarbonate-free Hanks with HEPES (CBFHH)	NaCl	137 mmol/l
	KCl	5.4 mmol/l
	KH_2PO_4	0.44 mmol/l
	Na_2HPO_4	0.34 mmol/l
	$MgSO_4$	0.81 mmol/l
	HEPES	20 mmol/l
	Glucose	5.6 mmol/l
	pH adjusted to 7.4, sterile filtered	

Table 22. Buffers for murine adult cardiomyocyte isolation

Perfusion buffer	NaCl	120.4 mmol/l
	KCl	14.7 mmol/l
	KH_2PO_4	0.6 mmol/l
	Na_2HPO_4	0.6 mmol/l
	$MgSO_4$	1.2 mmol/l
	HEPES	10 mmol/l
	$NaHCO_3$	4.6 mmol/l
	Taurin	30 mmol/l
	BDM	10 mmol/l
	Glucose	5.5 mmol/l
	adjust pH to 7.4	
Digestion buffer	Collagenase B	2 mg / ml
	$CaCl_2$	40 µmol/l
	diluted in Perfusion buffer	
Stop buffer	FCS	10%
	$CaCl_2$	12.5 µmol/l
	diluted in Perfusion buffer	
Calcium increasing all in Stop buffer	Step 2	100 µmol/l $CaCl_2$
	Step 3	400 µmol/l $CaCl_2$
	Step 4	900 µmol/l $CaCl_2$

6.16. Chromatin Immunoprecipitation

Table 23. Buffers for Chromatin Immunoprecipitation

FA in PBS	Formaldehyde 16%	for 2% 1,25 ml
	PBS	ad 10 ml
	directly before use add 1 tablet of Proteinase Inhibitors / 10 ml	
Glycin (10x)	Glycin	208,95 g/l
Hypotonic buffer	HEPES	2,38 g/l
	KCl	0,75 g/l
	$MgCl_2$ (Hexahydrat)	0,41 g/l
	EDTA	0,037 g/l
	DTT	0,154 g/l
	directly before use add 1 tablet of Proteinase Inhibitors / 10 ml	
Sonication Buffer I	Tris-HCl	7,88 g/l
	EDTA	2,92 g/l
	SDS	10,00 g/l
	adjust pH to 8, directly before use add 1 tablet of Proteinase Inhibitors / 10 ml	
Sonication Buffer II	Tris-HCl	7,88 g/l
	EDTA	5,84 g/l
	NP-40	10,00 g/l
	NaCl	8,77 g/l
	NaF	0,84 g/l
	adjust pH to 8, directly before use add 1 tablet of Proteinase Inhibitors / 10 ml	

ChIP incubation buffer	NaCl	2,92 g/l
	Tris-Cl	7,88 g/l
	EDTA	1,46 g/l
	adjust pH to 7.5, directly before use add 1 tablet of Proteinase Inhibitors / 10 ml	
Wash buffer 1	NaCl	4,38 g/l
	Tris-Cl	7,88 g/l
	EDTA	2,92 g/l
	adjust pH to 7.5	
Wash buffer 2	NaCl	7,31 g/l
	Tris-Cl	7,88 g/l
	EDTA	2,92 g/l
	adjust pH to 7.5	
Wash buffer 3	NaCl	10,23 g/l
	Tris-Cl	7,88 g/l
	EDTA	2,92 g/l
	adjust pH to 7.5	
ChIP Elution Buffer	NaCl	2,92 g/l
	Tris-Cl	7,88 g/l
	EDTA	1,46 g/l
	SDS	10,00 g/l
	adjust pH to 7.5	

7. Methods

7.1. TBX5 mice

All animal experiments were approved by the local competent authority (Lower Saxony State Office for Consumer Protection and Food Safety - LAVES; AZG15/2029).

7.1.1. Characterization of the TBX5 KO mouse model

To obtain a cardiomyocyte specific TBX5 KO mouse model, two previously published mouse strains were crossed (Figure 6A) as described by [Renger, 2012]. The *Myh6*-MerCreMer mouse encodes Cre-recombinase fused to a modified estrogen-receptor under control of the Myosin heavy chain, alpha isoform (*Myh6*) promoter. Thus the MerCreMer is expressed exclusively in cardiomyocytes and only activated once the selective estrogen receptor modulator (SERM) Tamoxifen is administered [Sohal Dawinder S. et al., 2001]. These mice were crossed with the TBX5$^{LDN/LDN}$ mouse model, harbouring loxP sites flanking Exon3 of the *Tbx5* gene. The resulting mouse model thereby allows removal of the DNA-binding domain of the TBX5 transcription factor [Mori et al., 2006] upon Tamoxifen exposure. We detected MerCreMer expression specifically in the nuclei of cardiomyocytes from atrial and ventricular tissue (Figure 6B). All crossings were done on a C57BL/6N background.

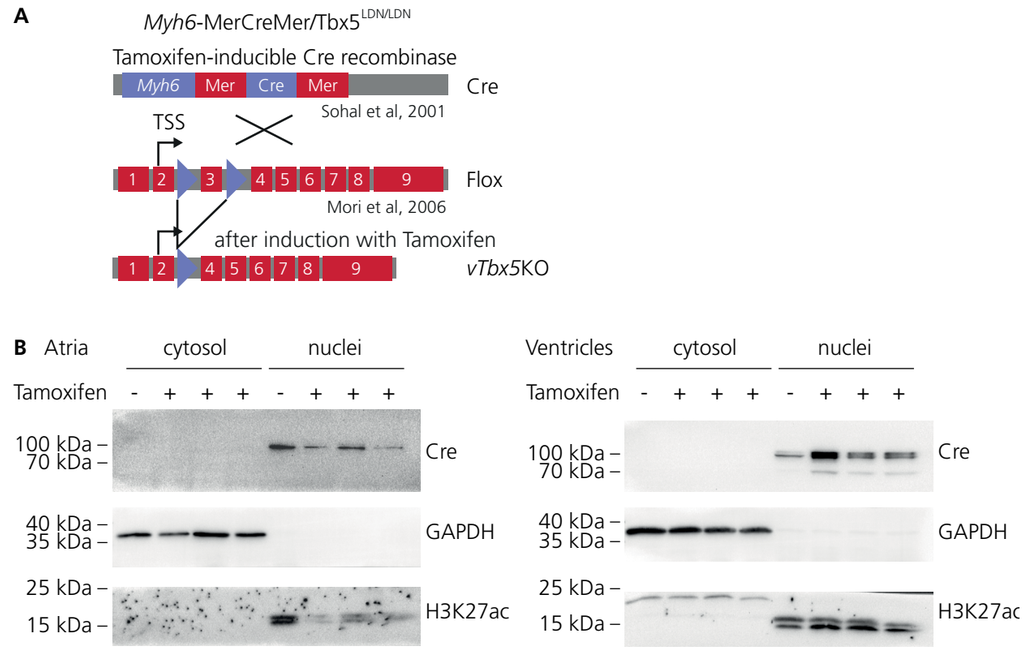

Figure 6. Generation of a cardiac specific TBX5 KO mouse model. A. A transgenic mouse strain with Tamoxifen-inducible Cre recombinase under the control of the Myosin heavy chain, alpha isoform (*Myh6*) was crossed with a mouse model containing loxP sites flanking Exon 3 of the *Tbx5* gene to obtain a cardiomyocyte specific inducible KO model. **B.** The MerCreMer fusion protein is exclusively expressed in the nuclei of cardiomyocytes.

7.1.2. Tamoxifen induction

For the activation of Cre recombinase by Tamoxifen, mice were injected with 30 mg Tamoxifen per kg body weight at the age of 8-12 weeks for consecutive 3 days in a row. Tamoxifen was dissolved in Ethanol at 75 mg/ml while warming at ~35°C for ~10 minutes. This solution was further diluted in Miglyol to a final concentration of 7.5 mg/ml and subsequently used for intraperitoneal (i.p.) injections.

7.1.3. Telemetry implantation and recordings

Telemetry devices were implanted before injection of Tamoxifen according to [Vettel Christiane et al., 2017]. Briefly described, electrocardiograms (ECG) were recorded for 24 hours each. They were evaluated with Ponemah P3, Version 6.33 using template based analysis for PR-, QRS- and QT-determination. For heart rate variability analysis RR-intervals were exported from Ponemah for intervals of 5 mins, which were manually checked and adjusted for correct R-placements. These data were imported and evaluated to HRVAS as ibi-files, which allowed calculation of standard-deviations [Ramshur, 2010].

7.1.4. Echocardiography

Mouse heart dimension and function was assessed by echocardiography in unconscious mice (2% isofluran inhalation) using the Visual Sonics Vevo 2100 Imaging System equipped with a 45 MHz MS-550D MicroScan transducer. Measurements and evaluation was performed by the SFB 1002 service unit S01 according to standard operating procedures in a blinded fashion as described previously [Zafiriou et al., 2014].

The evaluated parameters and their relationships with each other are listed in (Table 24).

Table 24. Echocardiographic parameters

Parameter	short	unit	calculation
Length systole	L_s	mm	measured directly
Length diastole	L_d	mm	measured directly
Area systole	Area s	mm²	measured directly
Area diastole	Area d	mm²	measured directly
Anterior wall thickness systole	AWThs	mm	measured directly
Anterior wall thickness diastole	AWThd	mm	measured directly
Posterior wall thickness systole	PWThs	mm	measured directly
Posterior wall thickness diastole	PWThd	mm	measured directly
Epicardial area systole	Epi s	mm²	measured directly
heart rate	HR	bpm	measured directly
body weight	BW	g	measured directly
fractional area shortening	FAS	%	(Area d / Area s) / Area d x 100
Volume in systole	Vol s	µl	(5/6) x (Area s x Ls)
Volume in diastole	Vol d	µl	(5/6) x (Area d x Ld)
Ejection fraction	EF	%	SV / Vol d x 100
Stroke volume	SV	µl	Vol d - Vol s
Cardiac output	CO	ml/min	SV / 1000 x HR
Cardiac index	CI	l / (min*g)	CO / BW x 1000
heart weight	HW	mg	1,05 x (5/6) x ((Epi s x (Ls + (AWThs+PWThs)/2))) - (Area s x Ls))
heart weight to body weight	HW/BW	mg/g	HW / BW

7.1.5. Organ Harvest

To harvest organs, mice were either anaesthetized with Isofluran and subsequently killed by cervical dislocation or received terminal anaesthesia by injection of Ketamin (ca. 160 mg/kg) and Xylazin (ca. 16 mg/kg) until loss of reflexes. The mice were opened at the chest and the heart was removed and rinsed in PBS to remove blood. Atria were kept separately in liquid nitrogen, the central part of the ventricles (cross-section) was fixed for histology in 4 % PFA at 4°C over night. Upper and apical parts of the ventricles were meshed and snap-frozen in liquid nitrogen before storing them at -80°C for later isolation of RNA or protein.

7.1.6. Ex vivo electrophysiological recordings

The method of ex vivo recordings of arrhythmia induction and measurement of activation times has been described previously [Wittköpper et al., 2010]. All experiments have been done at the University of Birmingham by Fahima Syeda, Nashita Kabir and Larissa Fabritz.

In brief, hearts were excised under deep terminal anaesthesia. The aorta was cannulated for retrograde perfusion with Krebs-Henseleit buffer on a Langendorff apparatus.

After inserting an octapolar mouse electrophysiologic catheter in the right atrium and ventricle, monophasic action potentials were recorded continuously and simultaneously on the right ventricular free wall, septum and on the left ventricular free wall epicardium. To measure activation times from right atrium to right ventricle, atrial S1 pacing was used. To determine ventricular activation times, the right ventricular endocardium was paced.

Ventricular arrhythmia inducibility was determined by programmed ventricular stimulation with a single encroaching premature stimulus (S2). Experiments were performed and analysed when the observer was unaware of the mouse genotype.

7.1.7. AAV-injections

Adeno-associated viral particles were produced and purified by the research group of Prof. Dr. Oliver Müller according to [Jungmann et al., 2017]. Briefly, the helper plasmid pDP9rs (a derivate of pDP2rs) was co-transfected with the respective AAV vector genome plasmid (either pdsTnT-rluc or pds-TnT-mTBX5) in 293T cells. The obtained vectors AAV9-luc or AAV9-TBX5 were subsequently purified by lodixanol step gradient centrifugation. To achieve re-expression of TBX5 in the *vTbx5*KO hearts, the mice received an intravenous injection of 2 x 10^{12} viral particles similar to [Schwab et al., 2018]. The mice were subjected to short general anaesthesia with 1-2% isofluran inhalation. Then they received the injection of the viral particles in the tail vein with a 30-gauge cannula.

7.2. RNA analysis

7.2.1. RNA isolation

Total RNA was isolated using the RNA Isolation Kit according to manufacturers instructions. Concentrations were determined spectrophotometrically.

7.2.2. cDNA synthesis

To transcribe mRNA into copy DNA (cDNA) for quantification by quantitative PCR or amplification by regular PCR, the following protocol was used according to manufacturers instructions:

Table 25. Reagents used for reverse transcription

Reagent	Amount
OligodT (20x T) 500 ng/µl	1 µl
dNTPs (10mM)	1 µl
RNA	500 ng
Water	ad 15.5 µl
Incubation at 65°C for 5 minutes	
M-MLV RT 5x	4 µl
M-MLV RT (200u/µl)	0.5 µl
Reverse transcription for 50 min at 42°C	
Enzyme inactivation by incubation for 15 min at 70°C	

7.2.3. Quantitative PCR

Quantitative PCR with the SYBR Green dye was used for quantification of the expression of mRNA transcripts or ChIP samples according to manufacturers instructions. Master mixes with primers specific for the target sequence were prepared:

Table 26. Reagents used for qPCR (per well)

Reagent	Amount
Sybr Green 2x Master mix	5 µl
CXR reference dye	0.1 µl
Primer fwd	to 0.3 µmol/l
Primer rev	to 0.3 µmol/l
Sample	1 µl cDNA (1:10) or ChIP sample
Water	ad 10 µl

9 µl of each master mix were pipetted on a 384-well plate. Subsequently 1 µl of 1:10 diluted cDNA or Standard curve (10^3 to 10^8 copies per µl) or ChIP sample was added per well.

Table 27. Program used for qPCR

Step	Temperature	Time
Initial denaturation	95°C	10 min
Denaturation	95°C	15 sec
Annealing + extension	60°C	1 min
Final extension	95°C	15 sec
Cycles	40	
+ Dissociation stage	60°C - 95°C	

Evaluation was done by quantification against the individual standard curve.

7.3. Protein analysis

7.3.1. Protein isolation from cells / tissue

Protein isolation and immunoblots were done according to established protocols described e.g. in [Noack et al., 2019]. According to these protocols, protein was isolated from cells or tissue for determination of protein expression levels by immunoblot:

7.3.1.1. Isolation from cells

Medium was removed from the cell culture dish and the cells were washed with PBS. On ice, Bäuerle buffer (~100 µl per 1 million of cells) including inhibitors was added to the dish, then cells were scraped of and the buffer with cells was gently mixed at 4°C for 20 mins. Cells were disrupted by passing them 10 times through a 20 Gauge cannula.

7.3.1.2. Isolation from mouse tissue

Bäuerle buffer (~500 µl for a third of a heart) with inhibitors was added to the frozen tissue. The tissue was disrupted into a homogeneous suspension using the tissue lyser. The homogeneous suspension was transferred to a fresh tube to remove the metal bead of the tissue lyser.

7.3.1.3. Clearing and Protein quantitation

Lysates were centrifuged for 20 mins at maximum speed (>10 000 x g). The supernatant was used for protein quantification and subsequent immunoblotting. To determine protein concentration, a 96-well Bradford assay against a standard curve of BSA with protein amounts ranging from 1 to 16 µg per well was performed.

7.3.2. Western Blot

Immunoblot analysis was performed to determine and quantify protein expression levels in protein lysates (7.3.1 describes preparation). Polyacrylamide gels for the SDS-PAGE were prepared depending on the expected protein size (8-12% Acrylamide). Protein samples (50 µg for tissue lysates, 20-30 µg for cell lysates) were mixed with water and 4x Lämmli buffer and heated to 95°C for 5 min. After cooling, samples were loaded on the gel and electrophoresis was started.

Gels were blotted on methanol-activated PVDF membranes by semi-dry transfer. To confirm blotting and protein loading, Ponceau staining was performed. Membranes were blocked with 5% milk powder dissolved in TBS-T and primary antibody incubation was carried out at 4°C over night under constant rotation. Membranes were washed three times with TBS-T and incubated with the corresponding secondary antibody coupled to horseradish peroxidase for 1 hour shaking at room temperature. Subsequently membranes were washed three times with TBS-T and imaged in the Chemiluminescent imager after adding FemtoLucent.

If required, protein expression was quantified by densitometric analysis using the ImageLab software. Protein expression was normalized to GAPDH expression as a housekeeping protein as described previously [Zafiriou et al., 2014][Iyer et al., 2018].

7.3.3. Preparation of cells for immunostaining

Cells were washed 3 times for 2 minutes with PBS, then fixed by incubating with Roti-Histofix (4% PFA) for 15 minutes and washed 3 times for 5 minutes with PBS. Then they were incubated in Permeabilisation Buffer for 10 minutes at room temperature according to established procedures described e.g. by [Zafiriou et al., 2014].

7.3.4. Preparation of tissue sections for immunostaining

Tissues were dehydrated for paraffin embedding with a series of solutions (Table 28) according to established procedures described e.g. by [Zafiriou et al., 2014].

Table 28. Paraffin embedding

Solution	Incubation time
Roti-Histofix	24 hours, 4°C, rotating
Ethanol 70%	until further processing, at least 72 h, 4°C
Ethanol 80%	30 min
Ethanol 90%	30 min
Ethanol 99%	30 min
Ethanol / Roti-Histol (1:1)	30 min
Roti-Histol	1 hour
Roti-Histol / Paraffin (heated)	1 hour
Paraffin (heated)	over night, 60°C

After dehydration, sections were placed in molten paraffin (~60°C) and left to solidify at 4°C over night. Thin (~5 µm) sections were cut with a microtome and placed on glass slides, which were store at 4°C until deparaffinisation. Deparaffinisation was carried out by a series of incubation steps in solutions to gradually rehydrate the sections (Table 29).

Table 29. Deparaffinisation

Solution	Incubation time
Roti Histol	10 min (twice)
Ethanol 100%	10 min (twice)
Ethanol 96%	5 min (twice)
Ethanol 80%	5 min
Ethanol 70%	5 min
Water	5 min
PBS	5 min
10 mM Sodium citrate (pre-heated)	15 min in microwave at 180 W Cooling for 20 min at room temperature
PBS	5 min (twice)

The rehydrated sections were used for immunostaining.

7.3.5. Immunostaining

Coverslips or slides were incubated with Blocking Buffer for one hour. Afterwards, the coverslips were incubated with primary antibodies over night at 4°C. After washing 3 times with PBS for 10 minutes, the incubation with the secondary antibody (diluted 1:200, room temperature, 1 hour) followed. Next, the samples were washed three times with PBS for 10 minutes, then stained with Nuclear Staining buffer for 5-10 minutes and washed 3 times for 5 minutes with PBS and rinsed with water. Then the coverslips or slides were put on glass slides with Mowiol. Visualization was done with confocal microscope.

7.4. Cloning

To validate putative enhancers found in the ChIP-Seq analysis, luciferase assays were performed. The pGL4.25 vector was chosen, as it encodes a luc2CP reporter gene under the control of a minimal promoter. When an enhancer sequence is inserted upstream of the minimal promoter its activation by a transcription factor can increase luciferase expression, measurable in a multiwell-plate assay. To clone the enhancer fragments, murine genomic DNA was amplified with specific primers containing restriction sites for the multiple cloning site (MCS) of the pGL4.25 vector. The PCR product was A-tailed and ligated into the pGEM-T Easy subcloning vector according to manufacturers instructions, from which it could be restricted and ligated in the final pGL4.25 plasmid (Figure 7).

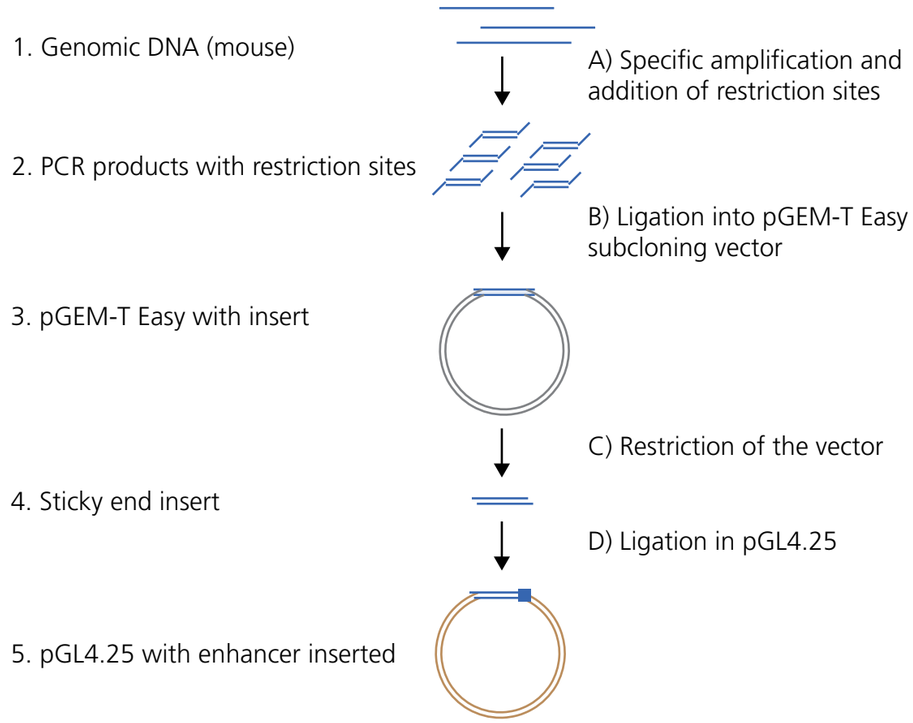

Figure 7. Cloning of putative enhancers The enhancer sequence was amplified and restrictions sites were added by PCR. The resulting product was sub-cloned into the pGEM-T Easy vector. After restriction from this vector, the resulting fragment was ligated into the final pGL4.25 plasmid.

Tbx5, *Gja1* and *Kcnj5* plasmids for transfections and AAV-production were prepared in a similar manner, which has been previously described [Rathjens, 2015]. For transfections the pCMV2c-flag backbone was used, for AAV-production the pds-hTnnT-vector (provided by Oliver Müller, Heidelberg/Kiel) was used.

7.4.1. PCR

For Cloning, Phusion polymerase was used according to manufacturers instructions.

Table 30. Reagents used for Phusion PCR

Reagent	amount
HF buffer (5x)	4.0 µl
10 mM dNTPs	0.4 µl
primer fwd (10 µM)	1.0 µl
primer rev (10µM)	1.0 µl
template (ca. 200 ng/tube)	x µl
water	ad 20µl
Phusion	0.2 µl

Table 31. Program for Phusion PCR

Step	Temperature	Time
Initial denaturation	98°C	5 min
denaturation	98°C	30 sec
annealing	primer specific	30 sec
extension	72°C	3 min
final extension	72°C	8 min
cycles	35	

7.4.2. A-Tailing

The Phusion polymerase generates blunt end PCR products, but for subcloning in pGEM-T Easy a PCR product with A-overhangs is required. Therefore, fragments were A-tailed using DreamTaq Polymerase according to manufacturers instructions.

Table 32. Reagents used for A-Tailing

reagent	amount
Phusion PCR product (directly)	ad 10 µl
Dream Taq buffer	1.00 µl
dATPs	1.00 µl
DreamTaq	0.20 µl

The solution was incubated at 70°C for 30 minutes, the products were cleaned using agarose gel electrophoresis followed by Gel extraction with a Kit according to manufacturers instructions.

7.4.3. Ligation

Table 33. Reagents used for Ligation	
reagent	**amount**
insert (purified PCR product or restricted fragment)	insert to vector ratio 3:1 to 9:1
vector	100 ng
10 x T4 Ligase buffer	2.00 µl
T4 Ligase	1.00 µl
water	ad 20 µl

Ligations in pGEM-T Easy were incubated over night at 4°C, other ligations were incubated at 16°C over night or at room temperature for 1-2 hours.

7.4.4. Transformation

The NEB 10-beta competent *Escherichia coli* strain was used for transformations, unless subsequent restrictions were predicted to be methylation sensitive, which made the use of *dam*$^-$/*dcm*$^-$ competent *E. coli* necessary.

To transform bacteria with a ligation product, 5 µl of the ligation preparation (about 25 to 50 ng of vector) were used. For a transformation with a validated plasmid, 1-2 µg of plasmid were used. The plasmids were gently mixed with 50 µl of the bacterial suspension and incubated on ice for 30 mins. Afterwards a 45 sec heat-shock at 42°C was performed followed by incubation on ice for 2 mins. 450 µl of SOC medium were added and the bacterial suspension was incubated for 1 h shaking at 37°C. This suspension was transferred to an agar plate containing the appropriate antibiotic for antibiotic selection and left to grow over night at 37°C.

7.4.5. Plasmid preparations

Small preparations (5 ml cultures) of plasmids were isolated using the plasmid purification kit mini; larger scale preparations (ca. 250 ml cultures) were purified with the Midi plasmid purification Kit according to manufacturers instruction.

7.4.6. Restriction

Restriction was done using FastDigest restriction enzymes according to manufacturers instructions. For restrictions intended for ligations, alkaline phosphatase was added to the restriction incubation of the plasmid. Fragments were analysed by gel electrophoresis, with size comparisons against the GeneRuler 1 kb DNA Ladder.

7.5. Cell culture methods

7.5.1. Transfection

HEK 293 cells were cultured in DMEM with 10% FCS and 1% Pen/Strep and passaged using 0.05% Trypsin once or twice a week depending on confluency levels. Cells were plated on 6-well-plates or 12-well-plates with coverslips coated with collagen on day 1. 24 hours later the DNA-Turbofect mixtures were prepared by mixing the plasmid, Turbofect™ and DMEM without FCS and Pen/Strep and incubating for 20 minutes. Then the cells were transfected by adding the mixtures. Four hours after applying the DNA/Turbofect mixture, medium was changed.

Table 34. Reagents used for Transfection for Luciferase assays (24-well plate)	
reagent	**amount**
plasmid DNA	500 ng
cells	100 000
Turbofect	2.0 µl
serum-free Medium	200 µl
total medium volume	1 ml

Table 35. Reagents used for Transfection for Western Blot (6-well plate)	
reagent	**amount**
plasmid DNA	3 µg
cells	500 000
Turbofect	6.0 µl
serum-free Medium	200 µl
total medium volume	4 ml

7.5.2. Isolation of neonatal rat cardiomyocytes and AAV6-transduction

Cardiomyocytes were isolated from neonatal rats (postnatal day 0 to 3). Hearts were excised and collected in Calcium and bicarbonate free Hanks with HEPES (CBFHH) after removal of atria (Table 21). The 'Neonatal Heart Dissociation Kit mouse and rat' was used to isolate neonatal rat cardiomyocytes (NRCM). Cardiomyocytes were separated from fibroblasts and other cells using a percoll gradient method. NRCMs were washed twice with NRCM medium and 1 million cells were plated in 6-well plates coated with collagen. Medium was changed every second day.

To transduce the NRCMs with AAV6-viruses encoding for TBX5, CX43 and GIRK4, the AAV6 were added at a ratio of 100 000 particles per cell and left to incubate for 48 hours. Cells were harvested after 2 weeks of infection.

7.5.3. Isolation of murine adult cardiomyocytes

Adult hearts were excised as described (7.1.5 for details) and blood was removed in ice-cold PBS. The heart was transferred into ice-cold perfusion buffer and a blunt-end 20 G cannula was inserted into the aorta. The aorta was fixed on the cannula with surgical yarn and slowly perfused to verify correct placement. The heart was connected to a Langendorff perfusion system for continuous retrograde perfusion at a flow rate of 4 ml/min at 37°C. Perfusion was done for 1 min with perfusion buffer, then 8-9 min with digestion buffer. After digestion, hearts were removed and ventricles were minced. The suspension was further homogenized by carefully pipetting up and down in stopping buffer. To remove bigger undigested fragments suspension was left for 1 min and supernatant containing cells was transferred to a fresh tube. To enrich for cardiomyocytes, the suspension was left to sediment by gravity for 8 min. This step was repeated 3 times using increasing Ca^{2+} concentrations. Supernatants were collected as non-myocyte fraction. For cardiomyocyte culture, sedimented cardiomyocytes were plated on laminin-coated glass cover slips and incubated for 1 hour at 37°C before fixation (7.3.3 for details).

7.5.4. Luciferase assays

Luciferasse assays were performed 24 hours after transfection according to manufacturers instructions. In brief, cells were lysed using the Passive Lysis Buffer. 20 µl of this lysate were transferred to a white 96-well plate and the assay was performed in the Luminometer. Firstly, Firefly Luciferase activity was measured, followed by Renilla activity detection for normalisation. Luminescence values of the Firefly were divided by Renilla and normalized to the condition without the enhancer and the empty pCMV2c-plasmid.

7.6. Chromatin Immunoprecipitation

To determine the binding sites of transcription factors or other DNA-binding proteins on native DNA, the technique of Chromatin Immunoprecipitation (ChIP) can be used. This technique consists of four basic steps (Figure 8): Firstly, the chromatin is covalently cross-linked to associated proteins. Secondly, the chromatin is sheared into fragments of an optimal size of 200 - 1000 bp, depending on downstream applications. The sheared chromatin can be immunoprecipitated with an antibody directed towards the protein of interest. After immunoprecipitation the DNA is isolated. It can be analysed by quantitative PCR for specific loci or subjected to next-generation sequencing for an unbiased approach. As controls, immunoprecipitation with an IgG control or total input (non-immunoprecipitated chromatin) can be used. The protocol described here was adapted from [Iyer et al., 2018] and [O'Geen et al., 2010].

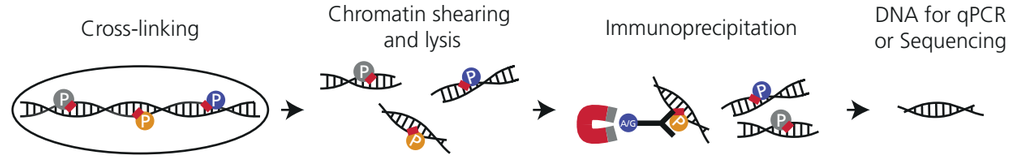

Figure 8. Schematic of Chromatin Immunoprecipitation Proteins binding to the chromatin are covalently cross-linked. Afterwards the chromatin is sheared into fragments of the correct size and nuclei are lysed. Immunoprecipitation enriches for fragments bound to a specific protein. The immunoprecipitated DNA is cleared and can be used for analysis by qPCR or next-generation sequencing.

7.6.1. Cross-linking

Fresh murine cardiac ventricles, prepared as described (7.1.5 for details), were dissected and incubated in 2% FA in PBS (1 ml for one ventricle) for 30 min constantly moving. Cross-linking was quenched by addition of glycine to a final concentration of 125 mmol/l with subsequent incubation for 5 min. Samples were centrifuged at 300 x g at 4 °C for 5 min. The supernatant was discarded and the pellet was washed with PBS (1 ml for one ventricle) containing protease inhibitors for 5 min. After centrifuging again, the supernatant was removed and the pellet was snap-frozen in liquid nitrogen and stored at -80°C or immediately proceeded with nuclei isolation.

7.6.2. Nuclei Isolation

To each ventricle, 500 µl of hypotonic buffer were added and the tissue was meshed in the tissue lyser for about 6 min at 30 Hz. This was incubated on ice for 5 min, NP-40 was added to a final concentration of 1 %, transferred to a fresh tube and incubated on ice for 10 min. Centrifugation was done at 12 000 x g and 4°C for 2 min, the supernatant was discarded. The pellet was resuspended in 500 µl of hypotonic buffer with 1% NP-40 and incubated on ice for 3 min. After another centrifugation for 3 min, the supernatant was discarded and the pellet was snap-frozen or immediately proceeded with sonication.

7.6.3. Sonication

To each ventricle, 750 µl of Sonication buffer I were added to resuspend the pellet, followed by 15 min incubation on ice. Secondly, 750 µl of Sonication buffer II were added and the mixture was distributed in 6 TPX tubes (250 µl each) for sonication. Samples were sonicated for 30 cycles with 30 sec ON/OFF and centrifuged at 8°C, 12 000 x g for 10 min. The supernatant was kept as chromatin fraction I. The pellet was resuspended in 750 µl Sonication buffer I and 750 µl Sonication buffer II and again distributed in 250 µl each in TPX tubes. Sonication and centrifugation were repeated and the supernatant was kept as chromatin fraction II for chromatin immunoprecipitation.

7.6.4. Shearing check

As a quality control, the fragment size after shearing was controlled by gel electrophoresis after elution. Therefore 10 µl of chromatin were incubated with 30 µl IP Elution buffer, 1.2 µl of 5 mol/l NaCl and 0.4 µl of Proteinase K (8 µg) shaking at 65°C for 1.5 hours. 12.5 µl of this mixture were added to 2.5 µl of loading dye (6x) and analysed on a 1% agarose gel.

7.6.5. ChIP

For each ChIP 350 µl chromatin fraction II, 1.4 ml ChIP Incubation buffer, 35 µl Protease Inhibitors (40 x stock) and 1.27 µg of antibody were incubated rotating at 4°C over night. The next day 35 µl ChIP grade Protein A/G magnetic beads were added and incubation was continued for 2 hours. Subsequently, the beads were washed with 1.2 ml of Wash Buffers 1 (once), 2 (three times) and 3 (once) for 5 min each rotating at room temperature.

7.6.6. Elution

To elute the DNA from the beads, a Proteinase K incubation was used to enzymatically remove the proteins from the solution. Each sample of beads was supplemented with 250 µl ChIP Elution buffer, 10 µl 5 mol/l NaCl and 3.33 µl of Proteinase K (67 µg). The input sample was prepared correspondingly from 35 µl chromatin fraction II, 150 µl ChIP Elution buffer, 6 µl 5 mol/l NaCl and 2 µl of Proteinase K (40 µg). Samples were vortexed and incubated at 65°C for 1.5 hours with vigorous shaking.

7.6.7. DNA recovery

The PCR and Gel Clean Up Kit was used with Buffer NTB for SDS-containing samples according to manufacturers instructions.

7.6.8. Analysis

Quantitative PCR was done as described (7.2.3). The sample quantities were calculated by regression from standard curves for each primer. The % input values were calculated by dividing the IP quantity by the 10% input value and multiplied by 10. The fold-enrichment was calculated by dividing the IP value by the corresponding IgG control.

Next-Generation Sequencing was carried out by the NGS Integrative Genomics Core Unit of the University Medical Centre Göttingen. In brief, ChIP-Seq library preparation was performed using NEBNext Ultra DNA library prep kit for Illumina (E7370) according to manufacturer's instructions. Quantitation of DNA libraries was done on an Invitrogen Qubit 2.0 Fluorometer and the size range of DNA libraries was performed on an Agilent Bioanalyzer 2100 (High Sensitivity DNA Assay). DNA libraries were amplified and sequenced by using cBot and HiSeq2500 from Illumina (20-25 million reads per sample).

7.7. Bioinformatic analysis

Basic ChIP-Seq analysis was performed on Galaxy [Afgan et al., 2016] on usegalaxy.org. In brief, the sequence reads were aligned to the mouse reference assembly (UCSC version mm9) using Bowtie [Langmead, 2010]. Model Based Analysis of ChIP-Seq (MACS2) version 2.1.0.20140616.0, which is the updated version of MACS [Zhang et al., 2008] was used for peak calling; IgG was used as a control file. Bedgraphs obtained from MACS2 were converted to bigwigs and visualized using the Integrative Genomics Viewer IGV 2.3.82 [Thorvaldsdóttir et al., 2013][Robinson et al., 2011]. To calculate the enriched genomic regions in the TBX5-ChIP-Seq dataset 'CEAS: cis-regulatory element annotation system' [Shin et al., 2009] was used on Cistrome [Liu et al., 2011]. GREAT analysis was performed to annotate the peaks to genes and calculate enrichment of gene ontology clusters for biological processes and human phenotypes for TBX5 [McLean et al., 2010]. Heatmaps were generated using deepTools-computeMatrix and heatmapper options for the ChIP-Seq signal (in RPKM) using bamCoverage [Ramírez et al., 2014]. Co-Occupancy correlation was statistically analyzed with multibigwig summary and plot correlation on Galaxy. To identify TBX5-peaks, that are overlapping with H3K27ac and POL2, the WindowBed function (500 bp up- and downstream) from BEDTools was used in Galaxy [Björn Grüning et al.,][Quinlan et al., 2010]. Motif Enrichment in the ChIP-Seq dataset was tested with AME [McLeay et al., 2010] using known motifs for TBX5, MEIS1 and MEIS2, GATA4 and NKX2.5. Motifs used were identified from previous studies [Ghosh et al., 2001] [Grau et al., 2013] and MotifMap [Daily et al., 2011] [Xie et al., 2009]. De novo motif discovery was carried out using HOMER [Heinz et al., 2010].InteractiVenn [Heberle et al., 2015] was used to analyse the intersection between TBX5 bound genes (found in ChIP-Seq) and genes differentially expressed in TBX5 KO ventricle (cutoff $p<0.05$; Log2-fold-change >0.8 or <-0.8 respectively). Gene ontology/pathway analyses were performed using a minimum of 4 genes per cluster and default parameters and stringency in 'ClueGO': a Cytoscape plug-in [Bindea et al., 2013][Bindea et al., 2009] and the significant ($p \leq 0.05$) cluster of 'Gene Ontology Biological Processes' were shown.

7.8. Statistical analysis

All data are displayed as individual values with mean (indicated by the line) or as box-and-whisker plot with the box extending from the 25th to 75th percentile, whiskers indicating min to max, + indicates the mean value and the line indicates the median. The statistical tests that were used are indicated in each figure legend.

Differences were considered statistically significant, when p value was below 0.05.

8. Results

8.1. Ventricular specific KO of TBX5

To characterize the effects of TBX5 in the adult heart, we used an inducible cardiomyocyte-specific loss-of-function mouse model [Renger, 2012] (7.1.1 for details). Recombination was confirmed by quantitative PCR for *Tbx5* mRNA. As expected, endogenous expression of *Tbx5* was stronger in the atria than in the ventricles. Surprisingly, recombination occurred robustly in the ventricles 4 weeks after induction, but no changes in the *Tbx5* expression levels in the atria could be observed (Figure 9A). Flox mice ($Tbx5^{LDN/LDN}$ without Cre) and Cre mice (*Myh6*-MerCreMer with homozygous wild-type alleles of *Tbx5*) injected with Tamoxifen served as control animals throughout the study. Neither Flox nor Cre mice showed any incidence of death in the months after recombination, whereas 60% of *vTbx5*KO mice died without showing any prior symptoms of disease (Figure 9B).

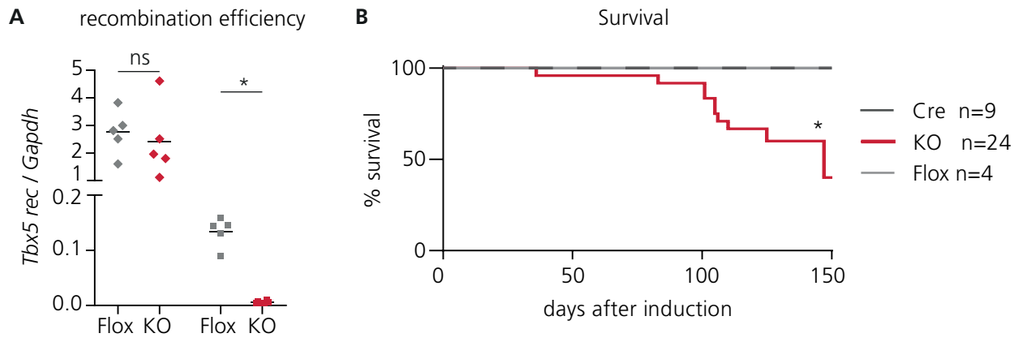

Figure 9. A ventricular specific KO of *Tbx5* results in a decreased survival rate A. Recombination of *Tbx5* was confirmed on mRNA level by quantitative PCR. Whereas the *Tbx5* levels strongly decreased in the ventricles, they remained unchanged in the atria, indicating ventricular specific recombination. **B.** The survival rate of *vTbx5*KO mice is severely decreased; after 5 months of recombination 40% of the mice are still alive. **Statistics:** * $p<0.05$ A. Unpaired students t-test in the atria and ventricle groups B. Differences in the survival rate were tested by logrank test (Mantel-Cox)

8.2. Cardiac function of TBX5 KO mice

Since the mice had a cardiac deficiency of *Tbx5*, we aimed to observe, if the decreased survival rate was due to functional impairments of the heart by echocardiography and electrocardiography.

8.2.1. Echocardiography

8.2.1.1. Absence of physiological hypertrophy

The heart dimension and function of Flox, Cre and KO mice were analysed by echocardiography prior and 8 and 16 weeks after recombination. Firstly, the heart grew physiologically in the Cre group along with the increase in body weight (BW), resulting in an unchanged heart weight to body weight ratio (HW/BW) (Figure 10A-C). In contrast to the Cre group, the heart weight (HW) in the *vTbx5*KO group did not change over time, although the body weight increased in a comparable manner (Figure 10A-B). This results in a reduced HW/BW ratio at 8 and 16 weeks after recombination (Figure 10C).

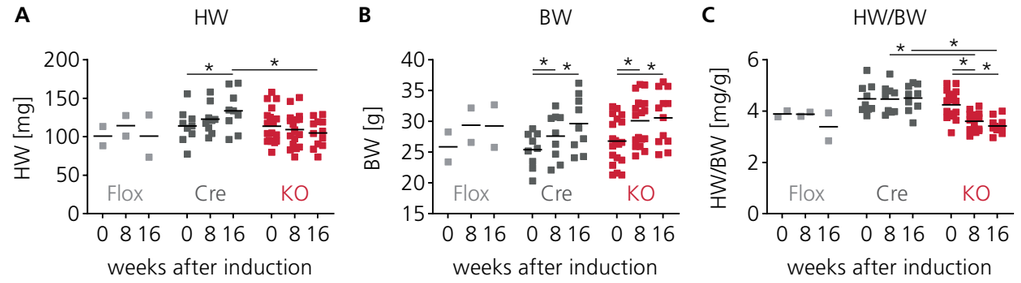

Figure 10. Tbx5 KO leads to reduced heart growth Echocardiographic analyses was performed before and 8 and 16 weeks after induction. **A.** Whereas the heart weight (HW) increases over time in the Cre control group, it does not change in the KO group. **B-C.** Since body weight increases normally in all groups, the heart weight to body weight ratio (HW/BW) in the KO group decreases. **Statistics:** Two-Way ANOVA, followed by Sidak's Multiple Comparison Test * $p<0.05$

8.2.1.2. Diastolic dysfunction in the absence of TBX5

Analysis of the cardiac contractile function revealed a reduction of fractional area shortening (FAS) and ejection fraction (EF) 16 weeks after recombination (Figure 11A-B). The stroke volume (SV) decreased over time in the KO hearts (Figure 11C), resulting from the decreased volume in diastole (Figure 11D). In contrast, the volume in systole remained unchanged (Figure 11E). Hence, cardiac output (CO) and cardiac index (CI) are as well decreasing over time (Figure 11F-G). Diastolic thickness of the anterior and posterior walls of the left ventricle did not change significantly in any group over time (Figure 11H-I).

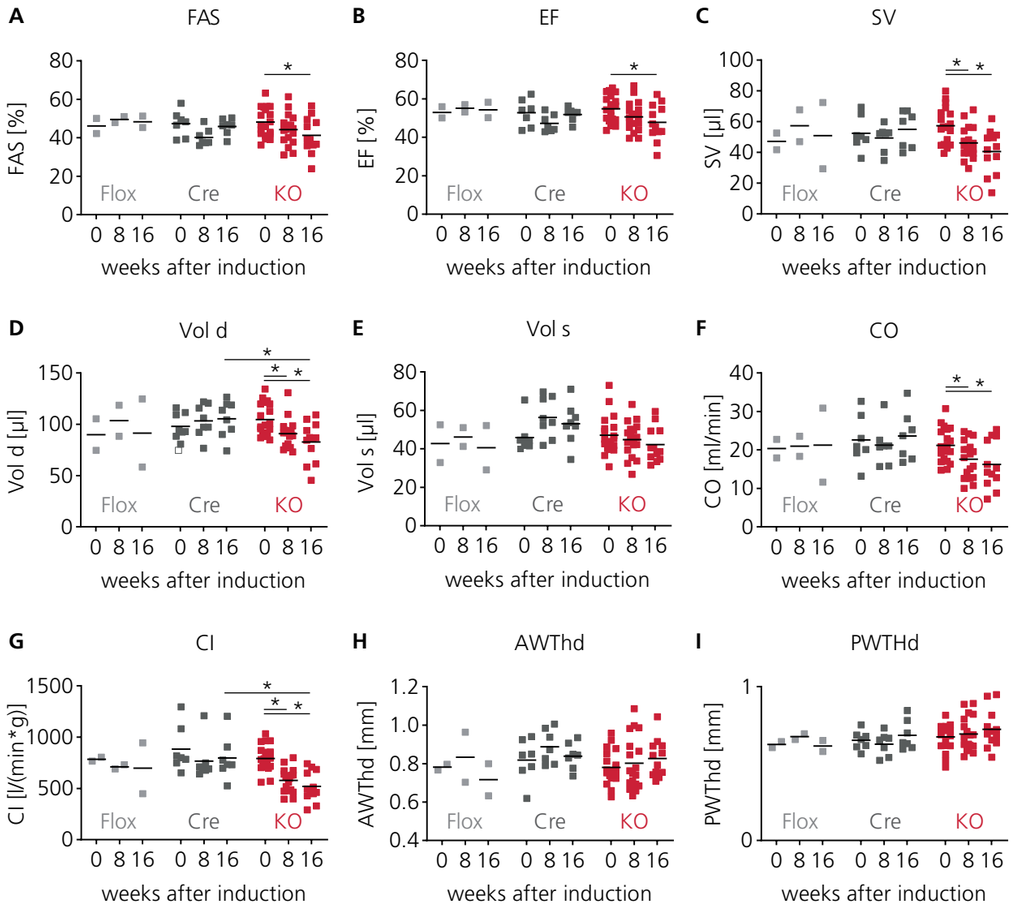

Figure 11. TBX5 KO leads to diastolic dysfunction Echocardiographic analyses was performed before and 8 and 16 weeks after recombination. **A-C.** Fractional area shortening (FAS), Ejection Fraction (EF) and Stroke volume (SV) are decreasing in the KO group. **D-E.** In contrast to the Volume in systole (Vol s), the Volume in diastole (Vol d) decreases over time in the KO group. **F-G.** Cardiac output (CO) and Cardiac index (CI) decrease over time in the KO group. **H-I.** The wall thickness in diastole of the anterior (AWThd) and posterior (PWThd) wall of the left ventricles remains unchanged in all groups. **Statistics:** Two-Way ANOVA, followed by Sidak's Multiple Comparison Test * p<0.05

8.2.2. Electrophysiological properties of *vTBX5*KO hearts

Telemetric ECG recordings over 24 hours before and one, two and four weeks after recombination show, that *vTbx5*KO mice have slower signal propagation compared to Flox and Cre control mice (Figure 12A). Statistical evaluation revealed increasingly longer PR, QRS and QT-intervals beginning from 1 week after recombination (Figure 12B). Along with this statistical variation of the cardiac cycle, mice showed different arrhythmias, like atrioventricular block, ventricular tachycardia and even asystoles (Figure 13), that could be causative of the observed sudden death in the *vTbx5*KO mice.

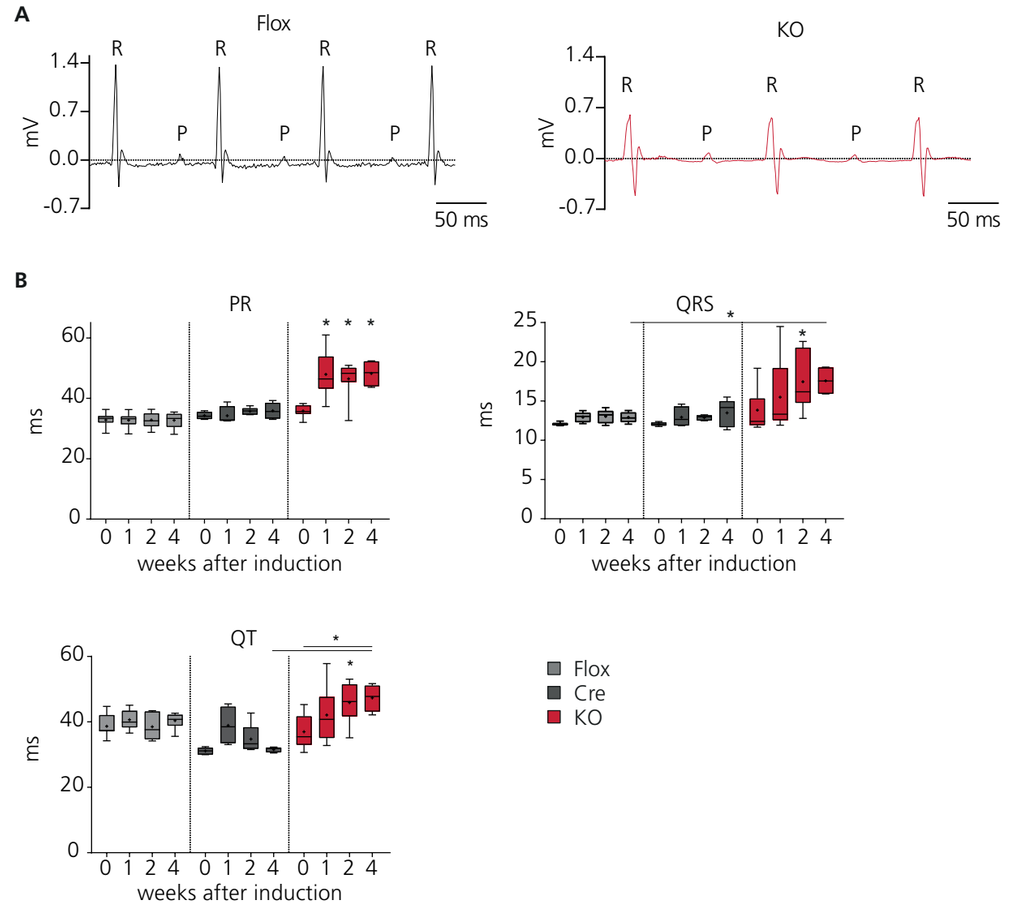

Figure 12. Timecourse analysis of ECG parameters shows gradual prolongation of PR- and QRS-intervals in *vTbx5*KO mice A. Representative ECG-traces of Flox and KO mice **B.** Time course evaluation of PR and QRS intervals revealed a prolongation of both conduction parameters over a course of 4 weeks in the TBX5 KO mice. **Statistics:** B: one-way ANOVA with Sidak's multiple comparison test; p-value-summary: * without lines - <0.05 for a comparison with the respective time point of Flox and Cre, as well as to the 0 week time point of the *vTbx5*KO . n=4-13/group. * with lines - <0.05 for the indicated comparison.

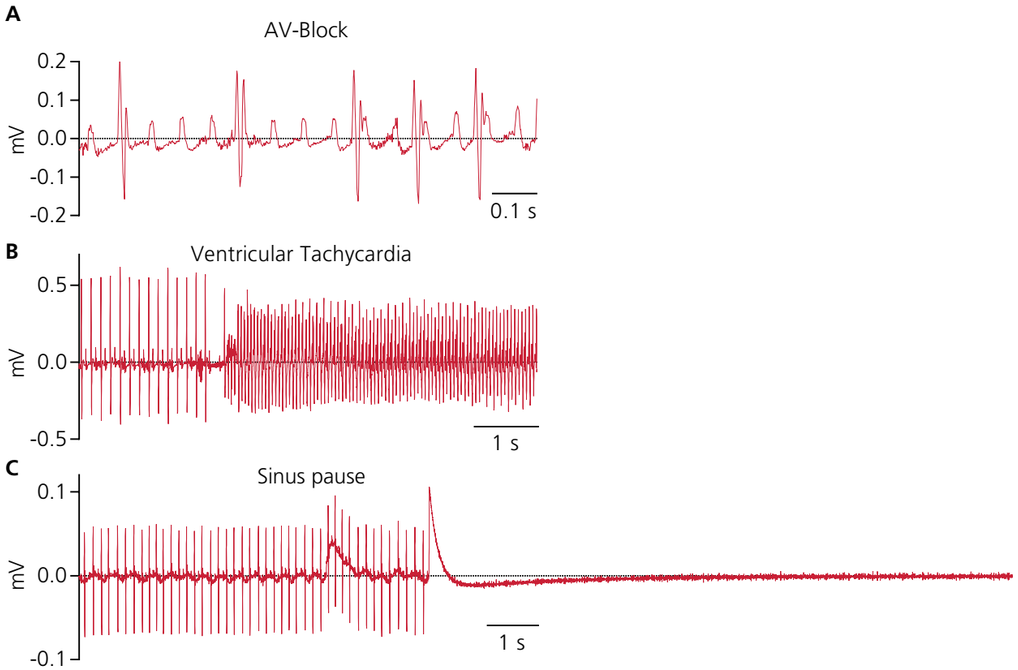

Figure 13. *vTbx5*KO mice develop ventricular and supraventricular arrhythmias A. Red traces show *vTbx5*KOmice experiencing third degree atrioventricular (AV) block, ventricular tachycardia (**B**) and sinus pauses (**C**).

More detailed electrophysiologic evaluation by ex vivo analysis (carried out by Fahima Syeda, Nashita Kabir and Larissa Fabritz, Birmingham) of the heart confirmed a tendency of increased arrhythmic activity in the *vTbx5*KO hearts upon S2 pacing (Figure 14A). Furthermore, these mice had longer activation times from right atrium to right ventricle, inside the right ventricle and from right ventricle to septum and left ventricle (Figure 14B), confirming the slower signal propagation in the working myocardium detected from the telemetric ECG recordings.

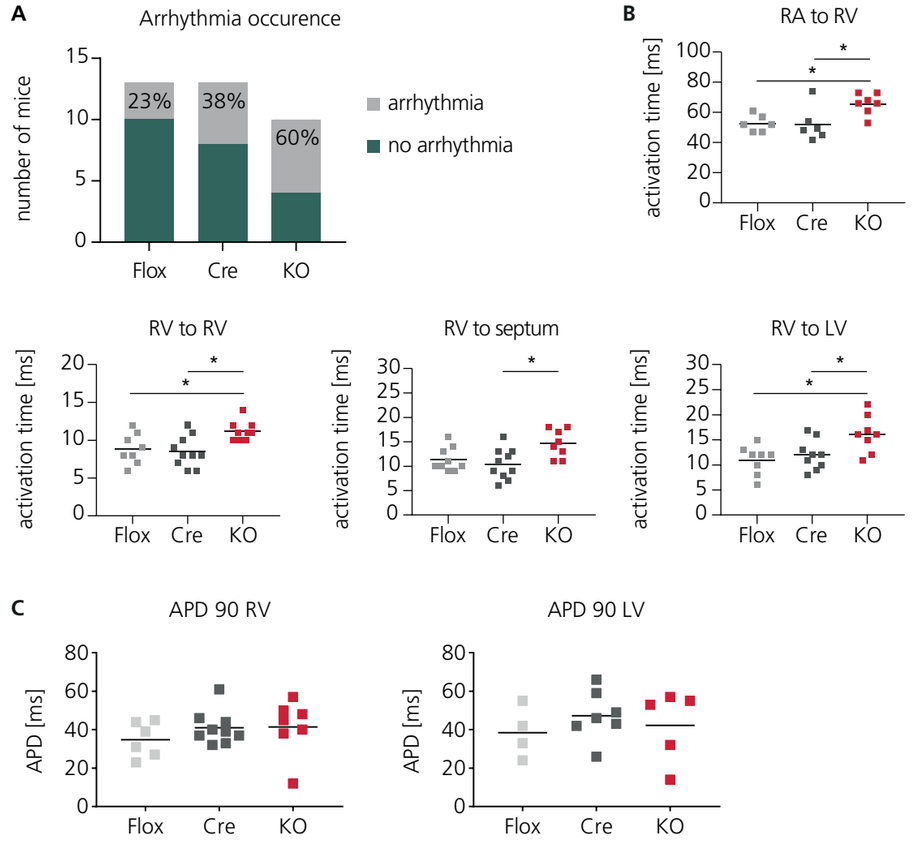

Figure 14. *vTbx5*KO hearts show slower signal propagation A. Ex vivo S2 pacing induced arrhythmia occurrence is higher (60%) in *vTbx5*KO mice vs Flox (23%) and Cre (38%) mice, although the level did not reach statistical significance **B.** Electrophysiological studies of isolated paced Flox, Cre and *vTbx5*KO hearts show prolonged activation times from right atrium (RA) to right ventricle (RV), endocardial RV to epicardial RV, RV to septum and RV to left ventricular epicardium (LV). **C.** Action potentials in the right and left ventricle were not different between the groups. APD90 measured at a cycle length of 100 ms. **Statistics:** B. One-way ANOVA followed by Tukey's multiple comparison test, * $p < 0.05$.

8.3. Chromatin binding of TBX5

To understand the underlying molecular mechanisms of the electric and contractile dysfunction in the absence of TBX5, we aimed to identify ventricular TBX5 target genes. Therefore we integrated chromatin binding sites from a TBX5 ChIP-Seq with dysregulated genes detected by RNA-Sequencing from *vTbx5*KO vs control ventricles.

8.3.1. Establishment of Chromatin Immunoprecipitation for TBX5 in adult hearts

The chromatin immunoprecipitation (ChIP) procedure was established to enable detection of new TBX5 binding sites on the chromatin in the adult mouse ventricle. In the process, an important step was to optimize the fractionation of the chromatin. An optimal size are chromatin fragments around 200-300 bp [Johnson et al., 2001]. Nuclei were sonicated for 30 cycles and the supernatant was collected, the remaining nuclei were re-sonicated for 30-55 cycles and the supernatant was again collected (7.6.3 for details). The supernatant of the first round contained Chromatin Fraction I, the supernatant of the second round Chromatin Fraction II (Figure 15A). It was chosen to use the chromatin from fraction II, sonicated for 30 cycles for further ChIP-Experiments because of optimal fragment size. Indeed, after Chromatin Immunoprecipitation, the size of precipitated chromatin analysed on the Bioanalyzer was 303 bp on average (ranging from 179 - 471 bp, n=3, used for sequencing).

To verify the success of the ChIP itself, we examined binding to the previously established *Scn5a* enhancer [Arnolds et al., 2012]. Quantitative PCR of the TBX5 precipitated DNA showed a reproducible enrichment on this enhancer (Figure 15B).

The obtained chromatin samples with a controlled fragment size and a validated enrichment of the *Scn5a* enhancer were subjected to next generation sequencing. A series of bioinformatic analysis was performed (7.7 for details). The enrichment of the *Scn5a* enhancer could be confirmed in the sequencing results from the TBX5-ChIP as well (Figure 15C, red traces).

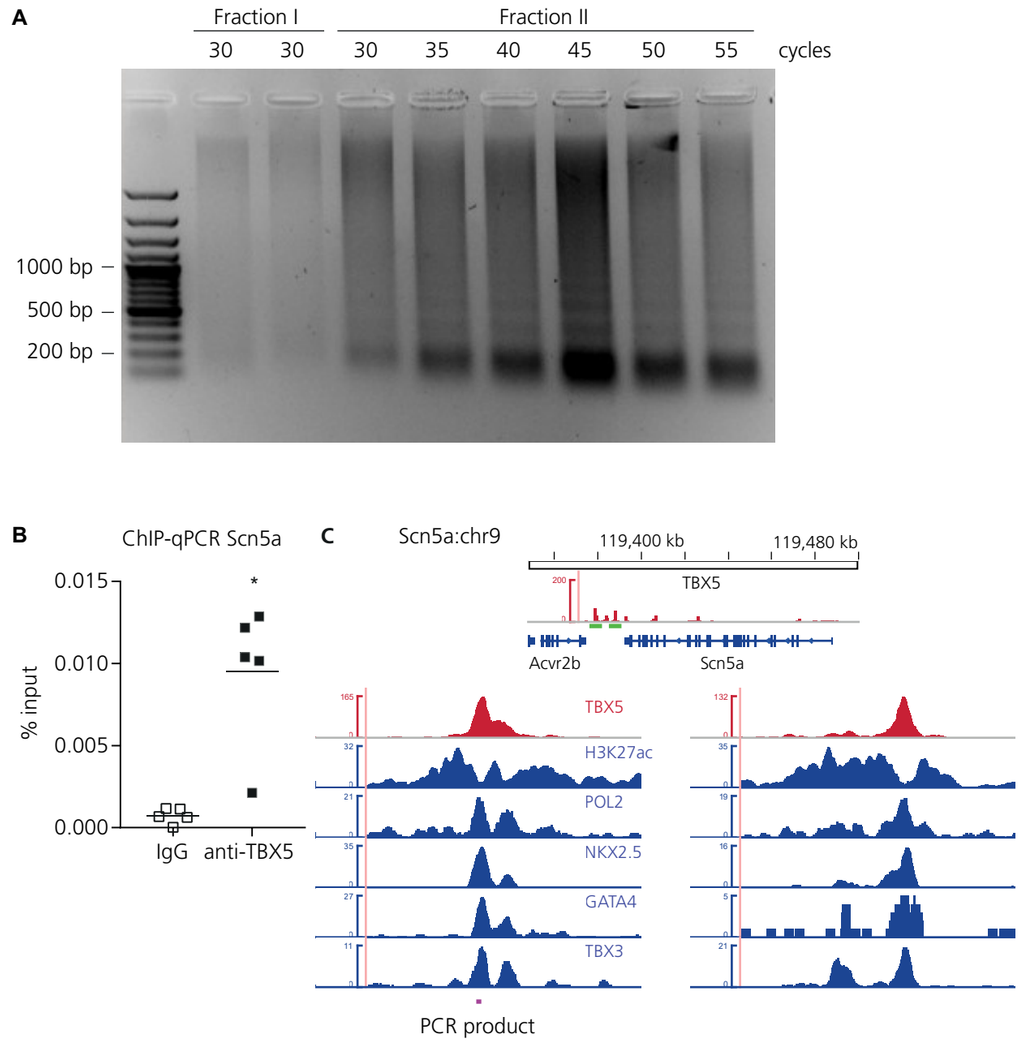

Figure 15. Establishment of the TBX5-ChIP-Seq A. Optimization of Chromatin Fractionation by Sonication: Fraction II, sonicated for 30 cycles was chosen for further experiments. **B.** ChIP-qPCR for the *Scn5a* enhancer revealed enrichment in the anti-TBX5 sample vs. the IgG sample. **C.** Sequencing showed a peak for the *Scn5a* enhancer in the TBX5-ChIP-Seq. The location of the PCR product from B is depicted in purple. **Statistics:** B: unpaired students t-test, * $p < 0.05$.

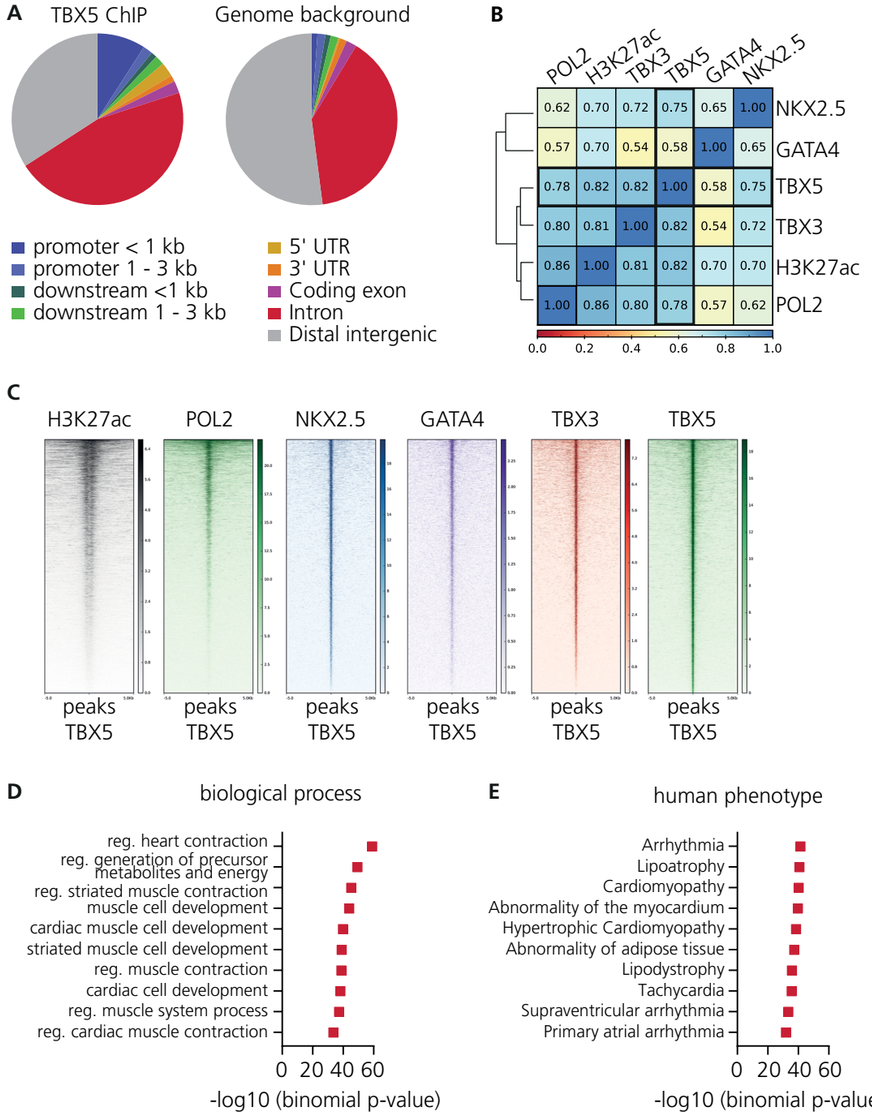

Figure 16. TBX5 co-occupies active enhancers with NKX2.5 and GATA4 A. Analysis of enriched genomic locations of TBX5-ChIP shows that TBX5 preferably binds to promoter sites, downstream of the gene body, in the 5‘ UTR and intronic regions (CEAS package[Shin et al., 2009], [Liu et al., 2011] on Cistrome). **B/C.** TBX5 bound regions show high co-occupancy with marks of active enhancers (H3K27ac, POL2) [He et al., 2014], known cofactors (NKX2.5, GATA4) and TBX3 [van den Boogaard et al., 2012]; analysed data from previously published datasets. Results are displayed in B as the statistical analysis of co-occupancy showing Pearson’s correlation coefficients and in C as heatmaps using deeptools [Ramírez et al., 2016] in Galaxy. The scale bar in B depicts co-occupancy percentage and in C normalized RPKM values. **D.** TBX5-bound regions were annotated to genes using GREAT [McLean et al., 2010]. These regions were analysed for the 10 most enriched biological process clusters (D) and the 10 most enriched human disease phenotype clusters (**E**) of TBX5 peaks.

To gain information about the genomic regions a transcription factor binds to, it can be evaluated in what distance to a transcription start site the ChIP-Seq peaks are located, an information that can be obtained using GREAT analysis [McLean et al., 2010]. However, the information which types of genomic regions (e.g. promoter, exon, intron) are bound by TBX5 provides a more sophisticated insight into the binding properties. Therefore an analysis with CEAS (cis-regulatory element annotation system) [Shin et al., 2009][Liu et al., 2011] was done. The binding patterns of TBX5 (Figure 16A - left panel) were then compared to the genomic background (Figure 16A - right panel). Compared to the genomic background an enrichment of promoter, 5’UTR, intronic regions and regions downstream to the gene body was found for the TBX5 bound regions (Figure 16A).

Next, we compared our TBX5 data to published data using deeptools [Ramírez et al., 2016]. We were interested in overlaps with marks of active enhancers (H3K27ac and POL2) [van den Boogaard et al., 2012] to determine whether TBX5 acts transcriptionally activating in the adult ventricle. Additionally, we studied peaks of the transcription factors NKX2.5 and GATA4, which are known to bind cooperatively with TBX5, and of TBX3 [He et al., 2014], known to bind to similar regions as TBX5. Indeed, we found a co-occupancy for the active enhancers as well as for the aforementioned transcription factors (Figure 16B and C).

Furthermore, we analysed the gene ontology annotations for genes bound by TBX5 in our ChIP-Seq dataset and found heart contraction and muscle development related biological processes and human disease phenotypes like arrhythmia and cardiomyopathy being overrepresented (Figure 16D and E).

8.3.2. TBX5 chromatin occupancy in the adult vs. the embryonic heart

As described, we performed ChIP sequencing in murine adult hearts. Since comparisons of ChIP-Seq datasets from different tissues or developmental stages can give insight into context-depent action of a transcription factor, we decided to perform a differential binding analysis. Therefore, we compared our dataset with a recently published ChIP-Seq for TBX5 in murine hearts from stage E9.5 [Steimle et al., 2018]. Both datasets are distinctly different based on principal component analysis (PCA) (Figure 17A). Nevertheless, when the E9.5 peaks were mapped to the regions bound by TBX5 in the adult heart using deeptools [Ramírez et al., 2016][Ramírez et al., 2014], embryonic TBX5 peaks showed an enrichment on the adult TBX5 peaks (Figure 17B).

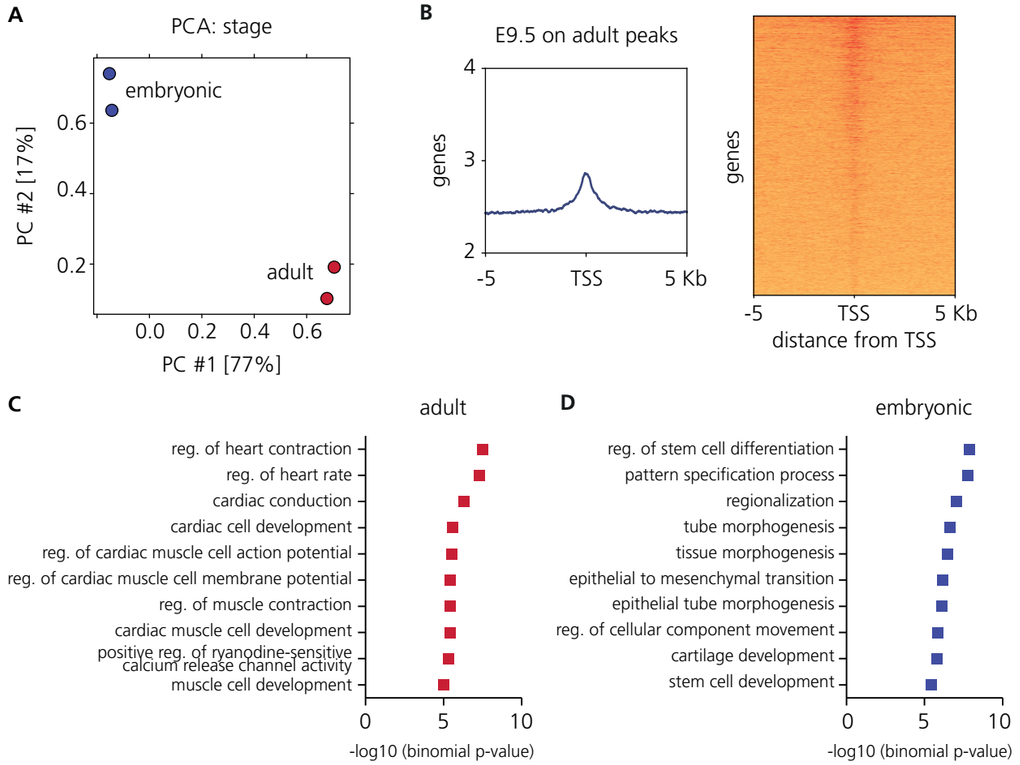

Figure 17. Comparison of adult and embryonic TBX5 ChIP-Seq A. Principal Component Analysis shows that the two embryonic and two adult ChIP-datasets cluster together. Analysis was performed by the DiffBind Package on differentially bound sites [Ross-Innes et al., 2012]. **B.** Summary and heatmap created with deeptools [Ramírez et al., 2016][Ramírez et al., 2014], showing that TBX5-peaks from the embryonic dataset are enriched on the adult dataset. **C-D.** DiffBind was also used to determine the differentially bound peaks of the adult and embryonic dataset (Cut-Off: 2-fold enrichment in each dataset). These peaks were annotated to genes and gene ontologies using GREAT [McLean et al., 2010]. Whereas the adult TBX5 target genes (**C**) bind to genes relevant for contraction and conduction, the embryonic genes (**D**) are associated with differentiation and developmental processes.

However, there are 500 peaks that are more than 2-fold enriched in the adult and 424 in the embryonic dataset. 122 peaks show similar binding patterns in the adult and embryonic stage. When these sets of differentially bound peaks were annotated to genes and the corresponding ontologies using GREAT [McLean et al., 2010], the adult peaks seem to be associated to cardiomyocyte homoeostasis and the embryonic to cardiomyocyte differentiation and development (Figure 17C-D). Common peaks are annotated to ventricular cardiac muscle tissue development and cardiac muscle contraction (annotation was performed with ClueGO [Bindea et al., 2013][Bindea et al., 2009] instead of GREAT due to the lower number of genes).

8.4. Integrative ChIP- and RNA-Sequencing

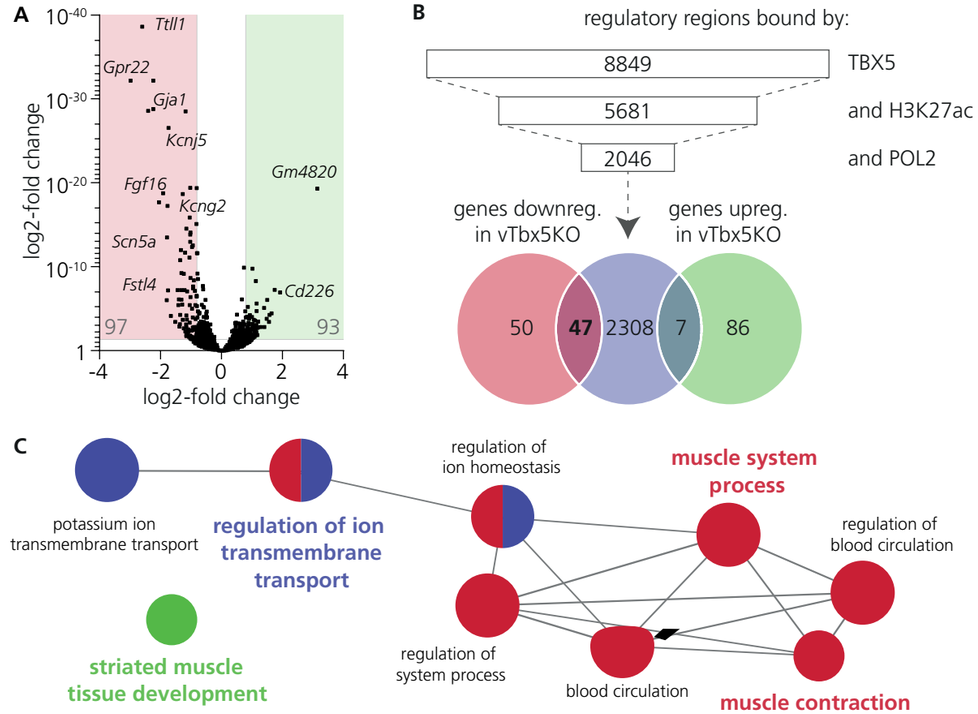

Figure 18. Integrative chromatin occupancy and transcriptome analysis identified clusters of novel putative TBX5 downstream targets in the adult ventricle A. RNA-Sequencing results displayed in a volcano plot. 97 genes are down- and 93 are upregulated in vTbx5KO ventricles using a cut-off of $p<0.05$ and log2-fold-change of > 0.8 or < -0.8. **B.** TBX5 co-occupancy with marks of active enhancers H3K27ac and POL2 identified 2,046 putative TBX5 active enhancers. These were annotated to genes with GREAT (*Gja1* and *Fgf16* enhancers were not annotated automatically by GREAT, but manually identified by BED file analysis in the IGV platform). Venn-diagram showing the intersection of those genes with the regulated transcripts of the RNA-Seq analysis. **C.** Gene ontology analysis of biological processes for 47 ventricular TBX5 targets.

In addition to the TBX5-ChIP-Seq, we performed RNA-Sequencing of *vTbx5*KO hearts vs. control hearts to determine which genes are differentially regulated in the absence of TBX5. This revealed 97 down- and 93 upregulated genes in the *vTbx*5KO mice (Figure 18A). The

upregulated genes are related to blood coagulation/platelet aggregation (*Ifi204, Ifit1/2, Gm4951*) and cellular response to interferon-alpha/beta (*Fermt3, Itga2b, Plek, P2ry12, F5, Gp9, Hpse*). Because these processes have little link to the phenotype of the *vTbx5*KO mice besides frequent blood clots in the atria, we decided to focus on the downregulated genes. To narrow down the number of peaks from the TBX5-ChIP-Seq relevant for the downregulated genes, we chose only the peaks that were marked as active enhancers by co-occupancy of H3K27ac and POL2. Of these 2046 genes, 47 were downregulated in the *vTbx5*KO model (Figure 18B). Gene ontology analysis for biological processes of these 47 genes revealed an enrichment of clusters relevant in muscle development, contraction and ion transmembrane transport (Figure 18C).

Validation of novel TBX5 target genes

Of those 47 genes we chose 12 genes, due to their (putative) role in cardiac electrophysiology (*Gja1, Kcnj5, Kcng2, Cacna1g, Chrm2*), cardioprotection (*Fhl2, Gpr22, Fgf16*) and contraction (*Fstl4, Cmya5, Emilin2, Pdlim4*) for further validation. The corresponding peaks from the TBX5 ChIP-Seq are displayed as an overview (Figure 19A).

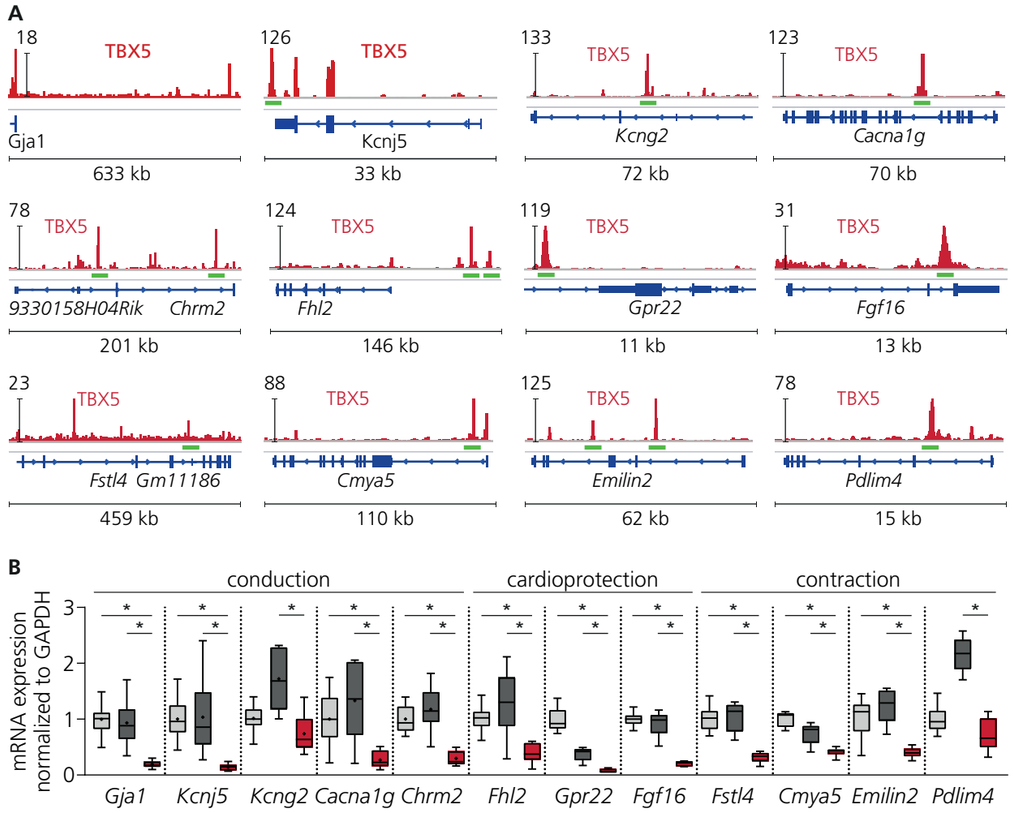

Figure 19. Validation of identified genes regulated in *vTbx5*KO A. Visualisation of TBX5 peaks on selected downregulated genes using IGV. The TBX5-ChIP-Seq is displayed in red and gene features in blue. The peaks investigated further are indicated in green. The y-axis represents the treatment pileup peak summit scores **B.** Validation of target gene expression by qPCR (Flox, light grey; Cre, dark grey; *vTbx5*KO, red) **Statistics:** B. One-way ANOVA for each transcript followed by Tukey's multiple comparison test * p < 0.05

We performed quantitative PCR to determine the mRNA expression in *vTbx5*KO hearts compared to Flox and Cre hearts. We indeed found each transcript to be downregulated in the *vTbx5*KO hearts (Figure 19B). Furthermore, CX43 (encoded by *Gja1*) and GIRK4 (encoded by *Kcnj5*) showed reduced expression on protein level as well (Figure 20A). Immunofluorescence analysis of cross-sections of the ventricular myocardium showed that CX43 is strongly downregulated homogeneously throughout the myocardium (Figure 20B).

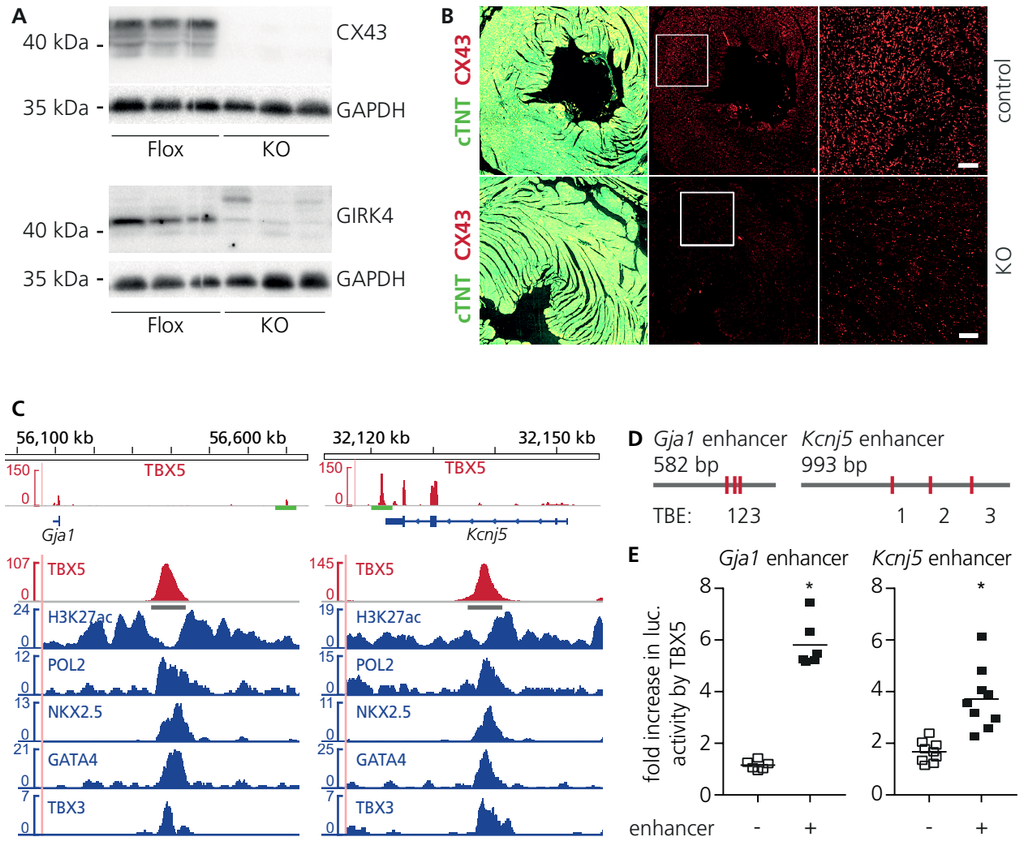

Figure 20. *Gja1* and *Kcnj5* are transcriptionally regulated by TBX5 A. Immunoblot analysis of CX43 (encoded by *Gja1*), GIRK4 (encoded by *Kcnj5*) and GAPDH shows a strong downregulation of CX43 and GIRK4 in *vTbx5*KO mice. Representative blot of n=6 per group. **B.** CX43 expression is strongly reduced in the ventricle of *vTbx5*KO mice shown by immunofluorescence staining for CX43 (red) and cTNT (green). Scale bars: 50 µm. **C.** The putative enhancers for *Gja1* (upstream) and *Kcnj5* (downstream) identified by ChIP-Seq are co-occupied by H3K27ac, POL2, NKX2.5, GATA4 and TBX3. **D.** Scheme indicating 3 predicted T-box elements (TBE) in the enhancer sequences for *Gja1* and *Kcnj5*. **E.** *Gja1* and *Kcnj5* enhancer activity analysis by luciferase measurements show enhancement of luciferase expression by TBX5 co-transfection. **Statistics:** ; E: unpaired, two-tailed student's t-test, p-value-summary: * - <0.05

We found a putative enhancer for *Gja1* ~600kb upstream of the TSS and for *Kcnj5* 700 bp downstream of the last exon. A closer look on the TBX5 ChIP-Seq results of the putative *Gja1* and *Kcnj5* enhancers showed a TBX5 peak consistent with NKX2.5, GATA4 and TBX3 ChIP results. These peaks were also marked as active by H3K27ac and POL2 occupancy (Fig-

ure 20C). Both enhancers harbour 3 potential T-box binding elements (TBE) (Figure 20D). We cloned these enhancers in a plasmid upstream of a firefly luciferase coding sequence with a minimal promoter. This plasmid has a low basic luciferase expression, that can be increased, when a co-expressed transcription factor activates the inserted enhancers. Indeed, co-expression with TBX5 led to a strong increase of luciferase, indicating TBX5 can bind and activate both enhancers (Figure 20E).

8.4.1. Armh4

Among the described targets, which functions are mostly known, one of the most down-regulated targets in the *vTbx5*KO hearts was armadillo-like helical domain containing 4 (*Armh4)*. There is very little knowledge about this protein, especially in the heart.

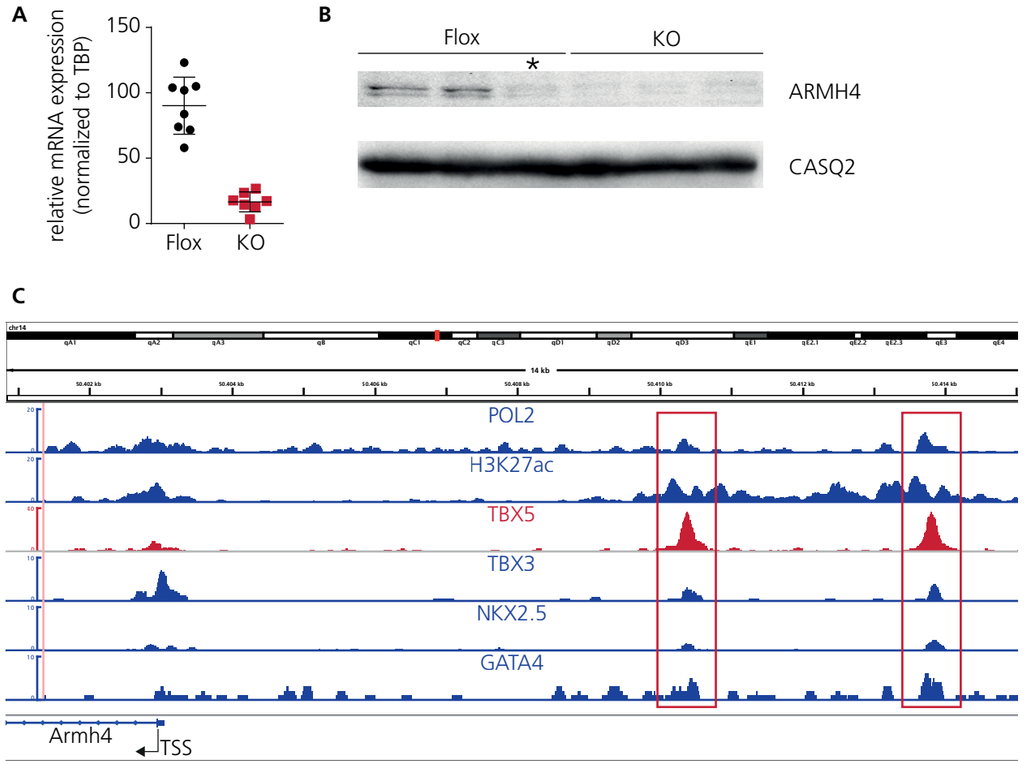

Figure 21. *Armh4* is downregulated on mRNA and protein levels in *vTbx5*KO hearts A. Transcript levels were analysed by qPCR and were normalized to the housekeeping gene TATA-binding protein (*Tbp*). **B.** Immunoblot was performed against ARMH4 (upper panel) and normalized to CASQ2 (lower panel). *This Flox mouse although it was not recombined, had low TBX5, GIRK4 and CX43 expression. **C.** TBX5 binds strongly to putative enhancers upstream of *Armh4*, indicated by ChIP-Seq also from POL2, H3K27ac, TBX3, NKX2.5 and GATA4 of data publicly available [He et al., 2014]; [van den Boogaard et al., 2012].

Validation of the next generation sequencing by qPCR and immunoblot analysis showed that *Armh4* expression in the mouse heart is significantly diminished on mRNA and protein level upon cardiomyocyte specific KO of TBX5 (Figure 21A-B). We analysed the chromatin-binding of TBX5 around the *Armh4* gene with the TBX5-ChIP-Seq data and revealed two putative TBX5-binding sites upstream of *Armh4* (Figure 21C). Both putative enhancers are bound by POL2 and H3K27ac marking active enhancers as well as by TBX3, NKX2.5 and GATA4 which are known to co-occupy chromatin together with TBX5.

In order to get some insight in the function of this protein in the heart, we performed immunostaining in isolated adult murine cardiomyocytes. ARMH4 is mainly localized at the Z-discs (white arrowheads), where it co-localises with alpha-actinin expression, intercalated discs (yellow arrows) and around the nuclei (Figure 22) similarly to sodium channels [Haufe et al., 2005].

In conclusion, the sub-cellular distributions as well as the structure of ARMH4 lead us to the hypothesis that it could be part of a membrane protein complex. Since it is found to be down-regulated in an arrhythmia model it may play a role in conduction and contraction.

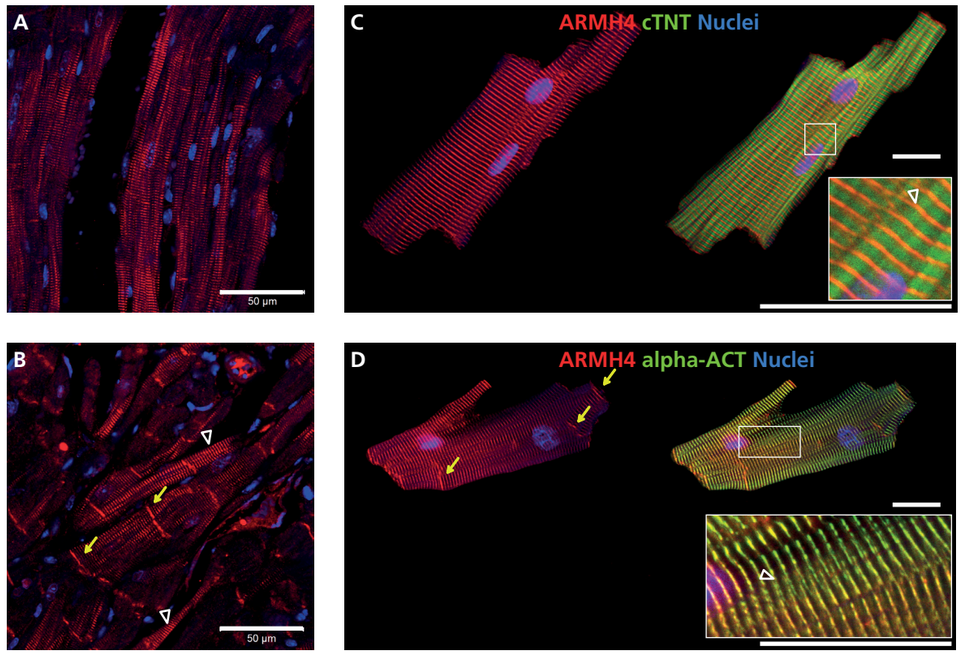

Figure 22. ARMH4 is localized mainly at the intercalated discs and z-discs of adult mouse cardiomyocytes. Sub-cellular distribution of ARMH4 protein in adult mouse CMs. **A+B.** ARMH4 (red) is expressed at the striations (white arrowheads) and at the intercalated discs (yellow arrows) of cardiomyocytes in the adult mouse heart. **C+D.** Isolated CMs co-stained for cTNT (green, **C**) and α-actinin (green, **D**) showed ARMH4 to be expressed mainly at the intercalated discs and Z-discs. Scale bar: 50 µm (panels A+B); 20µm (panels C + D)

8.5. Novel TBX5 co-factor in TBX5

Common analysis of ChIP-Seq data includes motif analysis, which can be applied for known or new (de novo) motifs. We used HOMER (Hypergeometric Optimization of Motif EnRichment) [Heinz et al., 2010] to detect both. In addition, AME (Analysis of Motif Enrichment) was used to obtain statistical results for known motif variants of relevant transcription factors [McLeay et al., 2010]. De novo motif analysis revealed motifs similar to TBX5 motifs, but also of motifs similar to known co-factors of TBX5, such as MEF2, NKX2.5 and GATA4 (Figure 23, see section (5.2.4 for background information). Startlingly, the highest significance had a de novo motif similar to MEIS1/2/3 (Figure 23A and F).

Figure 23. De-novo motifs found enriched in the TBX5-ChIP-Seq show motif similarity to transcription factors of the MEIS, MEF, TBX, NKX and GATA family. 10 most significant de-novo motifs using HOMER [Heinz et al., 2010], transcription factor similarity shown for all annotated mammalian transcription factors.

Therefore, we included MEIS1 and MEIS2 motifs along with motifs of TBX5, NKX2.5 and GATA4 in the AME analysis, which was applied on the total number of TBX5 peaks and for the subset of TBX5 enhancer peaks overlapping with H3K27ac- and POL2-occupancy. For the dataset of the total TBX5 peaks, again MEIS1 motif achieved the highest significance, whereas in the dataset of the TBX5 enhancer peaks a known motif of TBX5 itself showed the highest significance (Table 36).

Table 36. Motif analysis in TBX5-ChIP-Seq peaks

TF	Motif	p-value adj. total TBX5 peaks	p-value adj. TBX5 enh. peaks	Motif source
MEIS1	NHNTGACAGNNN	5.32×10^{-174}	3.92×10^{-18}	MotifMap
TBX5	RGGTGTBR	1.06×10^{-148}	9.91×10^{-43}	[Ghosh et al., 2001]
TBX5	NDAGGTGTBRNN	1.61×10^{-113}	1.53×10^{-35}	MotifMap
TBX5	TNACACCT	6.26×10^{-92}	8.21×10^{-21}	[Grau et al., 2013]
MEIS1	NDNBASCTGTCAWWNN	9.99×10^{-78}	9.16×10^{-09}	MotifMap
GATA4	AGATADMAGRSA	7.42×10^{-74}	7.92×10^{-09}	MotifMap
MEIS2	NDNBASCTGTCAAWNN	6.33×10^{-60}	2.37×10^{-05}	MotifMap
GATA4	ARAWWDMRGRSA	8.85×10^{-40}	7.92×10^{-07}	MotifMap
TBX5	BNDGGTGTKV	5.61×10^{-32}	1.54×10^{-15}	MotifMap
TBX5	YTCACACCTK	2.91×10^{-19}	1.14×10^{-04}	MotifMap
TBX5	DGGTGYBV	1.71×10^{-14}	6.19×10^{-07}	[Ghosh et al., 2001]
TBX5	SGGCGCCKS	7.08×10^{-04}	8.22×10^{-03}	[Grau et al., 2013]
NKX2.5	WTAAKWK	6.75×10^{-03}		MotifMap
NKX2.5	YBYCACTTSM		4.28×10^{-03}	MotifMap

These findings led us to take a closer look at MEIS1 targets. When comparing MEIS1 ChIP-Seq data publicly available from murine embryonic trunk to TBX5 ChIP-Seq data, MEIS1 shows some overlap with the TBX5 peaks (Figure 24A - analysis run by Lavanya Iyer). The overlapping peaks are related to regions annotating to cardiac morphogenesis and function (Figure 24B).

To gain more insights on the relationship between TBX5 and MEIS in the adult heart we performed ChIP-qPCRs for TBX5 and MEIS1 on different TBX5 targets (8.4 for information on the selected targets) in control and KO mice (ChIP and qPCRs were performed by Lavanya Iyer). We firstly found that no target sequence was bound by TBX5 in the *vTbx5*KO hearts (Figure 24C), thereby validating the newly identified targets.

Secondly, TBX5 presence influenced MEIS1 binding patterns. Three effects could be distinguished: On a first group of targets the binding of MEIS1 was diminished in the *vTbx5*KO hearts (Figure 24C - *Scn5a, Chrm2*) indicating a dependance on TBX5 presence. The second group of targets showed enhanced binding in the absence of TBX5 (Figure 24C - *Gja1, Gpr22*) pointing towards a competitive action of both factors. The third group did not display significant effects of TBX5 presence (Figure 24C - *Fhl2, Kcnj5, Cacna1g*).

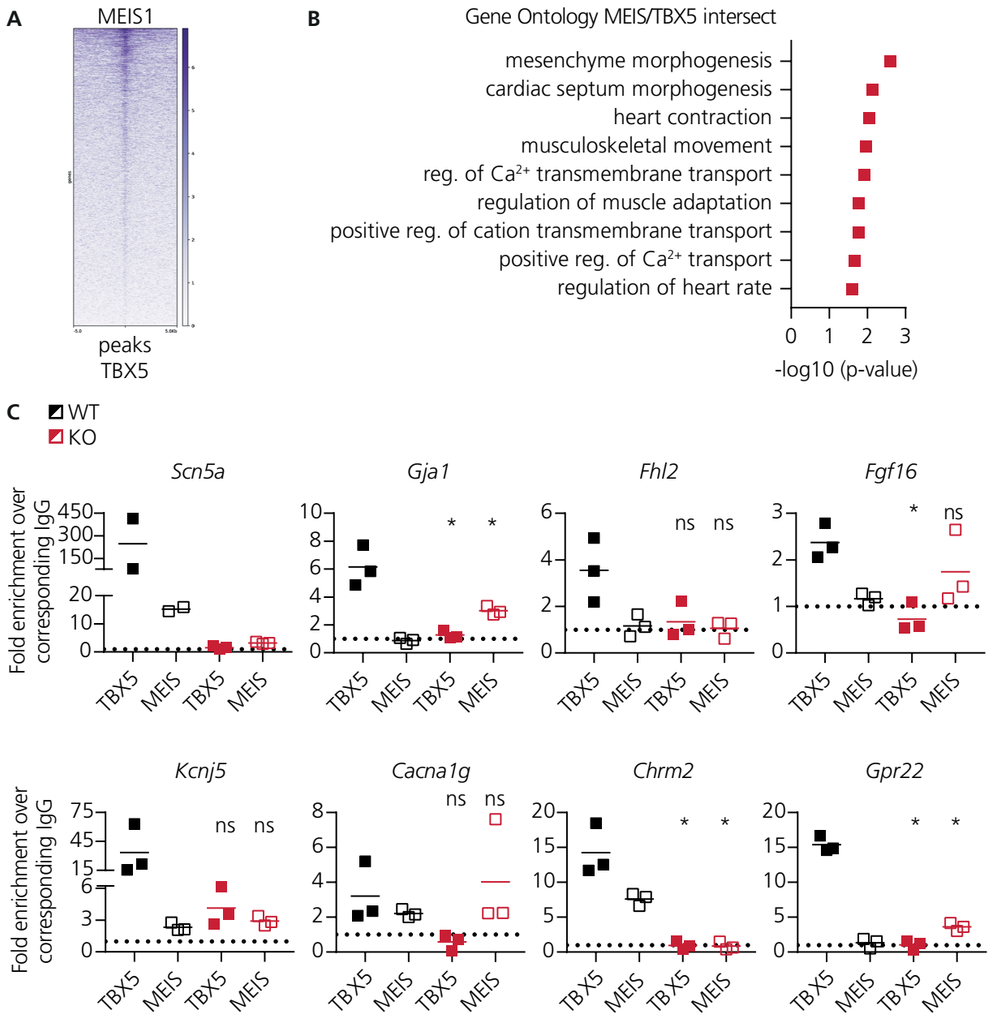

Figure 24. Chromatin occupancy by MEIS1 and TBX5 A. MEIS1 binding is enriched on TBX5 peaks. MEIS1 ChIP-Seq from E11.5 embryonic trunks [Penkov et al., 2013] **B.** Peaks from the intersect of MEIS1 and TBX5 bound regions are annotated with cardiac morphogenesis and heart contraction. **C.** ChIP-qPCRs in WT and KO hearts showed that TBX5 binding is diminished in the KO hearts. MEIS binding patterns change in the absence of TBX5. Experiments were performed by Lavanya Iyer **Statistics:** C. Unpaired students t-test was used to compare the enrichment in the KO hearts with the WT control hearts individually for each factor. p-value-summary: * - <0.05

8.6. Re-expression of TBX5

We established that TBX5 KO leads to conduction disturbances and diastolic dysfunction and this is mediated by the transcriptional dysregulation of several transcripts and their encoded proteins. Next, we tested if the reintroduction of TBX5 in the heart can lead to a reversal of the molecular consequences and thereby rescue the phenotype.

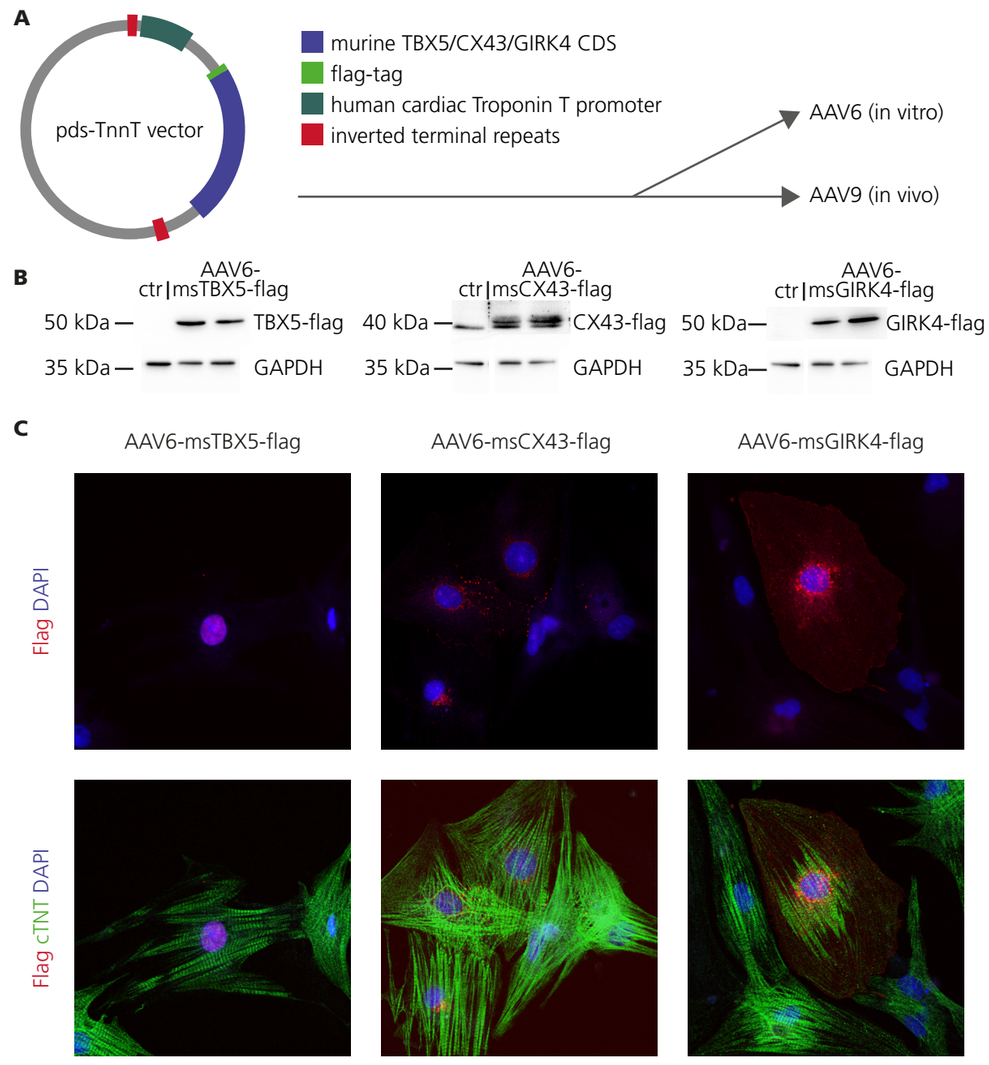

Figure 25. AAV6-*in vitro* validation in neonatal rat cardiomyocytes A. The coding sequences for TBX5/CX43/GIRK4 were flag-tagged and introduced into the pds-TnnT vector under the control of a *TnnT* promoter. **B.** Neonatal rat cardiomyocytes were transduced with adeno-associated virus serotype 6 at a multiplicity of infection of 100.000. Expression analyses by immunoblot showed a successful transduction **C.** TBX5-flag is localized in the nucleus of the NRCMs; CX43 appears mainly at connections between the cardiomyocytes. KIR3.4 showed a dotted expression mainly perinuclear.

To reintroduce TBX5 and its target genes into the hearts of *vTbx5*KO mice, we used adeno-associated virus (AAV) (5.6 for details). The coding DNA sequence of murine TBX5, CX43 and GIRK4 was tagged with a flag-tag and cloned into the pds-TnnT vector, which allows cardiomyocyte-specific expression (Figure 25A). This vector can be used to generate AAV6 for *in vitro* and AAV9 for *in vivo* transduction with a cardiac tropism.

8.6.1. *In vitro* validation

To test the expression prior to *in vivo* experiments, AAV6 were generated to infect neonatal rat cardiomyocytes in vitro. Protein expression of TBX5, CX43 and GIRK4 could be detected by immunoblot (Figure 25B). The correct intracellular localization was confirmed by immunofluorescence (Figure 25C). TBX5 localized in the nucleus whereas CX43 localized at cell-to-cell junctions and GIRK4 localized at the cell surface/perinuclear.

8.6.2. *In vivo* re-expression

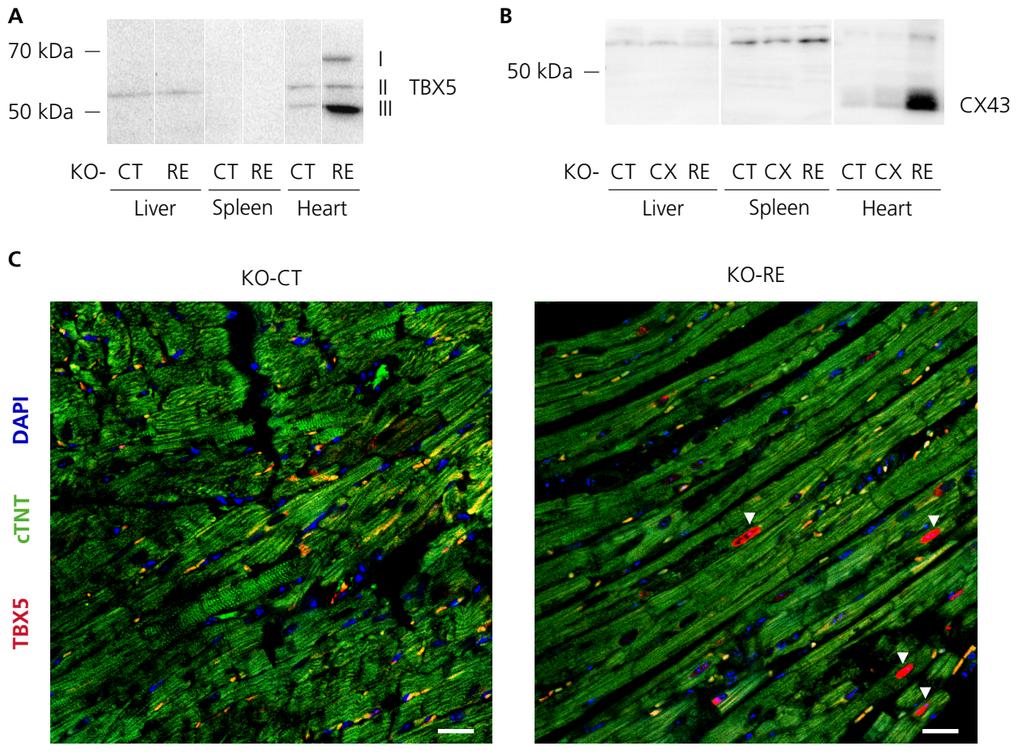

Figure 26. AAV9-mediated TBX5 delivery leads to cardiac specific re-expression of TBX5 A. Immunoblot analysis directed against TBX5 revealed a specific re-expression in the heart upon AAV9-TBX5 delivery (KO-RE) compared to AAV9-LUC (KO-CT). Band I represents the flagged-tagged TBX5, band III the endogenous TBX5, Band II is unspecific staining. **B.** AAV9-CX43 (KO-CX) did not lead to a detectable CX43 expression, but AAV9-TBX5 did. **C.** In the KO-RE hearts, TBX5 is expressed in the nuclei of cardiomyocytes (white arrowheads). Scale bar: 20 µm Immunostaining performed by Yelena Sargsyan.

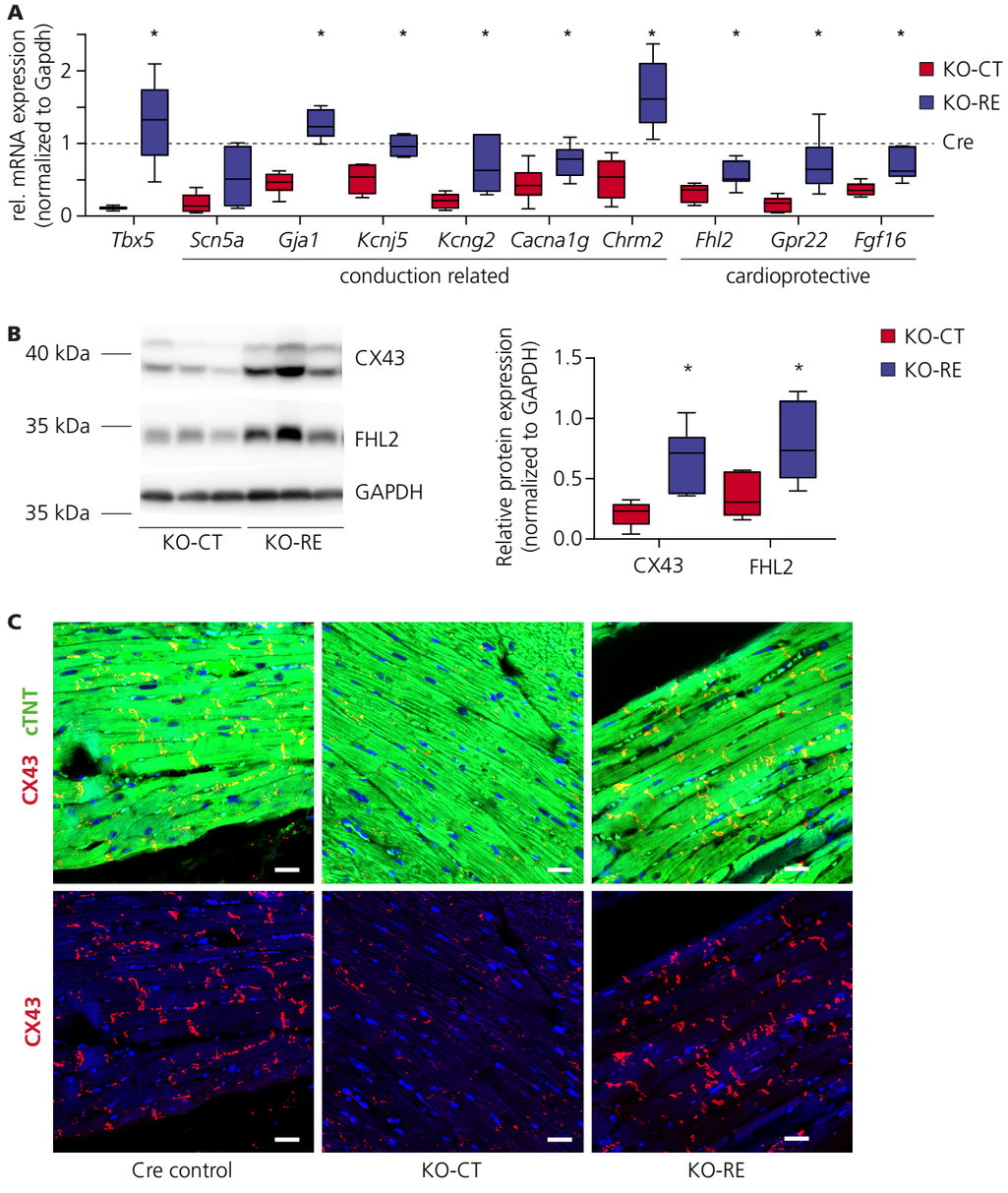

Figure 27. *In vivo* re-expression of TBX5 restores TBX5 mediated transcription A. The transcript levels of newly identified ventricular TBX5 targets are significantly enhanced by TBX5 re-expression (KO-RE, blue) as compared to control groups (KO-CT, red). The only target that was not significantly induced was *Scn5a*. **B.** CX43 and FHL2 protein levels are increased by TBX5 re-expression determined by immunoblot with densitometric quantification **C.** Representative immunofluorescence picture detected CX43 at the intercalated disks of KO-RE ventricles similar to Cre controls. In contrast, KO-CT ventricles show almost no CX43 expression. **Statistics:** A, one-way-ANOVA for each transcript; B, Student's-t-test. * $p < 0.05$ vs. KO-CT.

After *in vitro* validation of the AAV6 constructs, we used AAV9 to re-express TBX5 *in vivo*, after inducing TBX5 KO. TBX5 protein was found to be expressed in the heart, but not in the liver or spleen (Figure 26A) of re-expression mice (KO-RE). AAV9-TBX5 delivery could induce expression of CX43, but AAV9-CX43 could not (Figure 26B). Moreover, TBX5 was localized in the nuclei of cardiomyocytes in the KO-RE mice (Figure 26C).

As a consequence of the TBX5 re-expression in the cardiomyocyte nuclei, we expected re-expression of its target genes. Quantitative qPCR for mRNA expression showed a robust re-expression of *Tbx5* itself along with its targets *Gja1*, *Kcnj5*, *Kcng2*, *Cacna1g*, *Chrm2*, *Fhl2*, *Gpr22* and *Fgf16* (Figure 27A) comparable with Cre controls.

Exemplary, we confirmed the expression of the targets CX43 and FHL2 by immunoblot, showing a similar re-expression on protein level (Figure 27B). In the KO-RE hearts CX43 was distributed homogeneously throughout the myocardium and correctly located within the cell at comparable levels to Cre controls, whereas its expression was almost absent in KO-CT hearts (Figure 27C).

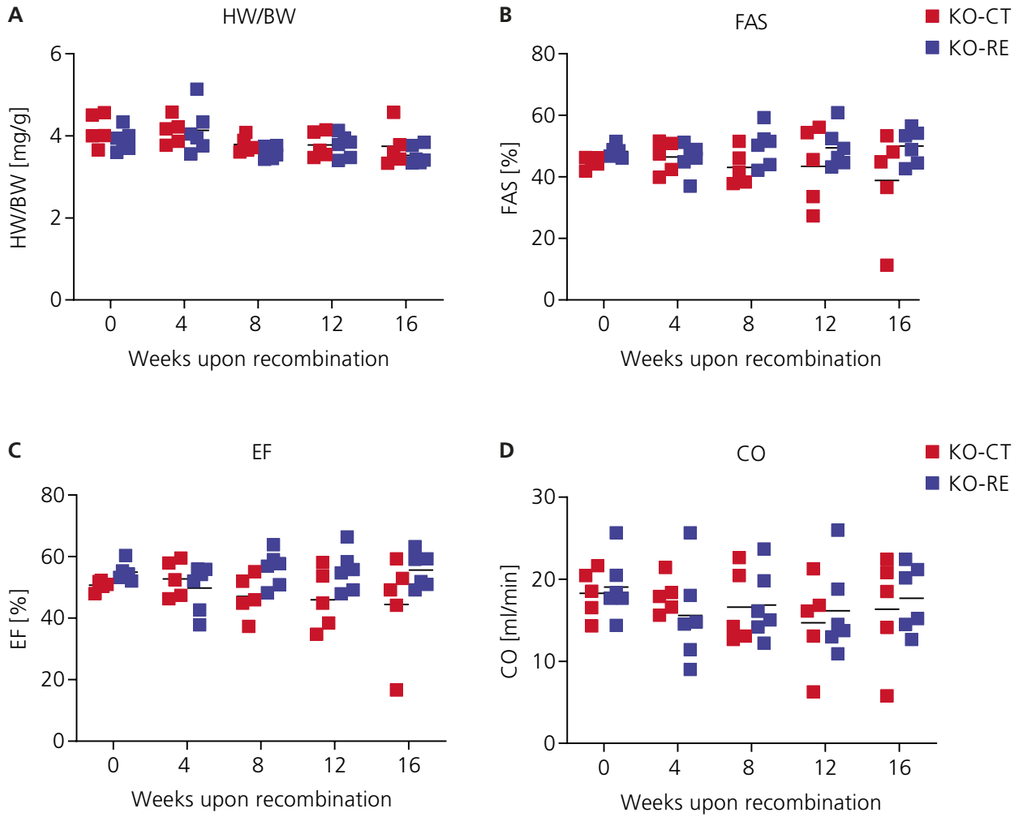

Figure 28. *In vivo* TBX5 re-expression has no significant effect on functional parameters measured by echocardiography No statistical differences could be observed between KO-CT and KO-RE groups, neither for HW/BW ratio (**A**), FAS (**B**), EF (**C**) or CO (**D**) **Statistics:** Two-Way ANOVA (repeated measures)

After verifying that the molecular signature is reversed after re-expression of TBX5, we performed echocardiography analysis over a time course of 16 weeks after recombination. None of the measured parameters showed any statistical differences between the KO group receiving the control AAV and the KO group receiving AAV9-TBX5 (Figure 28) due to the low number of mice. Although not statistically significant, the KO-CT mice showed a tendency of progressive deterioration of cardiac function at 12 - 16 weeks measured by FAS and EF (Figure 28B and C). The contractile function of the KO-RE mice remained stable over time.

As a consequence of normalized target gene expression, a rescue of the arrhythmic phenotype seen in the TBX5-KO mice (8.2.2 for details) would be expected. Thus, we examined the cardiac rhythmicity of Cre control, KO-CT and KO-RE hearts over 1000 consecutive beats using Poincaré RR-plots and calculation of the standard deviation 1 (SD1). Indeed, KO-RE mice show a more regular beating pattern than KO-CT mice, represented by a smaller SD1(-Figure 29A-C). Moreover, TBX5 re-expression was able to reduce the prolongation of the QRS interval caused by the KO of TBX5 (Figure 29D).

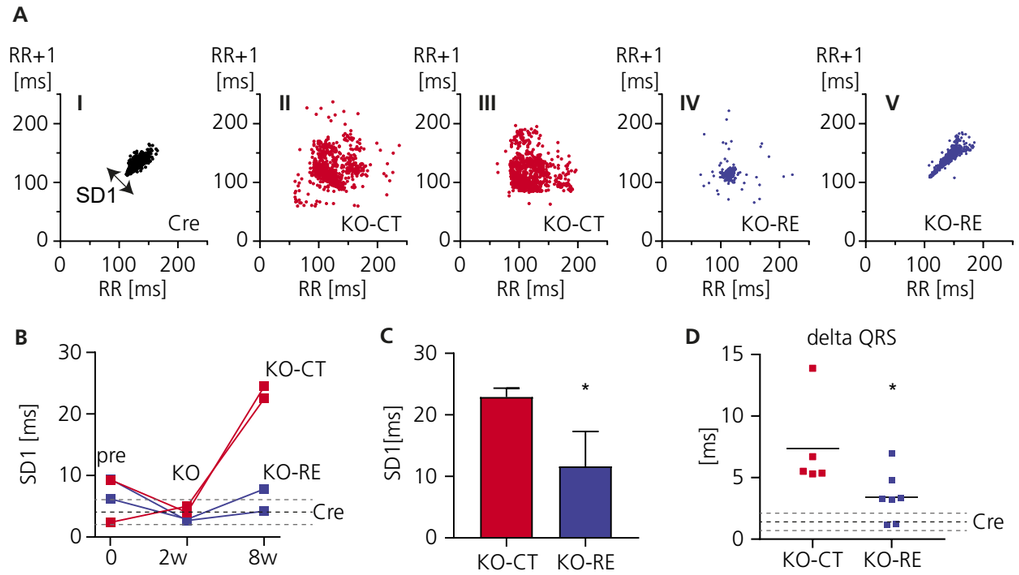

Figure 29. *In vivo* TBX5 re-expression rescues arrhythmic phenotype of *vTbx5*KO mice A. Heart-rate-variability (HRV) represented by Poincaré plots is lower in KO-RE indicative of less AV blocks than KO-CT. 1000 consecutive beats per mouse/plot. **B,** The Poincaré plots were statistically analysed with HRVAS [Ramshur, 2010]. Standard deviation of the HRV (SD1) increased in KO-CT mice with time, while remaining stable in KO-RE mice. Dashed lines indicated Cre-average values ± SEM. **C.** Statistical analysis of SD1 from HRV analysis, shows significantly lower HRV in KO-RE vs. KO-CT mice. **D.** QRS prolongation in the KO-RE mice is partially reversed after TBX5 re-expression. **Statistics:** C+D: Student's-t-test. * $p < 0.05$ vs. KO-CT.

Although the low number of mice did not allow a thorough survival study, it is important to note, that all KO-RE mice (n=5) survived at least 170 days after recombination, whereas 2 out of 6 KO-CT mice died during that time span.

In summary, larger studies including more animals are needed to prove if the TBX5 normalization can improve contractile function and survival. But this study could already show that TBX5 normalization can restore target gene expression and rescue the arrhythmic phenotype.

9. Discussion

The major global health burden of cardiac disease requires new therapies. Interestingly the transcription factor TBX5, which was mainly investigated in the context of development, has recently been found dysregulated in cardiac disease [Baurand Anthony et al., 2007], [Horton et al., 2016] (own unpublished data) (5.5.2 for details). Therefore, we hypothesized that TBX5 could be required for homoeostasis of the working myocardium and its dysregulated expression in cardiomyopathies contributes to a deterioration of cardiac function. In order to proof this, we investigated the phenotypical and molecular consequences using an inducible cardiac specific TBX5 KO mouse model.

9.1. Basic Phenotype of the *vTbx5*KO mice

9.1.1. Ventricular specific recombination

The aforementioned model was generated by mating the TBX5$^{LDN/LDN}$ model (harbouring loxP sites flanking Exon 3 of the *Tbx5* gene) with the *Myh6*-MerCreMer mouse strain, in which the expression of the tamoxifen-inducible Cre recombinase is controlled by the *Myh6*-promoter. This promoter is supposedly active in all types of cardiomyocytes [Lyons et al., 1990] and thus the MerCreMer should be expressed in the whole heart. Indeed, we found Cre expression in the nuclei of atrial and ventricular tissue (7.1.1 for details). A number of publications, including the first description of the *Myh6*-MerCreMer mouse strain [Sohal Dawinder S. et al., 2001] show recombination throughout the whole heart. But to our surprise, robust TBX5 recombination did not occur in atrial cardiomyocytes, but was restricted to the ventricles. Inefficient atrial recombination in adult *Myh6*-MerCreMer mice has been described previously [Shen et al., 2011] [Hsieh et al., 2007].

Interestingly, in embryonic and early postnatal stages high atrial recombination efficiency was described, but the same study showed low efficiency in the atria at postnatal day 12 [Sereti et al., 2018]. The same decreasing atrial recombination efficiency was observed, when MerCreMer was inserted after the endogenous *Myh6*-promoter into the locus [Yan et al., 2015] and even the original publication showed stronger atrial recombination at the age of 17 days compared to three months old mice [Sohal Dawinder S. et al., 2001]. In line with these observations, a recent publication showed much lower reporter gene expression under the control of a *Myh6*-promoter in atria compared to ventricles in 6 week old mice [Carroll et al., 2016].

Another factor influencing the recombination efficiency could be the genetic background of the mice. The original characterization of the *Myh6*-MerCreMer mouse was performed in the FVB mouse strain and showed atrial recombination [Sohal Dawinder S. et al., 2001]. After the initial characterization these mice were backcrossed into a background of C57BL/6SV129. These mice were mated with ZEG mice and C57BL/6J mice to generate a transgenic model which showed no atrial recombination [Hsieh et al., 2007]. The other study demonstrating inefficient atrial recombination used a mixed 129 / black swiss background [Shen et al., 2011], the study showing differences in atrial recombination depending on the developmental stage used an undefined mixed background [Sereti et al., 2018] and the *vTbx5*KO mice were maintained in a C57BL/6N strain.

These data suggest that atrial recombination efficiency might be due to reduced Cre expression in the atria depending on the development stage and further influenced by differences in the genetic background of the mice that greatly varied among studies.

Although we cannot fully explain the molecular background of this compartment specific recombination, it provides us with a model to specifically study the role of TBX5 in the adult working myocardium.

9.1.2. Reduced heart growth and diastolic dysfunction

To study the functional consequences of the ventricular loss of TBX5 we performed a time series of echocardiographic examinations. This revealed that the *vTbx5*KO mice had no physiological heart growth after recombination and cardiac function deteriorated over time indicated by a decrease of ejection fraction and diastolic volume (8.2.1 for details). These observations show a more severe phenotype compared to a heterozygous constitutive KO model. This model was observed with reduced ventricular diameter and prolonged relaxation, but no changes in contractile function [Zhou et al., 2005] in contrast to the *vTbx5*KO. Because these heterozygous mice had mostly presented cardiac structural abnormalities, another study investigated the cardiac function in mice with a haploinsufficient KO of TBX5 under the control of *Nkx2.5*-Cre. These mice did not have atrial or septal defects, but still suffered from diastolic dysfunction, indicated by lower E/A ratio as well [Zhu et al., 2008]. Both studies using haploinsufficient mice did not find problems in systolic function and fractional shortening was unchanged. Our study confirmed the previously shown diastolic dysfunction and reduced end-diastolic ventricular dimension, but also found a reduced ejection fraction. This can be explained by the homozygous loss of TBX5 from the ventricles, but also by the extended time period in our study (16 weeks after KO - 28-30 weeks of age; whereas the other studies used 8-10 week old mice). Both circumstances might lead to the development of a more severe phenotype.

9.1.3. Conduction defects, arrhythmia and sudden cardiac death

Because of the known association of TBX5 with cardiac rhythm and arrhythmias observed during echocardiographic analysis, we examined the cardiac rhythm of the *vTbx5*KO mice by telemetric electrocardiography. The *vTbx5*KO mice presented conduction defects and arrhythmia, most prominently slower signal propagation (8.2.2).

Similar conduction problems also occur in constitutive globally haploinsufficient KO models with a varying range of TBX5 expression levels summarized by [Mori et al., 2006], mainly describing prolonged PQ-intervals, third degree AV-Block, sinoatrial pauses and tachycardia.

Inducible removal of TBX5 from the cardiac conduction system (CCS) leads to conduction problems and SCD, but only ~25% of the mice die up until 300 days after recombination [Arnolds et al., 2012]. In our model, 60% of the mice died until 150 days after recombination

was induced. Nevertheless, QRS- and PR-interval duration in both models were comparable (QRS CCS-KO: 15.3 ± 2.6; *vTbx5*KO: 17.6 ± 1.9; PR CCS-KO: 51.8 ± 1.2; *vTbx5*KO: 48.3 ± 4.5). This indicates, that TBX5 plays an important role for cardiomyocyte homoeostasis beyond the conduction system.

A study focusing on the effects of TBX5-loss in the atria used an inducible global TBX5-KO model [Nadadur et al., 2016]. This led to irregular heart rate and atrial fibrillation. The authors observed ventricular arrhythmias happening at later time points than atrial arrhythmias and thus claimed, that they are only a secondary effect of the atrial arrhythmias [Nadadur et al., 2016]. However, after observing several ventricular arrhythmias in the absence of atrial recombination and atrial fibrillation, we hypothesised, the ventricular arrhythmias, although less prominent, are a direct effect of ventricular TBX5-loss.

Besides the PR- and QRS-prolongation, we found a prolongation of the QT-interval in the *vTbx5*KO hearts, which would be indicating a prolonged repolarisation phase in the human ECG. However, the action potential duration measured in isolated *vTbx5*KO hearts was unchanged. Indeed, in mice the measurement of the QT-interval is problematic due to the fast cardiac cycle in the murine heart [Zhang et al., 2014]. QT-prolongations can be a consequence of a longer QRS-complex, therefore a sign of slower signal propagation occurring in the *vTbx5*KO model.

9.2. Integrative Target Gene Analysis

After we found that a homozygous loss of TBX5 in the adult ventricle leads to reduced heart growth, diastolic dysfunction, arrhythmia and sudden cardiac death, we intended to investigate the underlying molecular mechanism. Therefore, we aimed to uncover the chromatin binding sites of TBX5 in the adult ventricle and to reveal the differentially regulated genes in *vTbx5*KO vs. control hearts.

This RNA-Sequencing revealed upregulated genes, that were not directly linked to the contractile and conduction defects of the *vTbx5*KO mice, but were instead related with blood coagulation. Since TBX5 is neither known to be involved in blood coagulation nor to be expressed in thrombocytes, the appearance of this gene cluster can probably be attributed to blood clots observed in the atria of the *vTbx5*KO mice. These clots are possibly an adverse effect of abnormal blood flow caused by the arrhythmia and diastolic dysfunction. Diastolic dysfunction is associated with bigger atrial volumes [Pritchett et al., 2005][Aouar et al., 2013]. Along with the atrioventricular block observed in the *vTbx5*KO mice, this might lead to problems with the ejection of blood from atria to ventricles resulting in blood clotting. In contrast to the upregulated genes that were not clearly connected to the phenotype, the downregulated targets are directly implicated in heart contraction and electrophysiology.

In addition to the analysis of differentially regulated genes upon TBX5 loss, we established a protocol for chromatin immunoprecipitation of TBX5 from adult heart tissue to detect a direct transcriptional regulation by TBX5. Although TBX5 ChIP-Seq results have been published

from immature cells like differentiated cardiomyocytes [Luna-Zurita et al., 2016] or embryonic heart [Steimle et al., 2018], we decided on an adult ventricular specific analysis, since the targets of TBX5 in the adult heart might be different from early developmental stages

The sequencing of this TBX5-bound chromatin showed the TBX5 genomic occupancy in the adult heart. In line with previous studies (5.2.4 for details) proving the interaction of TBX5 with NKX2.5 and GATA4, we found a correlation between the binding regions of those transcription factors as well as an enrichment of their corresponding motifs in the TBX5 peaks. Not only did TBX5 occupancy overlap with other transcription factors, but also with marks of active enhancers. Accordingly, the TBX5-bound regions marked by active enhancers showed a greater overlap with the genes downregulated (47 of 97) in the *vTbx5*KO hearts compared to the upregulated genes (7 out of 93) detected by transcriptomic analysis. This points towards a rather transcriptionally activating role of TBX5 in the adult heart. Indeed, the transcriptionally repressive role of TBX5 has so far been established in the developmental stage only [Waldron et al., 2016].

9.3. TBX5 targets

The aforementioned novel targets of TBX5 include transcripts important for cardiac conduction, cardioprotection and cardiomyocyte structure. These affected transcripts might be crucial to understand the phenotype of the *vTbx5*KO mice, since they show conduction defects, exacerbated hypertrophic response upon stress [Renger, 2012] and problems with cardiomyocyte growth.

9.3.1. TBX5 targets implicated in cardiac conduction

9.3.1.1. *Gja1*

One of the identified targets with a severely reduced expression in the *vTbx5*KO was *Gja1* (encoding for CX43), the dominant gap junction protein in the adult ventricle (5.3.1.2 for details). This severely reduced expression can explain the significantly slower ventricular conduction and incidence of SCD, since loss of CX43 leads to arrhythmias and SCD as well [Gutstein et al., 2001].

Since [Nadadur et al., 2016] already identified *Gja1* as a target of TBX5 in the atria, they looked for a specific enhancer and investigated this putative enhancer (mm9 chr10:88816980–88817471). Activation of this candidate enhancer by TBX5 was confirmed, although no direct link of this enhancer to *Gja1* expression was established. We could not detect binding of TBX5 to this enhancer in TBX5-ChIP-Seq neither in adult ventricular myocardium nor in the embryonic [Steimle et al., 2018] nor in differentiated cardiomyocytes [Luna-Zurita et al., 2016]. However, the binding might be tissue-specific. Instead, the enhancer we identified as a candidate enhancer for *Gja1* in the ventricular myocardium is significantly closer to the gene body (although still 600 kb away) in contrast to 32 mb and consistent over all published TBX5-datasets. Moreover, this enhancer has been found to drive embryonic expression specifically in the heart (data from Vista enhancer browser [Visel et al., 2007], ID mm74). These

results strongly suggest that this enhancer downstream of the *Gja1* gene body mediates TBX5-initiated expression.

9.3.1.2. *Kcnj5*

Along with *Gja1, Kcnj5* was suggested as a TBX5 target gene in the atria as well, because of its reduced expression upon TBX5 loss [Nadadur et al., 2016]. Indeed, we found reduced *Kcnj5* expression in the ventricles of *vTbx5*KO mice as well. Moreover, we showed transcriptional activation by TBX5 on an enhancer located less than 1 kb downstream of the *Kcnj5* gene (8.6.1 for details).

Kcnj5 is expressed in atria and ventricles. Although it contributes to repolarisation in both compartments, its expression and its functional relevance seem to be higher in the ventricle [Liang et al., 2014] [Anderson et al., 2018]. *Kcnj5* KO mice show no difference in their basal heart rate, but react differently to parasympathetic stimuli [Wickman et al., 1998] [Anderson et al., 2018]. Consistent with that, *vTbx5*KO mice do not show differences in their basal heart rate. KCNJ5 is associated with long-QT syndrome in humans and long-QT syndrome is a risk factor for SCD [Yang et al., 2010]. The *vTbx5*KO mice showed longer QT-intervals as well, but since in mice this is not always indicative of a prolonged repolarisation phase (9.1.3 for details), it requires further investigation if aberrant *Kcnj5* expression is contributing to the SCD phenotype observed in our study.

9.3.1.3. *Kcng2, Cacna1g* and *Chrm2*

Three other genes dysregulated in the *vTbx5*KO model, bound by TBX5 and related to electrophysiology are *Kcng2, Cacna1g* and *Chrm2.*

Kcng2 encodes for potassium voltage-gated channel, subfamiliy G, member 2 and is dysregulated upon TBX5 loss in the atria as well [Nadadur et al., 2016]. This protein is a subunit of a propafenone-sensitive potassium-channel expressed in the heart [Zhu et al., 1999]. It is not known, how it is regulated and how relevant it is for cardiomyocyte electrophysiology.

Cacna1g encodes for calcium channel, voltage-dependent, T-type, alpha 1G subunit, a subunit of a T-type calcium channel on the surface of cardiomyocytes. A KO of *Cacna1g* leads to adverse cardiac remodelling upon cardiac stress, with more hypertrophy and disturbed electrophysiology [Le Quang Khai et al., 2013], reviewed by [Fabritz et al., 2011].

Polymorphisms in the cholinergic receptor, muscarinic 2, cardiac (*CHRM2)* gene are significantly associated with the heart rate adjustment and cardiac death [Hautala et al., 2009]. Patients with a missense mutation in *CHRM2* present with dilated cardiomyopathy, suffer from arrhythmia and are at higher risk for sudden cardiac death [Zhang Lin et al., 2008].

Because a number of transcripts with a role in cardiac electrical signal propagation show a reduced expression in the *vTbx5*KO model, the slower signal propagation of the hearts can be explained. We hypothesise, that *Gja1* plays the main role in the slower signal propagation, but disturbed expression of *Kcnj5*, *Kcng2*, *Cacna1g* and *Chrm2* is likely to further increase the risk for arrhythmia and sudden cardiac death.

9.3.2. TBX5 target genes with a role in cardioprotection

Besides the genes implicated in cardiac electrophysiology, we identified targets known to protect the heart from cardiac stress:

9.3.2.1. *Fhl2*

Firstly, *Fhl2* has been found to be downregulated upon TBX5 loss by us and others [Mori et al., 2006]. *Fhl2* increases upon β-adrenergic stress induced by Isoproterenol [Hojayev et al., 2012]. Moreover, *Fhl2*KO-hearts respond to this cardiac stress by increased hypertrophy, indicated by higher HW/BW ratio and elevated ANP and BNP levels [Hojayev et al., 2012][Kong et al., 2001]. FHL2 in turn induces TBX5 expression by direct activation of the TBX5 promoter [Renger, 2012].

9.3.2.2. *Gpr22* and *Fgf16*

Secondly, *Gpr22* is an orphan G-protein coupled receptor mainly expressed in the heart and brain with reduced expression after TAC [Adams et al., 2008] and upon TBX5 loss. A global KO of *Gpr22* leads to exacerbated cardiac function upon aortic banding [Adams et al., 2008].

Finally, we show that fibroblast growth factor 16 (*Fgf16*) expression is reduced upon TBX5 loss. This is in agreement with previous studies, showing *Fgf16* expression to be activated by GATA4 [Yu et al., 2016]. FGF16 itself represses *Nppa* and *Nppb* and overexpression of FGF16 protects the hearts from cryoinjury [Yu et al., 2016].

9.3.2.3. Cardiac function of *vTbx5*KO mice upon cardiac stress

Due to these cardioprotective factors being expressed at reduced levels in the *vTbx5*KO model, it would be plausible, if those hearts show increased response to cardiac stress. Indeed, when *vTbx5*KO mice are treated with Angiotensin II, they respond with a decrease in ejection fraction (EF) and increase in hypertrophy [Renger, 2012]. Furthermore, hypertrophy occurs at a single cell cardiomyocyte level by an increase in cross-sectional area [Renger, 2012]. At the same time, the hearts react by developing fibrosis at a higher extent than the hearts of Flox mice [Renger, 2012].

We hypothesise that this phenotype can be explained by the dysregulation of *Fhl2*, *Gpr22*, *Fgf16* and potentially *Cacna1g* and that those factors might be relevant for the diastolic dysfunction of the *vTbx5*KO model in general.

9.3.3. TBX5 target genes with other functions

To gain further insight into the role of TBX5 in cardiac homoeostasis we looked into novel target genes possibly important in cardiac remodelling.

9.3.3.1. *Armh4*

One of the most down-regulated transcripts in the TBX5 KO was *Armh4* (armadillo-like helical domain containing 4). We verified, that it is downregulated on mRNA and protein level and identified two possible TBX5 binding sites in its promoter region. ARMH4 was found to be expressed in the z- and intercalated discs of cardiomyocytes (8.4.1 for details).

Armh4 was initially identified during mESC differentiation to cardiomyocytes [Christoforou et al., 2008]. *In situ* hybridization verified transcript expression rising in embryonic heart at E7.5 [Christoforou et al., 2008]. Public data (EUREXPRESS DATABASE) show that in the mouse embryo the transcript expression of *Armh4* and *Tbx5* strongly correlate at dorsal root ganglia, retina, and regions of the brain suggesting a link between the two proteins that is not only restricted to the heart.

Interestingly, the human homologue of ARMH4 is predicted to be a glycosylated single pass membrane protein type I (similar to beta subunits of sodium channels, integrins and cadherins) (Uniprot) [Huttlin et al., 2017]. In human leukaemia cells ARMH4 (in this context named upstream of mTORC2 (UT2)) inhibits RICTOR, a component of the mTORC2 signalling complex [Lee et al., 2014]. Additionally, ARMH4 interacts with GP130 to inhibit phosphorylation of STAT3, thereby reducing cytokine signalling in hematopoetic malignancies [Lee et al., 2016]. Both studies detected UT2 to act as a tumorsuppressor, resulting in reduced proliferation and prolonged survival.

A conditional cardiomyocyte-specific Rictor KO mouse model simulates mTORC2 up-regulation [Shende et al., 2016]. These mice have normal survival and cardiac function on a basal level, but upon cardiac stress by transaortic constriction (TAC) they show dilation and reduced ejection fraction and fractional area shortening already one week after TAC, when control mice are only in the compensatory phase of hypertrophy [Shende et al., 2016].

The function of ARMH4 in the heart remains unknown so far, but if it interferes with mTORC2 signalling in the heart in a similar manner like in leukaemia cells, its KO might be protective upon cardiac stress.

9.3.3.2. *Cmya5*

Cmya5 (Cardiomyopathy associated 5) encodes for the Myospryn protein and its expression is regulated by MEF2A [Durham et al., 2006]. *Cmya5* expression is altered after aortic banding [Knyazeva et al., 2019] and an association between a polymorphism in the *CMYA5* gene (rs2278239) and cardiac disease has been found [Nakagami et al., 2007]. Myospryn interacts with ryanodine receptors and plays a role in their assembly in the sarcoplasmic reticulum [Benson et al., 2017].

9.3.3.3. *Emilin2*

Emilin2 (Elastin microfibril interface located protein 2) has been identified as a protein on the cardiomyocyte cell surface [Van Hoof et al., 2010]. A loss of *Emilin2* leads to congenital cardiac anomalies, like ventricular septal defects, atrioventricular canal defects and hypoplastic ventricles potentially through interference with the TGF-β1 pathway [Guggilam et al., 2016]. *Emilin2* expression is upregulated upon isoproterenol induced hypertrophy [Molojavyi et al., 2010].

9.3.3.4. *Pdlim4*

Pdlim4 (PDZ and LIM domain 4) directly interacts with F-actin [Vanaja et al., 2009]. It is expressed in the heart at higher levels than in skeletal muscle [Komurcu-Bayrak et al., 2012].

There is no information on the function of *Pdlim4* in the heart, but it might play a role in cytoskeleton organisation.

Although a possible implication of *Armh4, Cmya5, Emilin2* and *Pdlim4* in cardiac remodelling requires more in depth studies of their function, observations indicate that these proteins are expressed in cardiomyocytes and show aberrant expression in the context of disease or are even directly linked to a cardiomyopathy phenotype. The dysregulation of these factors in the *vTbx5*KO hearts probably contributes to a worsening of the phenotype.

9.4. Chromatin Occupancy of TBX5

As no chromatin occupancy studies of TBX5 have been performed in adult hearts, we were interested to compare our model to existing studies examining chromatin binding properties of TBX5 in mouse, using embryonic hearts from E9.5 [Steimle et al., 2018], *in vitro* differentiated cardiac progenitor cells / cardiomyocytes [Luna-Zurita et al., 2016] or overexpressed tagged-TBX5 protein in the HL-1 cell line [He et al., 2011]. Specifically, we were interested to examine differences and similarities between these and our dataset. This could allow insights into stage-specific functions of TBX5.

In the adult heart TBX5 shows enriched binding to promoter, 5'UTR, intronic and downstream of the gene body regions compared to the genome background (8.3.1 for details). This is comparable to the data from E9.5 hearts [Steimle et al., 2018] and HL1-cells [He et al., 2011], both showing enrichment of promoter and downstream peaks (Table 37). However, TBX5 promoter binding was less in differentiated cardiac progenitor cells and cardiomyocytes [Luna-Zurita et al., 2016]. This might be confounded by differences in the methods, since these differentiated cells were subjected to ChIP-Exo resulting in narrower peaks.

Although the datasets obtained from heart tissue show overlapping peaks on regions active both in the embryonic and adult state, they have distinct binding patterns. A high number of regions is highly conserved for all published TBX5 datasets [Steimle et al., 2018], [He et al., 2011], [Luna-Zurita et al., 2016] like the *Scn5a*, *Gja5*, *Gja1*, *Kcnj5*, *Cacna1g*, *Fhl2* and *Cmya5* enhancer. Other regions are exclusively bound in the embryonic (e.g. *Wnt2*, *Fgf10*, *Rictor*) or in the adult stages (*Fgf16*, other *Scn5a* enhancers). Interestingly, in the immature stages TBX5 shows higher affinity to regions related to differentiation and development, whereas in the adult stages the affinity to regions related with cardiac homoeostasis and electrophysiology is higher (Table 37).

This allows the conclusion that factors implicated in cardiac electrophysiology are regulated by TBX5 independent of the developmental stage, although they are partially bound on different enhancers. In the immature stages enhancers involved in muscle development and cardiac morphogenesis require activation by TBX5. In contrast, the adult heart requires a stronger emphasis on cardioprotective factors indicated by stronger binding of *Fhl2*, *Fgf16* or *Emilin2*.

Table 37. Comparison of different TBX5-ChIP-Seq datasets

sample	adult ventricle	E9.5 hearts	cardiomyocytes	cardiac progenitor cells	HL-1 cells (overexpression of tagged TBX5)
number of peaks	8849	3534	8952	4985	55872
percentage of genes	34.0%	21.0%	35.0%	23.0%	73.0%
promoter < 3kb	10.9%	11.2%	3.4%	2.5%	11.4%
downstream < 3kb	2.9%	2.9%	2.4%	2.4%	3.9%
intronic	45.8%	40.6%	47.7%	44.2%	44.3%
Coding exon	2.3%	3.1%	2.2%	1.4%	10.4%
GO Biological Processes	Actin filament-based process, muscle cell development, regulation of heart contraction	Chromatin assembly or disassembly, cardiac muscle tissue development, epigenetic regulation of gene expression	Striated muscle cell development, muscle cell development, cardiac cell development	Cardiac chamber morphogenesis, heart morphogenesis, cardiac muscle tissue development	Heterochromatin organization, regulation of generation of precursor metabolites and energy, regulation of mitochondrial membrane permeability
Reference	own unpublished data	[Steimle et al., 2018]	[Luna-Zurita et al., 2016]	[Luna-Zurita et al., 2016]	[He et al., 2011]

9.5. Biological interaction between MEIS1 and TBX5

Because *de novo* motif analysis of the adult TBX5 ChIP-Seq data showed a strong enrichment of a motif similar to MEIS1/2 motifs, we became interested in looking into a possible relationship between the two transcription factors. The MEIS1 motif core (TGACAG) had been found previously in ChIP-Exo against TBX5 in cardiac progenitor cells and cardiomyocytes [Luna-Zurita et al., 2016]. The authors suggested, this finding could be attributed to its close similarity to the 3'end of alternate motifs of TBX3/5 and 20. But interestingly, a SNP in the *MEIS1* gene is associated with prolonged PR-intervals, as are SNPs in *TBX5*, its co-factor *NKX2-5* and its target *SCN5A* [Pfeufer et al., 2010] [Smith et al., 2011]. TBX5 and MEIS transcription factors are both involved in limb development. TBX5 is required for patterning of the forelimb identity [Rodriguez-Esteban et al., 1999] [Bruneau et al., 2001], whereas MEIS1/2 are involved in the proximal-distal organization of the limbs [Mercader et al., 1999] [Capdevila et al., 1999]. Moreover, MEIS1 and NKX2-5 as a known co-transcription factor of TBX5 bind mutually exclusive to overlapping motifs [Dupays et al., 2015]. In murine hearts with a KO of *Meis1*, *Tbx5* was found to be twofold upregulated [Mahmoud et al., 2013], possibly a compensatory mechanism. Finally a KO of *Meis1* in the peripheral nervous system can lead to conduction defects and sudden cardiac death [Bouilloux et al., 2016] similar to *Tbx5* loss. These data pinpoint towards a biological relevance of the appearance of a MEIS motif in the TBX5-ChIP-Seq dataset instead of a coincidence of motif similarity.

Therefore, we investigated a potential interaction between MEIS1 and TBX5. *In silico* analysis showed an enrichment of MEIS1 binding in a ChIP-Seq from embryonic trunks [Penkov et al., 2013] on TBX5 bound regions. These common regions are related to cardiac morphogenesis and muscle function, indicating a possible biologically relevant relationship between both transcription factors. Moreover, ChIP of MEIS1 and TBX5 in the heart showed enrichment of both transcription factors on the enhancers of *Scn5a*, *Kcnj5*, *Cacna1g* and *Chrm2*. Interestingly, MEIS1 was able to bind the enhancers of *Gja1* and *Gpr22* stronger in the absence of TBX5, but lost the ability to bind the *Scn5a* and the *Chrm2* enhancer, when TBX5 was not present.

These data indicate a biological interaction between TBX5 and MEIS1, since both bind to the same enhancer regions. However, further investigations need to identify whether the two factors act in a competing or synergistic fashion.

9.6. Re-expression of TBX5

TBX5 is expressed at reduced levels in cardiac disease both in rodents [Baurand Anthony et al., 2007] [Horton et al., 2016] and humans (5.5 for details). This study showed, that a ventricular loss of TBX5 disrupts the transcriptional homoeostasis leading to heart failure, arrhythmia and sudden cardiac death. Hence, we hypothesized that a normalization of TBX5 expression could restore transcription of its target genes and ameliorate the phenotypic consequences of TBX5 loss. To test this hypothesis, we selected an adeno-associated viral (AAV) approach.

9.6.1. AAVs as a research tool and in a preclinical therapeutic concept

Lately, AAV became of interest as a research tool, since it allows testing of overexpression of a protein of interest as an alternative or combined approach to generating transgenic animal models. An example of this approach was a study overexpressing of *Rbm24* via AAV9 under the control of a CMV-promoter. This way it could be established that *Rbm24* led to fibrosis induction [Hoogenhof et al., 2018].

AAVs are not only used as a research tool, but also for therapeutic proof-of-concept studies in small animal models. One study presented the cardio-selective overexpression of junctophilin-2 under the control of a myosin-light-chain promoter. This AAV9-application was able to rescue the contractile dysfunction in mice after TAC [Reynolds et al., 2016]. Another publication selected a comparable approach to our study: They injected constitutive Desmin-KO mice with AAV9 encoding desmin with a *TNNT2*-promoter and were able to show an amelioration of cardiac function providing proof-of-principle for a potential gene therapy for desmin-related cardiac disease [Heckmann et al., 2016].

Based on this study we selected the serotype AAV9 and the TnnT2-promoter to drive TBX5 (or CX43) expression. The aim was to determine the therapeutic effect of TBX5 re-expression, but also to examine the effect of CX43 re-expression in the *vTbx5*KO model thereby determining the contribution of CX43-loss to arrhythmia development. The viral particles were applied two weeks after induction of the *vTbx5*KO, since at this timepoint the transcription of target genes is disrupted and conduction delays can be observed.

9.6.2. Tissue-specific re-expression of TBX5

TBX5 was re-expressed in a tissue-specific manner in mouse hearts after KO of TBX5 by the use of adeno-associated viruses. Indeed, this corroborates the finding, that AAV9 has the highest cardiac transduction efficiency compared to serotypes 1-8 [Zincarelli et al., 2008]. Even higher specificity was achieved by using the cardiomyocyte-specific Tnnt2 promoter described earlier [Heckmann et al., 2016]. The re-introduction of CX43 by injection of AAV9-CX43 however, did not lead to markable expression of CX43. This could be because of the higher expression of CX43 in general. Although *Gja1* expression is strongly diminished in *vTbx5*KO ventricles, it is still 25-fold higher than the corresponding expression of *Tbx5* (mRNA expression normalised to *Gapdh* was 0.061 ±0.018 for *Gja1* and 0.0025 ±0.0017 for *Tbx5* in left ventricles) [own unpublished data]. Considering that TBX5 as a transcription factor is only expressed at low levels, the specific - but comparably weak - promoter of Troponin T is able to induce significant expression of TBX5. For CX43 higher expression levels might be necessary to induce a significant change to the endogenous expression of CX43. This could be achieved by using for example a CMV-promoter associated with a higher risk of unspecific expression in other tissues. However, it might also be a technical issue, since the *in vitro* transduction of NRCMs with AAV6-CX43 lead to a markable induction of CX43 expression. A common issue in the production of AAVs is the contamination with empty capsids. These are not only reducing the number of particles able to transduce cells, but are also inhibiting the transduction efficiency of the fully packed particles [Gao et al., 2014]. Therefore, the batch of the AAV9-CX43 might not have been able to induce significant elevation of CX43 expression.

However, we think, that the specific expression of TBX5 is a more relevant therapeutic target, because it can induce the induction of several targets to physiological levels without unspecifically interfering with other organs.

9.6.3. Restoration of TBX5-target gene expression and rescue of the phenotype

Re-expression of TBX5 lead to an increase of all previously validated transcripts. The expression of the conduction related genes *Gja1, Kcnj5, Kcng2,Cacna1g* and *Chrm2* was normalized to levels similar to Cre control mice. CX43 protein expression was distributed in the ventricle comparable to Cre controls as well. The restoration of those target genes allowed a reversal of the QRS-prolongation and lead to a reduction of arrhythmia incidence.

Besides conduction, also cardioprotective genes like *Fhl2, Gpr22* and *Fgf16* were re-expressed. Although not reaching statistical significance due to a low number of animals examined, the KO animals transduced with a control virus showed a progressive deterioration of their contractile function, whereas the TBX5-normalized hearts remained stable. Further experiments inducing cardiac stress in the TBX5-normalized animals could reveal, if they are protected better against pathological hypertrophy.

The *Tbx5* re-expression only induced a weak and non-significant increase in *Scn5a* (8.6.2). *Scn5a* and *Tbx5* are expressed at higher levels in the conduction system than in the working myocardium [Arnolds et al., 2012]. Although TBX5 re-expression seemed to lead to a physiological expression level in the working myocardium, it might not reach its original expression levels in the conduction system, thus not being able to induce complete recovery of *Scn5a* expression.

Nevertheless, the re-expression of TBX5 led to a substantial rescue of the arrhythmic phenotype. KO-RE mice displayed lower heart-rate variability and less QRS-prolongation than KO-CT mice. Notably, there seemed to be a lower incidence of death in the TBX5-normalized mice.

A more extensive study would be able to answer the question if this rescue of the phenotype can indeed lead to a protection from sudden cardiac death. Furthermore, TBX5 re-expression in a cardiomyopathy model, that is not attributed to direct TBX5-loss, is of high importance for potential translational implications.

9.6.4. Adeno-associated viruses in larger animal models

After performing a larger study in small animals, an investigation in larger animals would be required before a translational into a clinical context. Already AAV9 with a cardiomyocyte-specific promoter have been successfully used in a pig model of ischemic heart failure, induced by temporary ischemia [Pleger et al., 2011]. The authors applied 1.5 x 10^{13} viral particles directly to the anterior cardiac vein to achieve higher concentrations in the heart. Indeed, they were able to achieve high protein expression specifically in the anterior wall, compared to much lower expression in the posterior wall and negligible liver expression [Pleger et al., 2011].

Altogether, several studies proof the feasibility of AAV9 transduction *in vivo* in smaller and larger animals. Our investigation showed, that TBX5 is able to revert a phenotype caused by loss of TBX5 in the working myocardium, as it occurs in heart failure patients.

9.7. Summary

TBX5 is an essential transcription factor in the heart. So far, studies focused mainly on its role in development and the cardiac conduction system. But besides these established functions TBX5 expression is reduced in cardiac disease models in rodents and in heart failure patients. Therefore, we hypothesised that TBX5 is required for homoeostasis of the working myocardium and thus used a ventricular specific inducible TBX5 KO model to explore the function of TBX5 in the working myocardium.

These KO mice exhibited higher incidence of sudden cardiac death. Their hearts show diminished heart growth during aging along with diastolic dysfunction. Furthermore, they have slower cardiac conduction and arrhythmias similar to known models of TBX5 loss, though the phenotype (e.g. the incidence of sudden cardiac death) is more severe due to a complete loss of TBX5 throughout the ventricle.

We provide for the first time a full profile of endogenous TBX5-chromatin binding in the adult working myocardium, which can be applied in other studies to get more insights on transcription factor interactions and epigenetics in the heart. The integration of these results with RNA-Seq data revealed a number of novel targets for TBX5 and new putative enhancers. We validated several targets with an emphasis on *Gja1* and *Kcnj5* and could show that TBX5 directly activates enhancers in their gene proximity.

Besides known cofactors, motifs annotating to MEIS transcription factors were enriched in the TBX5-ChIP-Seq data and we thus collected hints for a biological interaction between both transcription factors. More extensive studies are needed to determine the relationship of MEIS1 and TBX5 in the heart.

Furthermore, we provide first proof-of-concept for the therapeutic potential of TBX5 restoration in the diseased heart. As a potential approach, we tested TBX5 re-expression by AAVs *in vivo* in *vTbx5*KO hearts. Indeed, this re-expression led to a reversal of TBX5 expression and subsequently to a rescue of target gene expression and the arrhythmic phenotype.

In summary, our study suggests the potential of TBX5 as a target for arrhythmia and heart failure with underlying transcriptional dysregulation.

9.8. Translational Outlook

Heart failure and sudden cardiac death are a major health burden worldwide. From 2000 to 2016 only an improvement from 41% to 48% in the 5-year survival rate of heart failure patients could be achieved with current treatments [Taylor et al., 2019]. For patients with end-stage heart failure, the only option is a heart transplant. However, the shortage of donor organs and costs of ~170 000 € per patient [Schröder, Dieter, 2013] prohibit the standard use of this therapeutic option. Therefore, better therapies are needed by patients and physicians.

Recently, research has focused on transcriptionally reprogramming the diseased heart in order to halt disease progression or even reverse pathological remodelling. This could be achieved by introducing transcription factors to restore the expression of beneficial target genes. Our study demonstrates how re-expression of cardiac transcription factor TBX5 was able to reduce the risk for arrhythmia and improve survival in a *vTbx5*KO model. Thus, we provide proof of principle for transcriptional reprogramming as a therapeutic strategy in heart failure. Further, more extensive studies need to show, if restoration of TBX5 expression in a heart failure model can protect mice from sudden cardiac death.

Our study is however limited by the use of a small rodent model. While providing distinct advantages such as short generation time and easy handling, these models are limited when it comes to the translation of findings into human physiology. Therefore, further studies using large animal models of heart failure or engineered human tissues are required in order to evaluate the therapeutic potential of TBX5 normalisation for the prevention of arrhythmia and sudden cardiac death. Especially engineered human tissue models, such as the engineered human myocardium (EHM) model allow for the fast investigation of therapeutic strategies in human disease models. In EHM, heart failure can be mimicked by pharmacological induction of adverse remodelling and hypertrophy [Tiburcy et al., 2017]. In this kind of heart failure model, TBX5 normalisation by AAV delivery would be expected to halt disease progression and reverse functional phenotypes.

Considering the potential clinical application of TBX5, routes for transcription factor delivery need to be investigated. In our study we used recombinant adeno-associated viruses as two therapies using rAAVs have been previously approved for clinical use [Wang et al., 2019].

When these investigations can be confirmed in a large animal model of heart failure, they could translate from bench-to-bedside and lead to an amelioration of clinical therapies. An alternative to direct transcription factor delivery could be small molecules enhancing TBX5-expression or activity. In this context, stem-cell derived cardiomyocytes [Sharma et al., 2017] or EHM [Meyer et al., 2019] offer a fast and high-throughput platform for the screening of small molecule libraries targeting TBX5 to find suitable candidates for human therapy. The easier application routes and lower costs of a targeted small molecule would allow a wide clinical application of a TBX5 based therapy for heart failure patients.

10. References

1. Adabag, A., Luepker, R., Roger, V. and Gersh, B., „Sudden cardiac death: epidemiology and risk factors", in: Nature reviews. Cardiology, 2010 [1]
2. Adams, J., Wang, J., Davis, J., Liaw, C., Gaidarov, I., Gatlin, J., Dalton, N., Gu, Y., Ross, J., Behan, D., Chien, K. and Connolly, D., „Myocardial expression, signaling, and function of GPR22: a protective role for an orphan G protein-coupled receptor", in: American Journal of Physiology - Heart and Circulatory Physiology, 2008 [87]
3. Afgan, E., Baker, D., van den Beek, M., Blankenberg, D., Bouvier, D., αech, M., Chilton, J., Clements, D., Coraor, N., Eberhard, C., Grüning, B., Guerler, A., Hillman-Jackson, J., Von Kuster, G., Rasche, E., Soranzo, N., Turaga, N., Taylor, J., Nekrutenko, A. and Goecks, J., „The Galaxy platform for accessible, reproducible and collaborative biomedical analyses: 2016 update", in: Nucleic Acids Research, 2016 [57]
4. Anderson, A., Kulkarni, K., Marron Fernandez de Velasco, E., Carlblom, N., Xia, Z., Nakano, A., Martemyanov, K., Tolkacheva, E. and Wickman, K., „Expression and relevance of the G protein-gated K+ channel in the mouse ventricle", in: Scientific Reports, 2018 [86]
5. Aouar, L., Meyerfreud, D., Magalhães, P., Rodrigues, S., Baldo, M., Brasil, Y., Aouar, S., Aouar, N., Mill, J. and Campos Filho, O., „Relationship Between Left Atrial Volume and Diastolic Dysfunction in 500 Brazilian Patients", in: Arquivos brasileiros de cardiologia, 2013 [84]
6. Arnolds, D., Liu, F., Fahrenbach, J., Kim, G., Schillinger, K., Smemo, S., McNally, E., Nobrega, M., Patel, V. and Moskowitz, I., „TBX5 drives Scn5a expression to regulate cardiac conduction system function", in: The Journal of Clinical Investigation, 2012 [1], [1], [22], [23], [25], [64], [83], [93]
7. Bass-Stringer, S., Bernardo, B., May, C., Thomas, C., Weeks, K. and McMullen, J., „Adeno-Associated Virus Gene Therapy: Translational Progress and Future Prospects in the Treatment of Heart Failure", in: Heart, Lung & Circulation, 2018 [28]
8. Baurand Anthony, Zelarayan Laura, Betney Russell, Gehrke Christina, Dunger Sandra, Noack Claudia, Busjahn Andreas, Huelsken Joerg, Taketo Makoto Mark, Birchmeier Walter, Dietz Rainer and Bergmann Martin W., „α-Catenin Downregulation Is Required for Adaptive Cardiac Remodeling", in: Circulation Research, 2007 [27], [82], [92]
9. Benson, M., Tinsley, C., Waite, A., Carlisle, F., Sweet, S., Ehler, E., George, C., Lai, F., Martin-Rendon, E. and Blake, D., „Ryanodine receptors are part of the myospryn complex in cardiac muscle", in: Scientific Reports, 2017 [88]
10. Bindea, G., Mlecnik, B., Hackl, H., Charoentong, P., Tosolini, M., Kirilovsky, A., Fridman, W., Pagès, F., Trajanoski, Z. and Galon, J., „ClueGO: a Cytoscape plug-in to decipher functionally grouped gene ontology and pathway annotation networks", in: Bioinformatics, 2009 [57], [69]
11. Bindea, G., Galon, J. and Mlecnik, B., „CluePedia Cytoscape plugin: pathway insights using integrated experimental and in silico data", in: Bioinformatics, 2013 [57], [69]
12. Björn Grüning, Dilmurat Yusuf, Torsten Houwaart, Anika, Milad Miladi, Qiang Gu, Bérénice Batut, Nicola Soranzo, Hassan Gamaleldin, Greg Von Kuster, zwanli, Joerg Fallmann, Cameron Smith, pkohvaei, Florian Eggenhofer, M Bernt, DamCorreia, Youri Hoogstrate, Scott Ouellette, Clemens Blank, Eteri Sokhoyan, Bithiah Yuan, Sebastian Will, Brad Langhorst, mblue9, Devon Ryan, F. H., Annkatrin Göpfert, Lucille Delisle and Gianluca Corrado, „bgruening/galaxytools: September release 2019" [57]
13. Boogerd, C. and Evans, S., „TBX5 and NuRD Divide the Heart", in: Developmental cell, 2016 [1], [22]
14. Bouilloux, F., Thireau, J., Ventéo, S., Farah, C., Karam, S., Dauvilliers, Y., Valmier, J., Copeland, N., Jenkins, N., Richard, S. and Marmigère, F., „Loss of the transcription factor Meis1 prevents sympathetic neurons target-field innervation and increases susceptibility to sudden cardiac death", in: eLife, 2016 [1], [91]
15. Bruneau, B., Nemer, G., Schmitt, J., Charron, F., Robitaille, L., Caron, S., Conner, D., Gessler, M., Nemer, M., Seidman, C. and Seidman, J., „A Murine Model of Holt-Oram Syndrome Defines Roles of the T-Box Transcription Factor Tbx5 in Cardiogenesis and Disease", in: Cell, 2001 [1], [1], [22], [23], [91]
16. Camarata, T., Bimber, B., Kulisz, A., Chew, T., Yeung, J. and Simon, H., „LMP4 regulates Tbx5 protein subcellular localization and activity", in: The Journal of Cell Biology, 2006 [22], [23], [26]
17. Capdevila, J., Tsukui, T., Esteban, C., Zappavigna, V. and Belmonte, J., „Control of Vertebrate Limb Outgrowth by the Proximal Factor Meis2 and Distal Antagonism of BMPs by Gremlin", in: Molecular Cell, 1999 [91]
18. Carroll, K., Makarewich, C., McAnally, J., Anderson, D., Zentilin, L., Liu, N., Giacca, M., Bassel-Duby, R. and Olson, E., „A mouse model for adult cardiac-specific gene deletion with CRISPR/Cas9", in: Proceedings of the National Academy of Sciences of the United States of America, 2016 [82]
19. Cerrone, M. and Priori, S., „Genetics of sudden death: focus on inherited channelopathies", in: European Heart Journal, 2011 [1]
20. Christoforou, N., Miller, R., Hill, C., Jie, C., McCallion, A. and Gearhart, J., „Mouse ES cell–derived cardiac precursor cells are multipotent and facilitate identification of novel cardiac genes", in: The Journal of Clinical Investigation, 2008 [88]
21. Cunningham, T., Zhao, X., Sandell, L., Evans, S., Trainor, P. and Duester, G., „Antagonism between Retinoic Acid and Fibroblast Growth Factor Signaling during Limb Development", in: Cell reports, 2013 [26]
22. Daily, K., Patel, V., Rigor, P., Xie, X. and Baldi, P., „MotifMap: integrative genome-wide maps of regulatory motif sites for model species", in: BMC Bioinformatics, 2011 [57]
23. De Bono, C., Thellier, C., Bertrand, N., Sturny, R., Jullian, E., Cortes, C., Stefanovic, S., Zaffran, S., Théveniau-Ruissy, M. and Kelly, R., „T-box genes and retinoic acid signaling regulate the segregation of arterial and venous pole progenitor cells in the murine second heart field", in: Human Molecular Genetics, 2018 [26]
24. Dupays, L., Shang, C., Wilson, R., Kotecha, S., Wood, S., Towers, N. and Mohun, T., „Sequential Binding of MEIS1 and NKX2-5 on the Popdc2 Gene: A Mechanism for Spatiotemporal Regulation of Enhancers during Cardiogenesis", in: Cell Reports, 2015 [91]
25. Durham, J., Brand, O., Arnold, M., Reynolds, J., Muthukumar, L., Weiler, H., Richardson, J. and Naya, F., „Myospryn Is a Direct Transcriptional Target for MEF2A That Encodes a Striated Muscle, α-Actinin-interacting, Costamere-localized Protein", in: Journal of Biological Chemistry, 2006 [88]
26. Eckart, R., Shry, E., Burke, A., McNear, J., Appel, D., Castillo-Rojas, L., Avedissian, L., Pearse, L., Potter, R., Tremaine, L., Gentlesk, P., Huffer, L., Reich, S. and Stevenson, W., „Sudden Death in Young Adults: An Autopsy-Based Series of a Population Undergoing Active Surveillance", in: Journal of the American College of Cardiology, 2011 [1]
27. Elek, C., Vitéz, M. and Czeizel, E., „[Holt-Oram syndrome]", in: Orvosi Hetilap, 1991 [1]
28. Ellesøe, S., Johansen, M., Bjerre, J., Hjortdal, V., Brunak, S. and Larsen, L., „Familial Atrial Septal Defect and Sudden Cardiac Death: Identification of a Novel NKX2-5 Mutation and a Review of the Literature", in: Congenital Heart Disease, 2016 [1]
29. Fabritz, L. and Herzig, S., „Can T-type calcium channels make a change of heart after myocardial infarction? Fiction or fact, and for better or for worse?", in: Cardiovascular Research, 2011 [86]
30. Gao, K., Li, M., Zhong, L., Su, Q., Li, J., Li, S., He, R., Zhang, Y., Hendricks, G., Wang, J. and Gao, G., „Empty virions in AAV8 vector preparations reduce transduction efficiency and may cause total viral particle dose-limiting side effects", in: Molecular Therapy. Methods & Clinical Development, 2014 [93]
31. Garg, V., Kathiriya, I., Barnes, R., Schluterman, M., King, I., Butler, C., Rothrock, C., Eapen, R., Hirayama-Yamada, K., Joo, K., Matsuoka, R., Cohen, J. and Srivastava, D., „GATA4 mutations cause human congenital heart defects and reveal an interaction with TBX5", in: Nature, 2003 [1]
32. Ghosh, T., Packham, E., Bonser, A., Robinson, T., Cross, S. and Brook, J., „Characterization of the TBX5 binding site and analysis of mutations that cause Holt–Oram syndrome", in: Human Molecular Genetics, 2001 [57], [75]
33. Ghosh, T., Song, F., Packham, E., Buxton, S., Robinson, T., Ronksley, J., Self, T., Bonser, A. and Brook, J., „Physical Interaction between TBX5 and MEF2C Is Required for Early Heart Development", in: Molecular and Cellular Biology, 2009 [1], [23]
34. Grau, J., Posch, S., Grosse, I. and Keilwagen, J., „A general approach for discriminative de novo motif discovery from high-throughput data", in: Nucleic Acids Research, 2013 [57], [75]
35. Guggilam, A., Sannaningaiah, D., Gong, Y., Grondolsky, J., Huang, M., Nie, H., Davis, E., Liu, Y., Jenkins, M., Strainic, J. and Hoover-Plow, J., „Cardiac Malformations in EMILIN2 Deficient Mice", in: International Journal of Cardiovascular Research, 2016 [88]
36. Gutstein, D., Morley, G., Tamaddon, H., Vaidya, D., Schneider, M., Chen, J., Chien, K., Stuhlmann, H. and Fishman, G., „Conduction Slowing and Sudden Arrhythmic Death in Mice With Cardiac-Restricted Inactivation of Connexin43", in: Circulation research, 2001 [25], [85]
37. Haufe, V., Cordeiro, J., Zimmer, T., Wu, Y., Schiccitano, S., Benndorf, K. and Dumaine, R., „Contribution of neuronal sodium channels to the cardiac fast sodium current INa is greater in dog heart Purkinje fibers than in ventricles", in: Cardiovascular Research, 2005 [73]
38. Hautala, A., Tulppo, M., Kiviniemi, A., Rankinen, T., Bouchard, C., Mäkikallio, T. and Huikuri, H., „Acetylcholine receptor M2 gene variants, heart rate recovery, and risk of cardiac death after an acute myocardial infarction", in: Annals of Medicine, 2009 [86]

39. He, A., Kong, S., Ma, Q. and Pu, W., „Co-occupancy by multiple cardiac transcription factors identifies transcriptional enhancers active in heart", in: Proceedings of the National Academy of Sciences of the United States of America, 2011 [89], [90]

40. He, A., Gu, F., Hu, Y., Ma, Q., Yi Ye, L., Akiyama, J., Visel, A., Pennacchio, L. and Pu, W., „Dynamic GATA4 enhancers shape the chromatin landscape central to heart development and disease", in: Nature communications, 2014 [66], [67], [72]

41. Heberle, H., Meirelles, G., da Silva, F., Telles, G. and Minghim, R., „InteractiVenn: a web-based tool for the analysis of sets through Venn diagrams", in: BMC Bioinformatics, 2015 [57]

42. Heckmann, M., Bauer, R., Jungmann, A., Winter, L., Rapti, K., Strucksberg, K., Clemen, C., Li, Z., Schröder, R., Katus, H. and Müller, O., „AAV9-mediated gene transfer of desmin ameliorates cardiomyopathy in desmin-deficient mice", in: Gene Therapy, 2016 [92]

43. Heinz, S., Benner, C., Spann, N., Bertolino, E., Lin, Y., Laslo, P., Cheng, J., Murre, C., Singh, H. and Glass, C., „Simple combinations of lineage-determining transcription factors prime cis-regulatory elements required for macrophage and B cell identities", in: Molecular cell, 2010 [57], [74]

44. Hiroi, Y., Kudoh, S., Monzen, K., Ikeda, Y., Yazaki, Y., Nagai, R. and Komuro, I., „Tbx5 associates with Nkx2-5 and synergistically promotes cardiomyocyte differentiation", in: Nature Genetics, 2001 [1], [23]

45. Hojayev, B., Rothermel, B., Gillette, T. and Hill, J., „FHL2 Binds Calcineurin and Represses Pathological Cardiac Growth", in: Molecular and Cellular Biology, 2012 [87]

46. Holm, H., Gudbjartsson, D., Arnar, D., Thorleifsson, G., Thorgeirsson, G., Stefansdottir, H., Gudjonsson, S., Jonasdottir, A., Mathiesen, E., Njølstad, I., Nyrnes, A., Wilsgaard, T., Hald, E., Hveem, K., Stoltenberg, C., Løchen, M., Kong, A., Thorsteinsdottir, U. and Stefansson, K., „Several common variants modulate heart rate, PR interval and QRS duration", in: Nature Genetics, 2010 [1]

47. Holt, M. and Oram, S., „FAMILIAL HEART DISEASE WITH SKELETAL MALFORMATIONS", in: British Heart Journal, 1960 [1]

48. Hoogenhof, M., Made, I., Groot, N., Damanafshan, A., Amersfoorth, S., Zentilin, L., Giacca, M., Pinto, Y. and Creemers, E., „AAV9-mediated Rbm24 overexpression induces fibrosis in the mouse heart", in: Scientific Reports, 2018 [92]

49. Horb, M. and Thomsen, G., „Tbx5 is essential for heart development", in: Development, 1999 [1]

50. Horton, R., Yadid, M., McCain, M., Sheehy, S., Pasqualini, F., Park, S., Cho, A., Campbell, P. and Parker, K., „Angiotensin II Induced Cardiac Dysfunction on a Chip", in: PLoS ONE, 2016 [27], [82], [92]

51. Hsieh, P., Segers, V., Davis, M., MacGillivray, C., Gannon, J., Molkentin, J., Robbins, J. and Lee, R., „Evidence from a genetic fate-mapping study that stem cells refresh adult mammalian cardiomyocytes after injury", in: Nature medicine, 2007 [82]

52. Huttlin, E., Bruckner, R., Paulo, J., Cannon, J., Ting, L., Baltier, K., Colby, G., Gebreab, F., Gygi, M., Parzen, H., Szpyt, J., Tam, S., Zarraga, G., Pontano-Vaites, L., Swarup, S., White, A., Schweppe, D., Rad, R., Erickson, B., Obar, R., Guruharsha, K., Li, K., Artavanis-Tsakonas, S., Gygi, S. and Harper, J., „Architecture of the human interactome defines protein communities and disease networks", in: Nature, 2017 [88]

53. Iyer, L., Nagarajan, S., Woelfer, M., Schoger, E., Khadjeh, S., Zafiriou, M., Kari, V., Herting, J., Pang, S., Weber, T., Rathjens, F., Fischer, T., Toischer, K., Hasenfuss, G., Noack, C., Johnsen, S. and Zelarayán, L., „A context-specific cardiac α-catenin and GATA4 interaction influences TCF7L2 occupancy and remodels chromatin driving disease progression in the adult heart", in: Nucleic Acids Research, 2018 [48], [54]

54. Jeong, H., Jung, E., Sim, Y., Kim, S., Jang, J., Hong, K., Lee, W., Chung, H., Park, K., Jung, Y., Kim, C. and Kim, K., „Fbxo25 controls Tbx5 and Nkx2–5 transcriptional activity to regulate cardiomyocyte development", in: Biochimica et Biophysica Acta (BBA) - Gene Regulatory Mechanisms, 2015 [26]

55. Johnson, T., Wilson, H. and Roesler, W., „Improvement of the chromatin immunoprecipitation (ChIP) assay by DNA fragment size fractionation", in: BioTechniques, 2001 [64]

56. Jungmann, A., Leuchs, B., Rommelaere, J., Katus, H. and Müller, O., „Protocol for Efficient Generation and Characterization of Adeno-Associated Viral Vectors", in: Human Gene Therapy Methods, 2017 [46]

57. Knyazeva, A., Krutikov, A., Golovkin, A., Mishanin, A., Pavlov, G., Smolina, N., Hushkina, A., Sejersen, T., Sjoberg, G., Galagudza, M. and Kostareva, A., „Time- and Ventricular-Specific Expression Profiles of Genes Encoding Z-Disk Proteins in Pressure Overload Model of Left Ventricular Hypertrophy", in: Frontiers in Genetics, 2019 [88]

58. Koizumi, A., Sasano, T., Kimura, W., Miyamoto, Y., Aiba, T., Ishikawa, T., Nogami, A., Fukamizu, S., Sakurada, H., Takahashi, Y., Nakamura, H., Ishikura, T., Koseki, H., Arimura, T., Kimura, A., Hirao, K., Isobe, M., Shimizu, W., Miura, N. and Furukawa, T., „Genetic defects in a His-Purkinje system transcription factor, IRX3, cause lethal cardiac arrhythmias", in: European Heart Journal, 2016 [1]

59. Komurcu-Bayrak, E., Ozsait, B. and Erginel-Unaltuna, N., „Isolation and analysis of genes mainly expressed in adult mouse heart using subtractive hybridization cDNA library", in: Molecular Biology Reports, 2012 [88]

60. Kong, Y., Shelton, J., Rothermel, B., Li, X., Richardson, J., Bassel-Duby, R. and Williams, R., „Cardiac-Specific LIM Protein FHL2 Modifies the Hypertrophic Response to α-Adrenergic Stimulation", in: Circulation, 2001 [87]

61. Koshiba-Takeuchi, K., Takeuchi, J., Arruda, E., Kathiriya, I., Mo, R., Hui, C., Srivastava, D. and Bruneau, B., „Cooperative and antagonistic interactions between Sall4 and Tbx5 pattern the mouse limb and heart", in: Nature Genetics, 2006 [1], [22], [23]

62. Krapivinsky, G., Gordon, E., Wickman, K., Velimirović, B., Krapivinsky, L. and Clapham, D., „The G-protein-gated atrial K+ channel IKACh is a heteromultimer of two inwardly rectifying K(+)-channel proteins", in: Nature, 1995 [25]

63. Langmead, B., „Aligning short sequencing reads with Bowtie", in: Current Protocols in Bioinformatics, 2010 [57]

64. Le Quang Khai, Benito Begoña, Naud Patrice, Qi Xiao Yan, Shi Yan Fen, Tardif Jean-Claude, Gillis Marc-Antoine, Dobrev Dobromir, Charpentier Flavien and Nattel Stanley, „T-Type Calcium Current Contributes to Escape Automaticity and Governs the Occurrence of Lethal Arrhythmias After Atrioventricular Block in Mice", in: Circulation: Arrhythmia and Electrophysiology, 2013 [86]

65. Lee, D., Sykes, S., Kalaitzidis, D., Lane, A., Kfoury, Y., Raaijmakers, M., Wang, Y., Armstrong, S. and Scadden, D., „Transmembrane Inhibitor of RICTOR/mTORC2 in Hematopoietic Progenitors", in: Stem Cell Reports, 2014 [88]

66. Lee, D., Wang, Y., Kalaitzidis, D., Ramachandran, J., Eda, H., Sykes, D., Raje, N. and Scadden, D., „Endogenous transmembrane protein UT2 inhibits pSTAT3 and suppresses hematological malignancy", in: The Journal of Clinical Investigation, 2016 [88]

67. Lewandowski, S., Janardhan, H., Smee, K., Bachman, M., Sun, Z., Lazar, M. and Trivedi, C., „Histone deacetylase 3 modulates Tbx5 activity to regulate early cardiogenesis", in: Human Molecular Genetics, 2014 [26]

68. Liang, B., Nissen, J., Laursen, M., Wang, X., Skibsbye, L., Hearing, M., Andersen, M., Rasmussen, H., Wickman, K., Grunnet, M., Olesen, S. and Jespersen, T., „G-protein-coupled inward rectifier potassium current contributes to ventricular repolarization", in: Cardiovascular Research, 2014 [25], [86]

69. Liberatore, C., Searcy-Schrick, R. and Yutzey, K., „Ventricular Expression of tbx5 Inhibits Normal Heart Chamber Development", in: Developmental Biology, 2000 [26]

70. Liu, T., Ortiz, J., Taing, L., Meyer, C., Lee, B., Zhang, Y., Shin, H., Wong, S., Ma, J., Lei, Y., Pape, U., Poidinger, M., Chen, Y., Yeung, K., Brown, M., Turpaz, Y. and Liu, X., „Cistrome: an integrative platform for transcriptional regulation studies", in: Genome Biology, 2011 [57], [66], [67]

71. Luna-Zurita, L., Stirnimann, C., Glatt, S., Kaynak, B., Thomas, S., Baudin, F., Samee, M., He, D., Small, E., Mileikovsky, M., Nagy, A., Holloway, A., Pollard, K., Müller, C. and Bruneau, B., „Complex Interdependence Regulates Heterotypic Transcription Factor Distribution and Coordinates Cardiogenesis", in: Cell, 2016 [85], [89], [90], [91]

72. Lyons, G., Schiaffino, S., Sassoon, D., Barton, P. and Buckingham, M., „Developmental regulation of myosin gene expression in mouse cardiac muscle.", in: The Journal of Cell Biology, 1990 [82]

73. Mahmoud, A., Kocabas, F., Muralidhar, S., Kimura, W., Koura, A., Thet, S., Porrello, E. and Sadek, H., „Meis1 regulates postnatal cardiomyocyte cell cycle arrest", in: Nature, 2013 [91]

74. McLean, C., Bristor, D., Hiller, M., Clarke, S., Schaar, B., Lowe, C., Wenger, A. and Bejerano, G., „GREAT improves functional interpretation of cis-regulatory regions", in: Nature biotechnology, 2010 [57], [66], [67], [68], [69]

75. McLeay, R. and Bailey, T., „Motif Enrichment Analysis: a unified framework and an evaluation on ChIP data", in: BMC Bioinformatics, 2010 [57], [74]

76. Mearini, G., Stimpel, D., Geertz, B., Weinberger, F., Krämer, E., Schlossarek, S., Mourot-Filiatre, J., Stoehr, A., Dutsch, A., Wijnker, P., Braren, I., Katus, H., Müller, O., Voit, T., Eschenhagen, T. and Carrier, L., „Mybpc3 gene therapy for neonatal cardiomyopathy enables long-term disease prevention in mice", in: Nature Communications, 2014 [28]

77. Mendis, S., Norrving, B. and Puska, P., Edt., „WHO | Global atlas on cardiovascular disease prevention and control", 2011 [18]

78. Mercader, N., Leonardo, E., Azpiazu, N., Serrano, A., Morata, G., Martínez, C. and Torres, M., „Conserved regulation of proximodistal limb axis development by Meis1/Hth", in: Nature, 1999 [91]

79. Meyer, T., Tiburcy, M. and Zimmermann, W., „Cardiac macrotissues-on-a-plate models for phenotypic drug screens", in: Advanced Drug Delivery Reviews, 2019 [95]

80. Molojavyi, A., Lindecke, A., Raupach, A., Moellendorf, S., Köhrer, K. and Gödecke, A., „Myoglobin-deficient mice activate a distinct cardiac gene expression program in response to isoproterenol-induced hypertrophy", in: Physiological Genomics, 2010 [88]

81. Mori, A., Zhu, Y., Vahora, I., Nieman, B., Koshiba-Takeuchi, K., Davidson, L., Pizard, A., Seidman, J., Seidman, C., Chen, X., Henkelman, R. and Bruneau, B., „Tbx5-dependent rheostatic control of cardiac gene expression and morphogenesis", in: Developmental Biology, 2006 [23], [43], [83], [87]

82. Moskowitz, I., Pizard, A., Patel, V., Bruneau, B., Kim, J., Kupershmidt, S., Roden, D., Berul, C., Seidman, C. and Seidman, J., „The T-Box transcription factor Tbx5 is required for the patterning and maturation of the murine cardiac conduction system", in: Development, 2004 [1]

83. Nadadur, R., Broman, M., Boukens, B., Mazurek, S., Yang, X., van den Boogaard, M., Bekeny, J., Gadek, M., Ward, T., Zhang, M., Qiao, Y., Martin, J., Seidman, C., Seidman, J., Christoffels, V., Efimov, I., McNally, E., Weber, C. and Moskowitz, I., „Pitx2 modulates a Tbx5-dependent gene regulatory network to maintain atrial rhythm", in: Science translational medicine, 2016 [1], [1], [22], [23], [25], [84], [85], [86]

84. Nakagami, H., Kikuchi, Y., Katsuya, T., Morishita, R., Akasaka, H., Saitoh, S., Rakugi, H., Kaneda, Y., Shimamoto, K. and Ogihara, T., „Gene Polymorphism of Myospryn (Cardiomyopathy-Associated 5) Is Associated with Left Ventricular Wall Thickness in Patients with Hypertension", in: Hypertension Research, 2007 [88]

85. Naya, F., Black, B., Wu, H., Bassel-Duby, R., Richardson, J., Hill, J. and Olson, E., „Mitochondrial deficiency and cardiac sudden death in mice lacking the MEF2A transcription factor", in: Nature Medicine, 2002 [1]

86. Nishimoto, S., Wilde, S., Wood, S. and Logan, M., „RA Acts in a Coherent Feed-Forward Mechanism with Tbx5 to Control Limb Bud Induction and Initiation", in: Cell Reports, 2015 [26]

87. Noack, C., Iyer, L., Liaw, N., Schoger, E., Khadjeh, S., Wagner, E., Woelfer, M., Zafiriou, M., Milting, H., Sossalla, S., Streckfuss-Boemeke, K., Hasenfuß, G., Zimmermann, W. and Zelarayán, L., „KLF15-Wnt–Dependent Cardiac Reprogramming Up-Regulates SHISA3 in the Mammalian Heart", in: Journal of the American College of Cardiology, 2019 [47]

88. O'Geen, H., Frietze, S. and Farnham, P., „Using ChIP-seq Technology to Identify Targets of Zinc Finger Transcription Factors", in: Methods in molecular biology (Clifton, N.J.), 2010 [54]

89. Papadatos, G., Wallerstein, P., Head, C., Ratcliff, R., Brady, P., Benndorf, K., Saumarez, R., Trezise, A., Huang, C., Vandenberg, J., Colledge, W. and Grace, A., „Slowed conduction and ventricular tachycardia after targeted disruption of the cardiac sodium channel gene Scn5a", in: Proceedings of the National Academy of Sciences of the United States of America, 2002 [25]

90. Penkov, D., San Martín, D., Fernandez-Díaz, L., Rosselló, C., Torroja, C., Sánchez-Cabo, F., Warnatz, H., Sultan, M., Yaspo, M., Gabrieli, A., Tkachuk, V., Brendolan, A., Blasi, F. and Torres, M., „Analysis of the DNA-Binding Profile and Function of TALE Homeoproteins Reveals Their Specialization and Specific Interactions with Hox Genes/Proteins", in: Cell Reports, 2013 [76], [91]

91. Perera, J., Johnson, N., Judge, D. and Crosson, J., „Novel and Highly Lethal NKX2.5 Missense Mutation in a Family With Sudden Death and Ventricular Arrhythmia", in: Pediatric Cardiology, 2014 [1]

92. Pfeufer, A., van Noord, C., Marciante, K., Arking, D., Larson, M., Smith, A., Tarasov, K., Müller, M., Sotoodehnia, N., Sinner, M., Verwoert, G., Li, M., Kao, W., Köttgen, A., Coresh, J., Bis, J., Psaty, B., Rice, K., Rotter, J., Rivadeneira, F., Hofman, A., Kors, J., Stricker, B., Uitterlinden, A., van Duijn, C., Beckmann, B., Sauter, W., Gieger, C., Lubitz, S., Newton-Cheh, C., Wang, T., Magnani, J., Schnabel, R., Chung, M., Barnard, J., Smith, J., Van Wagoner, D., Vasan, R., Aspelund, T., Eiriksdottir, G., Harris, T., Launer, L., Najjar, S., Lakatta, E., Schlessinger, D., Uda, M., Abecasis, G., Müller-Myhsok, B., Ehret, G., Boerwinkle, E., Chakravarti, A., Soliman, E., Lunetta, K., Perz, S., Wichmann, H., Meitinger, T., Levy, D., Gudnason, V., Ellinor, P., Sanna, S., Kääb, S., Witteman, J., Alonso, A., Benjamin, E. and Heckbert, S., „Genome-wide association study of PR interval", in: Nature Genetics, 2010 [1], [1], [91]

93. Pleger, S., Shan, C., Ksienzyk, J., Bekeredjian, R., Boekstegers, P., Hinkel, R., Schinkel, S., Leuchs, B., Ludwig, J., Qiu, G., Weber, C., Kleinschmidt, J., Raake, P., Koch, W., Katus, H., Müller, O. and Most, P., „Cardiac AAV9-S100A1 gene therapy rescues postischemic heart failure in a preclinical large animal model", in: Science translational medicine, 2011 [94]

94. Pradhan, L., Gopal, S., Li, S., Ashur, S., Suryanarayanan, S., Kasahara, H. and Nam, H., „Intermolecular Interactions of Cardiac Transcription Factors NKX2.5 and TBX5", in: Biochemistry, 2016 [1], [23]

95. Pritchett, A., Mahoney, D., Jacobsen, S., Rodeheffer, R., Karon, B. and Redfield, M., „Diastolic dysfunction and left atrial volume: A population-based study", in: Journal of the American College of Cardiology, 2005 [84]

96. Quinlan, A. and Hall, I., „BEDTools: a flexible suite of utilities for comparing genomic features", in: Bioinformatics, 2010 [57]

97. Ramírez, F., Dündar, F., Diehl, S., Grüning, B. and Manke, T., „deepTools: a flexible platform for exploring deep-sequencing data", in: Nucleic Acids Research, 2014 [57], [68]

98. Ramírez, F., Ryan, D., Grüning, B., Bhardwaj, V., Kilpert, F., Richter, A., Heyne, S., Dündar, F. and Manke, T., „deepTools2: a next generation web server for deep-sequencing data analysis", in: Nucleic Acids Research, 2016 [66], [67], [68]

99. Ramshur, J., „Design, Evaluation, and Application of Heart Rate Variability Analysis Software (HRVAS)", Masters Thesis, University of Memphis, Memphis, TN, 2010 [44], [81]

100. Rathjens, F., „The role of TBX5 in arrhythmia development upon cardiac remodeling", Master's Thesis, Georg-August University, Göttingen, 2015 [50]

101. Renger, A., „Analyse von kardialen Wnt/α-Catenin Interaktionspartnern bezüglich ihrer Möglichkeit, die embryonale Kardiogenese zu aktivieren", 2012 [26], [43], [58], [85], [87]

102. Reynolds, J., Quick, A., Wang, Q., Beavers, D., Philippen, L., Showell, J., Barreto-Torres, G., Theurauf, D., Doroudgar, S., Glembotski, C. and Wehrens, X., „Junctophilin-2 gene therapy rescues heart failure by normalizing RyR2-mediated Ca2+ release", in: International journal of cardiology, 2016 [92]

103. Robinson, J., Thorvaldsdóttir, H., Winckler, W., Guttman, M., Lander, E., Getz, G. and Mesirov, J., „Integrative genomics viewer", in: Nature Biotechnology, 2011 [57]

104. Rodriguez-Esteban, C., Tsukui, T., Yonei, S., Magallon, J., Tamura, K. and Izpisua Belmonte, J., „The T-box genes Tbx4 and Tbx5 regulate limb outgrowth and identity", in: Nature, 1999 [91]

105. Ross-Innes, C., Stark, R., Teschendorff, A., Holmes, K., Ali, H., Dunning, M., Brown, G., Gojis, O., Ellis, I., Green, A., Ali, S., Chin, S., Palmieri, C., Caldas, C. and Carroll, J., „Differential oestrogen receptor binding is associated with clinical outcome in breast cancer", in: Nature, 2012 [68]

106. Schröder, Dieter, ., „Was Gesundheit kostet", in: fit! (DAK-Gesundheit), 2013 [95]

107. Schwab, D., Tilemann, L., Bauer, R., Heckmann, M., Jungmann, A., Wagner, M., Burgis, J., Vettel, C., Katus, H., El-Armouche, A. and Müller, O., „AAV-9 mediated phosphatase-1 inhibitor-1 overexpression improves cardiac contractility in unchallenged mice but is deleterious in pressure-overload", in: Gene Therapy, 2018 [28], [46]

108. Schwartz, P., Crotti, L. and George, A., „Modifier genes for sudden cardiac death", in: European Heart Journal, 2018 [1]

109. Sereti, K., Nguyen, N., Kamran, P., Zhao, P., Ranjbarvaziri, S., Park, S., Sabri, S., Engel, J., Sung, K., Kulkarni, R., Ding, Y., Hsiai, T., Plath, K., Ernst, J., Sahoo, D., Mikkola, H., Iruela-Arispe, M. and Ardehali, R., „Analysis of cardiomyocyte clonal expansion during mouse heart development and injury", in: Nature Communications, 2018 [82], [83]

110. Severs, N., Coppen, S., Dupont, E., Yeh, H., Ko, Y. and Matsushita, T., „Gap junction alterations in human cardiac disease", in: Cardiovascular Research, 2004 [25]

111. Sharma, A., Burridge, P., McKeithan, W., Serrano, R., Shukla, P., Sayed, N., Churko, J., Kitani, T., Wu, H., Holmström, A., Matsa, E., Zhang, Y., Kumar, A., Fan, A., del Álamo, J., Wu, S., Moslehi, J., Mercola, M. and Wu, J., „High-Throughput Screening of Tyrosine Kinase Inhibitor Cardiotoxicity with Human Induced Pluripotent Stem Cells", in: Science translational medicine, 2017 [95]

112. Shen, T., Aneas, I., Sakabe, N., Dirschinger, R., Wang, G., Smemo, S., Westlund, J., Cheng, H., Dalton, N., Gu, Y., Boogerd, C., Cai, C., Peterson, K., Chen, J., Nobrega, M. and Evans, S., „Tbx20 regulates a genetic program essential to adult mouse cardiomyocyte function", in: The Journal of Clinical Investigation, 2011 [82], [82]

113. Shende, P., Xu, L., Morandi, C., Pentassuglia, L., Heim, P., Lebboukh, S., Berthonneche, C., Pedrazzini, T., Kaufmann, B., Hall, M., Rüegg, M. and Brink, M., „Cardiac mTOR complex 2 preserves ventricular function in pressure-overload hypertrophy", in: Cardiovascular Research, 2016 [88]

114. Shin, H., Liu, T., Manrai, A. and Liu, X., „CEAS: cis-regulatory element annotation system", in: Bioinformatics (Oxford, England), 2009 [57], [66], [67]

115. Smith, J., Magnani, J., Palmer, C., Meng, Y., Soliman, E., Musani, S., Kerr, K., Schnabel, R., Lubitz, S., Sotoodehnia, N., Redline, S., Pfeufer, A., Müller, M., Evans, D., Nalls, M., Liu, Y., Newman, A., Zonderman, A., Evans, M., Deo, R., Ellinor, P., Paltoo, D., Newton-Cheh, C., Benjamin, E., Mehra, R., Alonso, A., Heckbert, S., Fox, E. and Consortium, C., „Genome-Wide Association Studies of the PR Interval in African Americans", in: PLOS Genetics, 2011 [1], [1], [91]

116. Sohal Dawinder S., Nghiem Mai, Crackower Michael A., Witt Sandra A., Kimball Thomas R., Tymitz Kevin M., Penninger Josef M. and Molkentin Jeffery D., „Temporally Regulated and Tissue-Specific Gene Manipulations in the Adult and Embryonic Heart Using a Tamoxifen-Inducible Cre Protein", in: Circulation Research, 2001 [43], [82]

117. Steimle, J., Rankin, S., Slagle, C., Bekeny, J., Rydeen, A., Chan, S., Kweon, J., Yang, X., Ikegami, K., Nadadur, R., Rowton, M., Hoffmann, A., Lazarevic, S., Thomas, W., Boyle Anderson, E., Horb, M., Luna-Zurita, L., Ho, R., Kyba, M., Jensen, B., Zorn, A., Conlon, F. and Moskowitz, I., „Evolutionarily conserved Tbx5-Wnt2/2b pathway orchestrates cardiopulmonary development", in: Proceedings of the National Academy of Sciences of the United States of America, 2018 [1], [22], [24], [68], [85], [89], [90]

118. Taylor, C., Ordóñez-Mena, J., Roalfe, A., Lay-Flurrie, S., Jones, N., Marshall, T. and Hobbs, F., „Trends in survival after a diagnosis of heart failure in the United Kingdom 2000-2017: population based cohort study", in: BMJ, 2019 [95]

119. Thorvaldsdóttir, H., Robinson, J. and Mesirov, J., „Integrative Genomics Viewer (IGV): high-performance genomics data visualization and exploration", in: Briefings in Bioinformatics, 2013 [57]

120. Tiburcy, M., Hudson, J., Balfanz, P., Schlick, S., Meyer, T., Liao, M., Levent, E., Raad, F., Zeidler, S., Wingender, E., Riegler, J., Wang, M., Gold, J., Kehat, I., Wettwer, E., Ravens, U., Dierickx, P., van Laake, L., Goumans, M., Khadjeh, S., Toischer, K., Hasenfuss, G., Couture, L., Unger, A., Linke, W., Araki, T., Neel, B., Keller, G., Gepstein, L., Wu, J. and Zimmermann, W., „Defined Engineered Human Myocardium with Advanced Maturation for Applications in Heart Failure Modelling and Repair", in: Circulation, 2017 [95]

121. van den Boogaard, M., Wong, L., Tessadori, F., Bakker, M., Dreizehnter, L., Wakker, V., Bezzina, C., 't Hoen, P., Bakkers, J., Barnett, P. and Christoffels, V., „Genetic variation in T-box binding element functionally affects SCN5A/SCN10A enhancer", in: The Journal of Clinical Investigation, 2012 [22], [23], [25], [66], [67], [72]

122. Van Hoof, D., Dormeyer, W., Braam, S., Passier, R., Monshouwer-Kloots, J., Ward-van Oostwaard, D., Heck, A., Krijgsveld, J. and Mummery, C., „Identification of cell surface proteins for antibody-based selection of human embryonic stem cell-derived cardiomyocytes", in: Journal of Proteome Research, 2010 [88]

123. Vanaja, D., Grossmann, M., Cheville, J., Gazi, M., Gong, A., Zhang, J., Ajtai, K., Burghardt, T. and Young, C., „PDLIM4, An Actin Binding Protein, Suppresses Prostate Cancer Cell Growth", in: Cancer investigation, 2009 [88]

124. Vanlerberghe, C., Jourdain, A., Ghoumid, J., Frenois, F., Mezel, A., Vaksmann, G., Lenne, B., Delobel, B., Porchet, N., Cormier-Daire, V., Smol, T., Escande, F., Manouvrier-Hanu, S. and Petit, F., „Holt-Oram syndrome: clinical and molecular description of 78 patients with TBX5 variants", in: European journal of human genetics: EJHG, 2019 [1]

125. Vettel Christiane, Lindner Marta, Dewenter Matthias, Lorenz Kristina, Schanbacher Constanze, Riedel Merle, Lämmle Simon, Meinecke Simone, Mason Fleur E., Sossalla Samuel, Geerts Andreas, Hoffmann Michael, Wunder Frank, Brunner Fabian J., Wieland Thomas, Mehel Hind, Karam Sarah, Lechêne Patrick, Leroy Jérôme, Vandecasteele Grégoire, Wagner Michael, Fischmeister Rodolphe and El-Armouche Ali, „Phosphodiesterase 2 Protects Against Catecholamine-Induced Arrhythmia and Preserves Contractile Function After Myocardial Infarction", in: Circulation Research, 2017 [44]

126. Visel, A., Minovitsky, S., Dubchak, I. and Pennacchio, L., „VISTA Enhancer Browser—a database of tissue-specific human enhancers", in: Nucleic Acids Research, 2007 [85]

127. Waldron, L., Steimle, J., Greco, T., Gomez, N., Dorr, K., Kweon, J., Temple, B., Yang, X., Wilczewski, C., Davis, I., Cristea, I., Moskowitz, I. and Conlon, F., „The cardiac TBX5 interactome reveals a chromatin remodeling network essential for cardiac septation", in: Developmental cell, 2016 [1], [24], [85]

128. Wang, C., Cao, D., Wang, Q. and Wang, D., „Synergistic Activation of Cardiac Genes by Myocardin and Tbx5", in: PLoS ONE, 2011 [1], [23]

129. Wang, F., Liu, J., Hong, L., Liang, B., Graff, C., Yang, Y., Christiansen, M., Olesen, S., Zhang, L. and Kanters, J., „The phenotype characteristics of type 13 long QT syndrome with mutation in KCNJ5 (Kir3.4-G387R)", in: Heart Rhythm, 2013 [25]

130. Wang, D., Tai, P. and Gao, G., „Adeno-associated virus vector as a platform for gene therapy delivery", in: Nature Reviews. Drug Discovery, 2019 [28], [95]

131. Wang F, Yang XY, Zhao JY, Yu LW, Zhang P, Duan WY, Chong M and Gui YH, „miR-10a and miR-10b target the 3'-untranslated region of TBX5 to repress its expression.", in: Pediatr Cardiol, 2014 [26]

132. Wickman, K., Nemec, J., Gendler, S. and Clapham, D., „Abnormal Heart Rate Regulation in GIRK4 Knockout Mice", in: Neuron, 1998 [86]

133. Wittköpper, K., Fabritz, L., Neef, S., Ort, K., Grefe, C., Unsöld, B., Kirchhof, P., Maier, L., Hasenfuss, G., Dobrev, D., Eschenhagen, T. and El-Armouche, A., „Constitutively active phosphatase inhibitor-1 improves cardiac contractility in young mice but is deleterious after catecholaminergic stress and with aging", in: The Journal of Clinical Investigation, 2010 [45]

134. Xie, X., Rigor, P. and Baldi, P., „MotifMap: a human genome-wide map of candidate regulatory motif sites", in: Bioinformatics, 2009 [57]

135. Yan, J., Sultana, N., Zhang, L., Park, D., Shekhar, A., Hu, J., Bu, L. and Cai, C., „Generation of a tamoxifen inducible Tnnt2MerCreMer knock-in mouse model for cardiac studies", in: Genesis (New York, N.Y. : 2000), 2015 [82]

136. Yang, Y., Yang, Y., Liang, B., Liu, J., Li, J., Grunnet, M., Olesen, S., Rasmussen, H., Ellinor, P., Gao, L., Lin, X., Li, L., Wang, L., Xiao, J., Liu, Y., Liu, Y., Zhang, S., Liang, D., Peng, L., Jespersen, T. and Chen, Y., „Identification of a Kir3.4 Mutation in Congenital Long QT Syndrome", in: American Journal of Human Genetics, 2010 [86]

137. Yu, W., Huang, X., Tian, X., Zhang, H., He, L., Wang, Y., Nie, Y., Hu, S., Lin, Z., Zhou, B., Pu, W., Lui, K. and Zhou, B., „GATA4 regulates Fgf16 to promote heart repair after injury", in: Development, 2016 [87]

138. Zafiriou, M., Noack, C., Unsöld, B., Didie, M., Pavlova, E., Fischer, H., Reichardt, H., Bergmann, M., El-Armouche, A., Zimmermann, W. and Zelarayan, L., „Erythropoietin Responsive Cardiomyogenic Cells Contribute to Heart Repair Post Myocardial Infarction", in: STEM CELLS, 2014 [44], [48]

139. Zhang, Y., Liu, T., Meyer, C., Eeckhoute, J., Johnson, D., Bernstein, B., Nusbaum, C., Myers, R., Brown, M., Li, W. and Liu, X., „Model-based Analysis of ChIP-Seq (MACS)", in: Genome Biology, 2008 [57]

140. Zhang, Y., Wu, J., King, J., Huang, C. and Fraser, J., „Measurement and interpretation of electrocardiographic QT intervals in murine hearts", in: American Journal of Physiology-Heart and Circulatory Physiology, 2014 [84]

141. Zhang Lin, Hu Aihua, Yuan Haixin, Cui Liang, Miao Guobin, Yang Xinchun, Wang Lefeng, Liu Jinchun, Liu Xiulan, Wang Shuyan, Zhang Zhiyong, Liu Lisheng, Zhao Rongrui and Shen Yan, „A Missense Mutation in the CHRM2 Gene Is Associated With Familial Dilated Cardiomyopathy", in: Circulation Research, 2008 [86]

142. Zhao, X., Sirbu, I., Mic, F., Molotkova, N., Molotkov, A., Kumar, S. and Duester, G., „Retinoic Acid Promotes Limb Induction through Effects on Body Axis Extension but is Unnecessary for Limb Patterning", in: Current biology : CB, 2009 [26]

143. Zhou, Y., Zhu, Y., Bishop, J., Davidson, L., Henkelman, R., Bruneau, B. and Foster, F., „Abnormal cardiac inflow patterns during postnatal development in a mouse model of Holt-Oram syndrome", in: American Journal of Physiology-Heart and Circulatory Physiology, 2005 [1], [83]

144. Zhu, X., Netzer, R., Böhlke, K., Liu, Q. and Pongs, O., „Structural and functional characterization of Kv6.2 a new gamma-subunit of voltage-gated potassium channel", in: Receptors & Channels, 1999 [86]

145. Zhu, Y., Gramolini, A., Walsh, M., Zhou, Y., Slorach, C., Friedberg, M., Takeuchi, J., Sun, H., Henkelman, R., Backx, P., Redington, A., MacLennan, D. and Bruneau, B., „Tbx5-dependent pathway regulating diastolic function in congenital heart disease", in: Proceedings of the National Academy of Sciences of the United States of America, 2008 [1], [23], [83]

146. Zincarelli, C., Soltys, S., Rengo, G. and Rabinowitz, J., „Analysis of AAV Serotypes 1–9 Mediated Gene Expression and Tropism in Mice After Systemic Injection", in: Molecular Therapy, 2008 [92]

11. Appendix

11.1. Plasmid maps

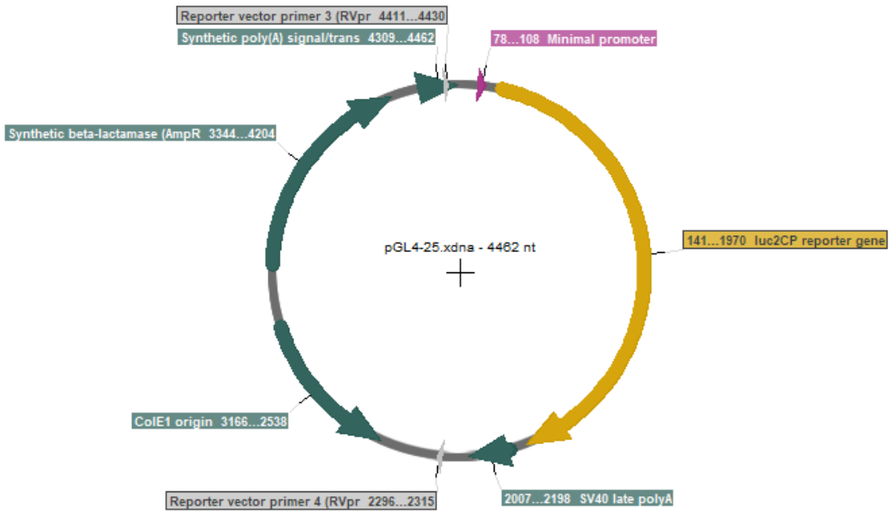

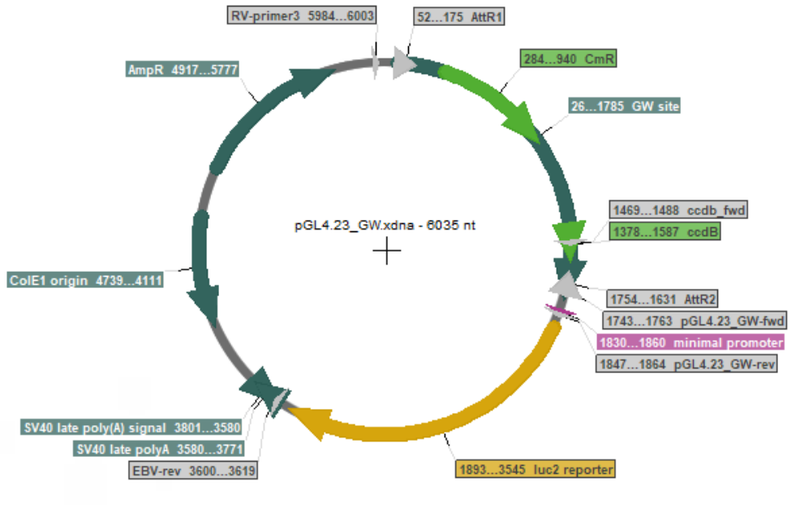

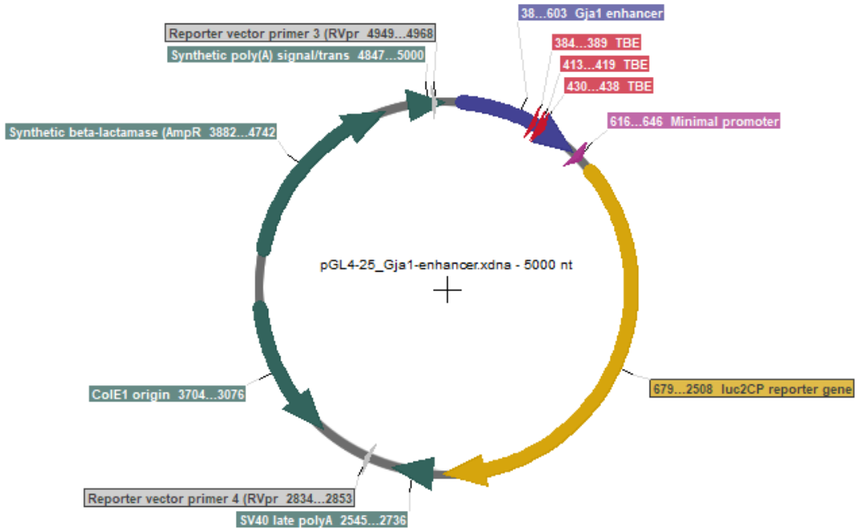

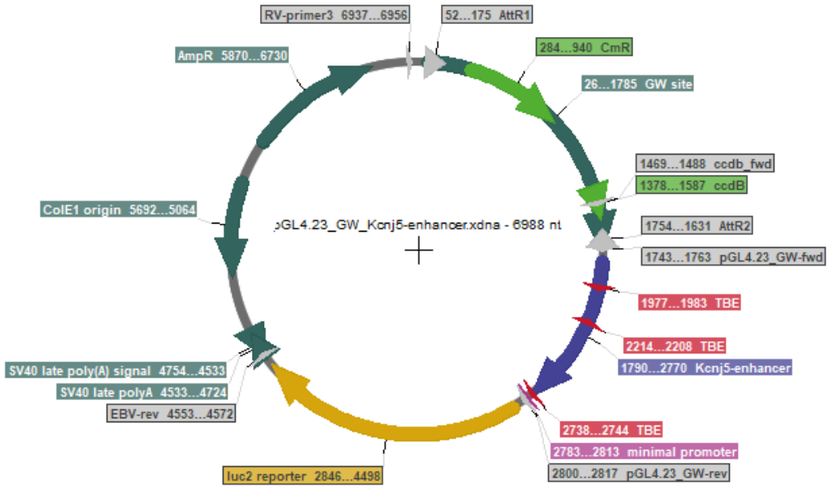

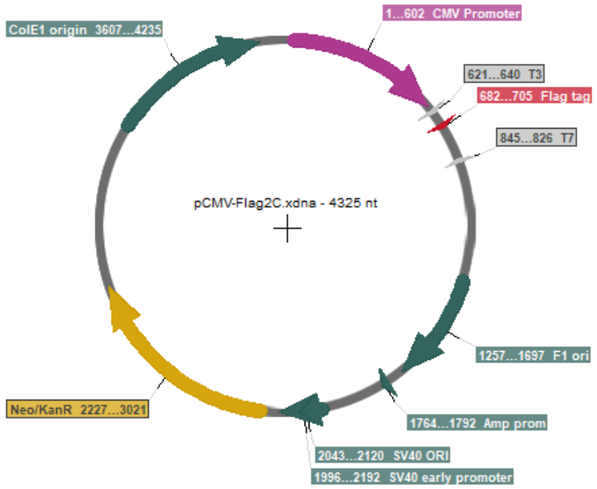
pCMV-Flag2C.xdna - 4325 nt
1...602 CMV Promoter
621...640 T3
682...705 Flag tag
845...826 T7
1257...1697 F1 ori
1764...1792 Amp prom
2043...2120 SV40 ORI
1996...2192 SV40 early promoter
Neo/KanR 2227...3021
ColE1 origin 3607...4235

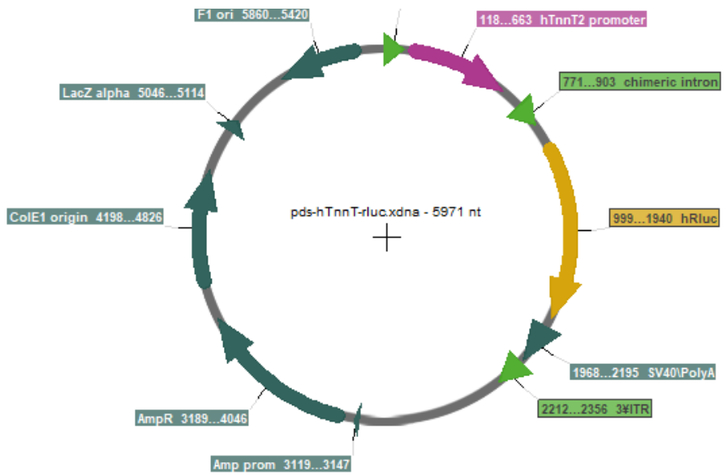
pds-hTnnT-rluc.xdna - 5971 nt
F1 ori 5860...5420
118...663 hTnnT2 promoter
771...903 chimeric intron
999...1940 hRluc
1968...2195 SV40\PolyA
2212...2356 3¥ITR
Amp prom 3119...3147
AmpR 3189...4046
ColE1 origin 4198...4826
LacZ alpha 5046...5114

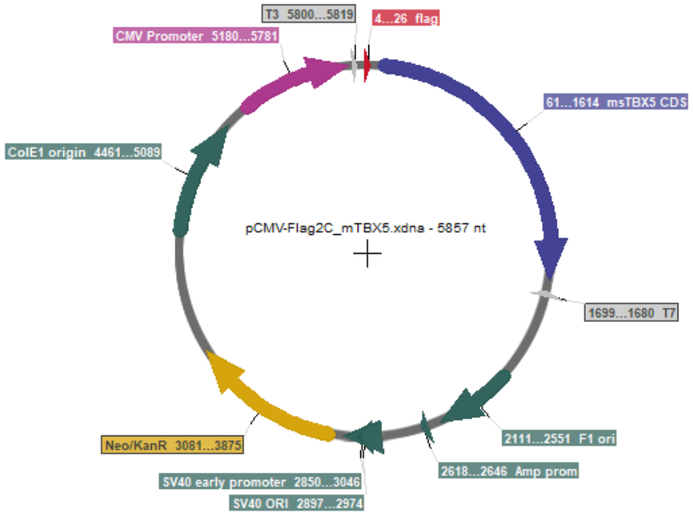
pCMV-Flag2C_mTBX5.xdna - 5857 nt
T3 5800...5819
4...26 flag
61...1614 msTBX5 CDS
1699...1680 T7
2111...2551 F1 ori
2618...2646 Amp prom
SV40 ORI 2897...2974
SV40 early promoter 2850...3046
Neo/KanR 3081...3875
ColE1 origin 4461...5089
CMV Promoter 5180...5781

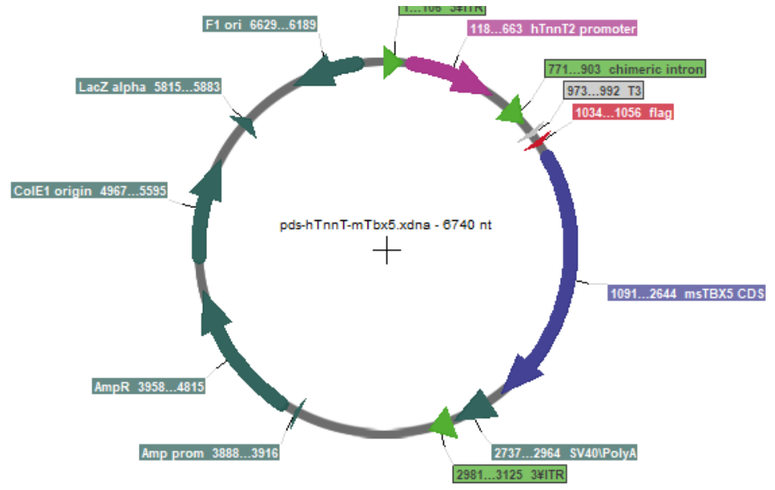
pds-hTnnT-mTbx5.xdna - 6740 nt
F1 ori 6629...6189
118...663 hTnnT2 promoter
771...903 chimeric intron
973...992 T3
1034...1056 flag
1091...2644 msTBX5 CDS
2737...2964 SV40\PolyA
2981...3125 3¥ITR
Amp prom 3888...3916
AmpR 3958...4815
ColE1 origin 4967...5595
LacZ alpha 5815...5883

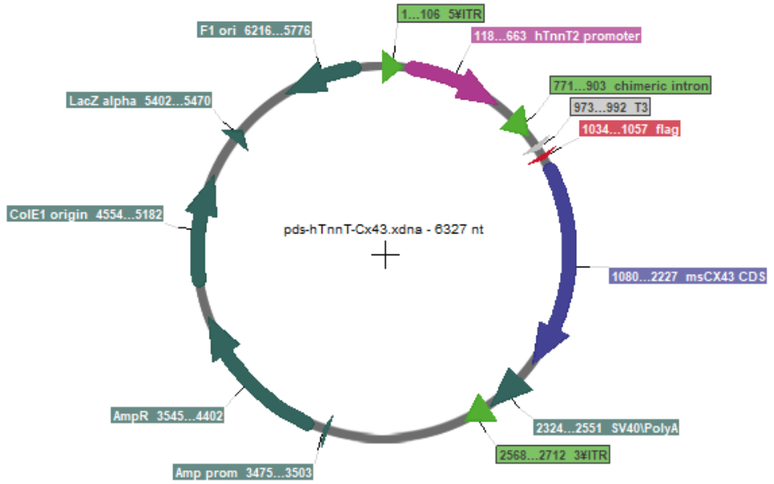

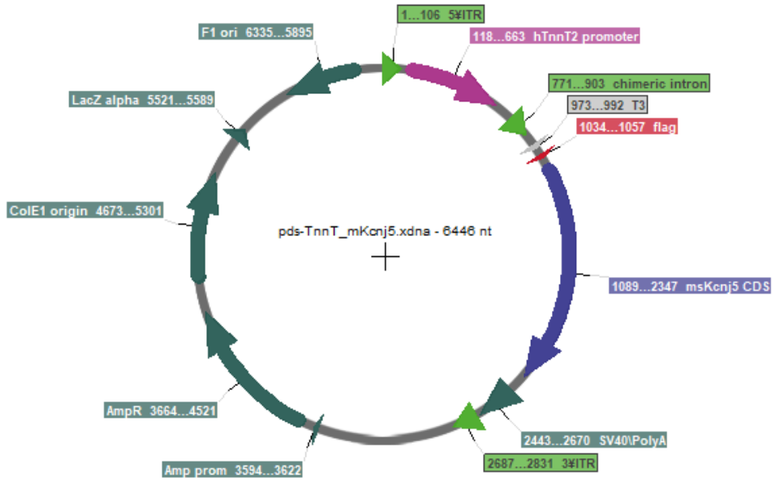

11.2. Dysregulated genes in *vTbx5*KO

Table 38. Downregulated genes with a log2-fold-change (L2FC) <-0.8 and p <0.05

external_gene_id	description	L2FC	padj
Gpr22	G protein-coupled receptor 22	-2.98	6.57E-33
Ttll1	tubulin tyrosine ligase-like 1	-2.60	2.30E-39
Aldob	aldolase B, fructose-bisphosphate	-2.40	2.51E-29
Gja1	gap junction protein, alpha 1	-2.23	1.60E-29
3632451O06Rik	RIKEN cDNA 3632451O06 gene	-2.23	6.43E-33
Cenpf	centromere protein F	-2.05	2.11E-18
Fgf16	fibroblast growth factor 16	-1.91	1.68E-19
Dbh	dopamine beta hydroxylase	-1.79	9.76E-07
Scn5a	sodium channel, voltage-gated, type V, alpha	-1.78	3.05E-14
9330158H04Rik	RIKEN cDNA 9330158H04 gene	-1.77	5.60E-18
Fstl4	follistatin-like 4	-1.75	6.29E-08
Kcnj5	potassium inwardly-rectifying channel, subfamily J, member 5	-1.73	2.72E-27
Gm16316	predicted gene 16316	-1.66	7.13E-05
Gm10801	predicted gene 10801	-1.51	3.78E-04
Lrrc4b	leucine rich repeat containing 4B	-1.44	6.12E-08
Pde11a	phosphodiesterase 11A	-1.41	3.60E-06
Gm14492	predicted gene 14492	-1.39	7.91E-07
B3galt2	UDP-Gal:betaGlcNAc beta 1,3-galactosyltransferase, polypeptide 2	-1.38	1.32E-03
Junb	Jun-B oncogene	-1.36	7.13E-04
Gm10435	predicted gene 10435	-1.35	5.45E-05
Fhl2	four and a half LIM domains 2	-1.35	1.64E-11
Chrm2	cholinergic receptor, muscarinic 2, cardiac	-1.33	1.04E-12
Emilin2	elastin microfibril interfacer 2	-1.32	5.82E-08
Plekhh1	pleckstrin homology domain containing, family H (with MyTH4 domain) member 1	-1.31	8.03E-07
Pdlim4	PDZ and LIM domain 4	-1.31	5.69E-10
Gm12295	predicted gene 12295	-1.28	3.11E-06
Gm16534	predicted gene 16534	-1.27	2.07E-04
Kcng2	potassium voltage-gated channel, subfamily G, member 2	-1.27	2.11E-19
Cyr61	cysteine rich protein 61	-1.23	2.11E-03
Polr1e	polymerase (RNA) I polypeptide E	-1.23	6.83E-10
Fitm1	fat storage-inducing transmembrane protein 1	-1.21	5.82E-08

Efnb3	ephrin B3	-1.19	2.03E-12
Sbk2	SH3-binding domain kinase family, member 2	-1.18	4.98E-03
Entpd5	ectonucleoside triphosphate diphosphohydrolase 5	-1.17	3.03E-29
Cntn5	contactin 5	-1.16	7.23E-04
Lgi3	leucine-rich repeat LGI family, member 3	-1.15	6.09E-05
Rbfox1	RNA binding protein, fox-1 homolog 1	-1.15	2.86E-15
Cacna1g	calcium channel, voltage-dependent, T type, alpha 1G subunit	-1.15	1.69E-03
Nppb	natriuretic peptide type B	-1.15	1.37E-02
Gm10800	predicted gene 10800	-1.15	1.87E-02
Abra	actin-binding Rho activating protein	-1.13	1.98E-04
Tbc1d10c	TBC1 domain family, member 10c	-1.12	8.35E-08
Fam81a	family with sequence similarity 81, member A	-1.11	7.57E-08
Adam11	a disintegrin and metallopeptidase domain 11	-1.11	7.36E-03
Ankrd63	ankyrin repeat domain 63	-1.09	2.90E-03
Slc17a7	solute carrier family 17 (sodium-dependent inorganic phosphate cotransporter), member 7	-1.08	5.05E-03
Gm26924	predicted gene, 26924	-1.06	2.26E-02
Egflam	EGF-like, fibronectin type III and laminin G domains	-1.05	7.75E-12
Sh3kbp1	SH3-domain kinase binding protein 1	-1.04	1.32E-16
Kcnv2	potassium channel, subfamily V, member 2	-1.04	3.80E-06
Crip2	cysteine rich protein 2	-1.04	4.64E-04
A530058N18Rik	RIKEN cDNA A530058N18 gene	-1.03	1.59E-02
Ier2	immediate early response 2	-1.02	3.38E-02
Lbh	limb-bud and heart	-1.02	3.78E-20
Pkig	protein kinase inhibitor, gamma	-1.02	1.06E-13
Cnga3	cyclic nucleotide gated channel alpha 3	-1.02	3.06E-06
C130080G10Rik	RIKEN cDNA C130080G10 gene	-1.02	1.49E-14
Pdzrn3	PDZ domain containing RING finger 3	-1.01	4.22E-07
Stk39	serine/threonine kinase 39	-1.01	7.95E-15
Fig4	FIG4 homolog (S. cerevisiae)	-1.01	2.15E-09
Gm17473	predicted gene, 17473	-0.99	2.12E-02
S1pr5	sphingosine-1-phosphate receptor 5	-0.99	4.28E-02
Lrrc3b	leucine rich repeat containing 3B	-0.98	3.77E-03
Ctgf	connective tissue growth factor	-0.98	4.19E-03

Lrrc10	leucine rich repeat containing 10	-0.96	1.02E-05
Ctnna1	catenin (cadherin associated protein), alpha 1	-0.96	4.30E-13
Ier5	immediate early response 5	-0.95	2.41E-02
Klhl34	kelch-like 34	-0.94	1.09E-04
Ano10	anoctamin 10	-0.94	2.74E-13
Ighg2c	immunoglobulin heavy constant gamma 2C	-0.94	1.78E-03
Aldh1l2	aldehyde dehydrogenase 1 family, member L2	-0.93	2.28E-08
Gm15770	predicted gene 15770	-0.93	4.18E-02
Cox17	cytochrome c oxidase assembly protein 17	-0.93	3.72E-08
Daam1	dishevelled associated activator of morphogenesis 1	-0.90	4.03E-09
Lclat1	lysocardiolipin acyltransferase 1	-0.89	1.51E-03
Cmya5	cardiomyopathy associated 5	-0.89	2.13E-03
Mrpl12	mitochondrial ribosomal protein L12	-0.88	4.95E-02
Amph	amphiphysin	-0.88	3.44E-03
Gm17281	predicted gene, 17281	-0.87	7.57E-08
4430402I18Rik	RIKEN cDNA 4430402I18 gene	-0.86	1.98E-03
Spint2	serine protease inhibitor, Kunitz type 2	-0.85	3.00E-02
Adrbk2	adrenergic receptor kinase, beta 2	-0.85	3.80E-06
Clasp1	CLIP associating protein 1	-0.84	1.64E-04
Ankrd23	ankyrin repeat domain 23	-0.83	1.69E-02
Pgf	placental growth factor	-0.82	1.56E-03
Ehbp1	EH domain binding protein 1	-0.82	8.08E-16
Myl1	myosin, light polypeptide 1	-0.82	3.72E-02
Il15	interleukin 15	-0.82	2.72E-03
Abca12	ATP-binding cassette, sub-family A (ABC1), member 12	-0.81	3.60E-07
Grb14	growth factor receptor bound protein 14	-0.81	4.08E-20
Tmem56	transmembrane protein 56	-0.81	9.98E-03
Hfe2	hemochromatosis type 2 (juvenile)	-0.81	2.86E-07
Adra1b	adrenergic receptor, alpha 1b	-0.80	4.95E-06
Cryab	crystallin, alpha B	-0.80	5.13E-03
Casq1	calsequestrin 1	-0.80	1.18E-02
Kcnip2	Kv channel-interacting protein 2	-0.80	2.46E-12
Hspb1	heat shock protein 1	-0.80	7.39E-03

Table 39. Downregulated genes with a log2-fold-change (L2FC) >0.8 and p <0.05

external_gene_id	description	L2FC	padj
Gm8420	predicted gene 8420	3.15	4.73E-20
Cd226	CD226 antigen	1.93	1.17E-07
AI593442	expressed sequence AI593442	1.75	5.63E-08
Ppbp	pro-platelet basic protein	1.65	3.63E-05
D630024D03Rik	RIKEN cDNA D630024D03 gene	1.58	5.45E-05
F5	coagulation factor V	1.56	3.62E-04
A930033H14Rik	RIKEN cDNA A930033H14 gene	1.50	9.10E-07
Btla	B and T lymphocyte associated	1.49	1.59E-04
Tubb1	tubulin, beta 1 class VI	1.41	1.55E-03
Gapdh	glyceraldehyde-3-phosphate dehydrogenase	1.40	8.28E-06
Lypd6	LY6/PLAUR domain containing 6	1.28	1.51E-03
Raph1	Ras association (RalGDS/AF-6) and pleckstrin homology domains 1	1.22	4.56E-04
Siglec1	sialic acid binding Ig-like lectin 1, sialoadhesin	1.21	3.52E-04
Gm15626	predicted gene 15626	1.19	1.93E-03
Itga2b	integrin alpha 2b	1.18	1.38E-02
Casc5	cancer susceptibility candidate 5	1.16	9.43E-04
Wisp2	WNT1 inducible signaling pathway protein 2	1.16	2.41E-06
Scgb1c1	secretoglobin, family 1C, member 1	1.16	1.93E-05
Vaultrc5	vault RNA component 5	1.15	7.36E-03
Cubn	cubilin (intrinsic factor-cobalamin receptor)	1.15	8.81E-04
Gm4951	predicted gene 4951	1.14	1.22E-03
Acox2	acyl-Coenzyme A oxidase 2, branched chain	1.14	4.62E-03
Gm10115	predicted gene 10115	1.13	1.25E-02
Ctla2a	cytotoxic T lymphocyte-associated protein 2 alpha	1.13	5.02E-09
Rgs18	regulator of G-protein signaling 18	1.13	1.69E-03
Gm17388	predicted gene, 17388	1.12	1.46E-02
Clec1b	C-type lectin domain family 1, member b	1.12	2.66E-02
Gp9	glycoprotein 9 (platelet)	1.11	2.78E-02
Mx2	myxovirus (influenza virus) resistance 2	1.11	2.56E-04
Snora23	small nucleolar RNA, H/ACA box 23	1.10	8.82E-03
Marveld2	MARVEL (membrane-associating) domain containing 2	1.09	4.12E-03
Psca	prostate stem cell antigen	1.09	2.26E-02
B230325K18Rik	RIKEN cDNA B230325K18 gene	1.07	1.73E-02
Gm12250	predicted gene 12250	1.06	2.90E-03
Gm25835	predicted gene, 25835	1.06	2.12E-04
Gm10615	predicted gene 10615	1.05	1.32E-02
Gm22710	predicted gene, 22710	1.04	2.69E-03
5430416N02Rik	RIKEN cDNA 5430416N02 gene	1.04	1.80E-02
A430110L20Rik	RIKEN cDNA A430110L20 gene	1.04	3.01E-02
Slfn8	schlafen 8	1.03	3.97E-02
Snord15a	small nucleolar RNA, C/D box 15A	1.02	9.62E-05
Gm15675	predicted gene 15675	1.02	2.30E-02
P2ry12	purinergic receptor P2Y, G-protein coupled 12	1.02	1.51E-03
Ddx60	DEAD (Asp-Glu-Ala-Asp) box polypeptide 60	1.02	1.72E-10
Angptl7	angiopoietin-like 7	1.02	6.64E-04
Trim59	tripartite motif-containing 59	1.00	1.99E-02
Trpc6	transient receptor potential cation channel, subfamily C, member 6	1.00	2.28E-02
Slc6a4	solute carrier family 6 (neurotransmitter transporter, serotonin), member 4	1.00	2.85E-02
Ckap2	cytoskeleton associated protein 2	1.00	3.60E-02
Gm16586	predicted gene 16586	1.00	9.42E-05
Rorb	RAR-related orphan receptor beta	0.98	1.36E-02
Trim67	tripartite motif-containing 67	0.98	2.65E-03
Mir1949	microRNA 1949	0.98	9.50E-03
Gm16340	predicted gene 16340	0.98	1.34E-02
Ccl8	chemokine (C-C motif) ligand 8	0.98	2.54E-02
Npas2	neuronal PAS domain protein 2	0.98	4.74E-02
Ikzf1	IKAROS family zinc finger 1	0.97	4.40E-03
A930039A15Rik	RIKEN cDNA A930039A15 gene	0.97	1.74E-02
S100a4	S100 calcium binding protein A4	0.96	4.96E-03
Gm25791	predicted gene, 25791	0.94	6.00E-05
Gm26165	predicted gene, 26165	0.93	1.21E-02
Ifi204	interferon activated gene 204	0.92	1.02E-02
Ifit1	interferon-induced protein with tetratricopeptide repeats 1	0.92	8.19E-05
H2-Q6	histocompatibility 2, Q region locus 6	0.92	2.82E-03
Tfcp2l1	transcription factor CP2-like 1	0.92	1.03E-02
Creb5	cAMP responsive element binding protein 5	0.92	8.35E-03
F630028O10Rik	RIKEN cDNA F630028O10 gene	0.91	1.24E-04

Prg4	proteoglycan 4 (megakaryocyte stimulating factor, articular superficial zone protein)	0.91	1.51E-04
2610203C20Rik	RIKEN cDNA 2610203C20 gene	0.91	1.74E-02
Zfhx4	zinc finger homeodomain 4	0.91	2.66E-02
Adam33	a disintegrin and metallopeptidase domain 33	0.90	3.69E-02
Gm23442	predicted gene, 23442	0.90	6.35E-04
Papd4	PAP associated domain containing 4	0.90	9.12E-03
Gm26397	predicted gene, 26397	0.89	7.54E-04
Cd84	CD84 antigen	0.89	4.60E-04
Gm21781	predicted gene, 21781	0.89	1.89E-02
Plek	pleckstrin	0.88	1.62E-02
Arhgap15	Rho GTPase activating protein 15	0.88	2.41E-02
Rbm3	RNA binding motif protein 3	0.87	6.07E-06
Clec10a	C-type lectin domain family 10, member A	0.87	1.75E-03
Myo1g	myosin IG	0.86	3.82E-02
Sntb1	syntrophin, basic 1	0.86	1.53E-03
Zfp960	zinc finger protein 960	0.85	5.60E-03
Irf7	interferon regulatory factor 7	0.84	8.99E-05
Mamld1	mastermind-like domain containing 1	0.84	4.80E-02
Clec5a	C-type lectin domain family 5, member a	0.84	3.46E-02
Fermt3	fermitin family homolog 3 (Drosophila)	0.84	3.88E-03
4931406C07Rik	RIKEN cDNA 4931406C07 gene	0.83	8.67E-05
Dlg2	discs, large homolog 2 (Drosophila)	0.83	2.06E-02
Hpse	heparanase	0.83	3.84E-02
Gm12940	predicted gene 12940	0.81	2.69E-02
Ifit2	interferon-induced protein with tetratricopeptide repeats 2	0.80	1.09E-04
4930529M08Rik	RIKEN cDNA 4930529M08 gene	0.80	1.66E-02